


9-27-2013

# Tubular and Sector Heat Pipes with Interconnected Branches for Gas Turbine and/or Compressor Cooling

Brian D. Reding II  
bredi001@fiu.edu

Follow this and additional works at: <http://digitalcommons.fiu.edu/etd>

 Part of the [Aerospace Engineering Commons](#), [Fluid Dynamics Commons](#), [Heat Transfer, Combustion Commons](#), [Other Mechanical Engineering Commons](#), and the [Thermodynamics Commons](#)

---

## Recommended Citation

Reding, Brian D. II, "Tubular and Sector Heat Pipes with Interconnected Branches for Gas Turbine and/or Compressor Cooling" (2013). *FIU Electronic Theses and Dissertations*. Paper 969.  
<http://digitalcommons.fiu.edu/etd/969>

This work is brought to you for free and open access by the University Graduate School at FIU Digital Commons. It has been accepted for inclusion in FIU Electronic Theses and Dissertations by an authorized administrator of FIU Digital Commons. For more information, please contact [dcc@fiu.edu](mailto:dcc@fiu.edu).

FLORIDA INTERNATIONAL UNIVERSITY

Miami, Florida

TUBULAR AND SECTOR HEAT PIPES WITH INTERCONNECTED BRANCHES  
FOR GAS TURBINE AND/OR COMPRESSOR COOLING

A dissertation submitted in partial fulfillment of

the requirements for the degree of

DOCTOR OF PHILOSOPHY

in

MECHANICAL ENGINEERING

by

Brian D. Reding II

2013

To: Dean Amir Mirmiran  
College of Engineering and Computing

This dissertation, written by Brian D. Reding II, and entitled Tubular and Sector Heat Pipes with Interconnected Branches for Gas Turbine and/or Compressor Cooling, having been approved in respect to style and intellectual content, is referred to you for judgment.

We have read this dissertation and recommend that it be approved.

---

Ali Ebadian

---

Ibrahim Tansel

---

Grover Larkins

---

Norman Munroe, Co-Major Professor

---

Yiding Cao, Co-Major Professor

Date of Defense: September 27, 2013

The dissertation of Brian D. Reding II is approved.

---

Dean Amir Mirmiran  
College of Engineering and Computing

---

Dean Lakshmi N. Reddi  
University Graduate School

Florida International University, 2013

© Copyright 2013 by Brian D. Reding II

All rights reserved.

## DEDICATION

I dedicate this dissertation to my family and loved ones. Without their patience, understanding, support, and most of all energy drinks, the completion of this work would not have been possible.

## ACKNOWLEDGMENTS

I wish to thank the members of my committee for their support, patience, and understanding during my research. Their constant support and invaluable knowledge has been much appreciated. I would like to thank Florida International University's Applied Research Center (ARC) for use of their lab and facilities. Without their lab and facilities, I would not have been able to finish my research. I would also like to thank Mr. Adrian Arbide for his help and expertise in setting up the testing apparatus and Mr. Mingcong Gao for his valuable assistance in heat pipe prototype testing.

I am also grateful for the following grant 58940-RT-REP from the Army Research Office that has enabled this work to be possible.

Finally, I would like to thank my major professor, Dr. Yiding Cao. From the beginning he had confidence in my abilities to complete a degree and to do it with excellence.

I have found my coursework throughout the curriculum to be stimulating and insightful, providing me with the tools and experience with which to excel in my field.

ABSTRACT OF THE DISSERTATION  
TUBULAR AND SECTOR HEAT PIPE WITH INTERCONNECTED BRANCHES  
FOR GAS TURBINE AND/OR COMPRESSOR COOLING

by

Brian D. Reding II

Florida International University, 2013

Miami, Florida

Professor Yiding Cao, Co-Major Professor

Professor Norman Munroe, Co-Major Professor

Designing turbines for either aerospace or power production is a daunting task for any heat transfer scientist or engineer. Turbine designers are continuously pursuing better ways to convert the stored chemical energy in the fuel into useful work with maximum efficiency. Based on thermodynamic principles, one way to improve thermal efficiency is to increase the turbine inlet pressure and temperature. Generally, the inlet temperature may exceed the capabilities of standard materials for safe and long-life operation of the turbine. Next generation propulsion systems, whether for new supersonic transport or for improving existing aviation transport, will require more aggressive cooling system for many hot-gas-path components of the turbine. Heat pipe technology offers a possible cooling technique for the structures exposed to the high heat fluxes. Hence, the objective of this dissertation is to develop new radially rotating heat pipe systems that integrate multiple rotating miniature heat pipes with a common reservoir for a more effective and practical solution to turbine or compressor cooling.

In this dissertation, two radially rotating miniature heat pipes and two sector heat pipes are analyzed and studied by utilizing suitable fluid flow and heat transfer modeling along with experimental tests. Analytical solutions for the film thickness and the lengthwise vapor temperature distribution for a single heat pipe are derived. Experimental tests on single radially rotating miniature heat pipes and sector heat pipes are undertaken with different important parameters and the manner in which these parameters affect heat pipe operation.

Analytical and experimental studies have proven that the radially rotating miniature heat pipes have an incredibly high effective thermal conductance and an enormous heat transfer capability. Concurrently, the heat pipe has an uncomplicated structure and relatively low manufacturing costs. The heat pipe can also resist strong vibrations and is well suited for a high temperature environment. Hence, the heat pipes with a common reservoir make incorporation of heat pipes into turbo-machinery much more feasible and cost effective.



## TABLE OF CONTENTS

CHAPTER	PAGE
1. Introduction .....	1
1.1 History of the Heat Pipe.....	1
1.2 Turbine Blade and Disk Cooling .....	18
1.3 Application of Radially Rotating Miniature Heat Pipes to the Turbine Blade and Disk.....	23
1.4 Objectives of this Study .....	27
2. Analysis of the Performance of a Single Radially Rotating Miniature Heat Pipe Derived from a Sector of the Turbine Disk.....	28
2.1 Analytical Solution for the Liquid Film Distribution in the Condenser Section of a Single Heat Pipe.....	31
2.2 General Solution of the Liquid Film Distribution in the Condenser Section with Consideration of the Tilt Angle .....	39
2.3 Axial Vapor Flow Analysis along the Single Heat Pipe Length .....	46
2.4 Analytical Results for the Heat Transfer Limitations and Temperature Drop in a Single Heat Pipe.....	54
3. Experimental Testing Procedures.....	63
3.1 High Speed Rotating Test Apparatus.....	63
3.2 Single Radially Rotating Miniature Heat Pipes .....	68
3.3 Sector Heat Pipe with Interconnected Branches (Design 1).....	73
3.4 Sector Heat Pipe with Interconnected Branches (Design 2).....	78
4. Experimental Results and Analysis.....	83
4.1 Operating Characteristics of Radially Rotating Miniature Heat Pipes .....	85
4.2 Effects of Heat Input.....	95
4.3 Effects of the Dimensionless Centripetal Forces .....	99
4.4 Effects of Fill Volume on the Sector Heat Pipe.....	102
4.5 Comparisons of the Theoretical Results with Experimental Data for the Lengthwise Temperature Distributions.....	105
4.6 Determination of the Effective Thermal Conductivity .....	109
4.7 Error Analysis for Experimental Measurements.....	113
5. Conclusions and Recommendations.....	116
5.1 Conclusions.....	116
5.2 Recommendations.....	118
Appendix.....	123
Vita.....	148

## LIST OF TABLES

TABLE	PAGE
Table 2-1 Parameters of Testing and Heat Pipes .....	54
Table 4-1 Comparison of Heat Pipe and Heat Pipe Shell ( $d_i = 1.5 \text{ mm}$ and $f = 30 \text{ Hz}$ )..	86
Table 4-2 Comparison of Heat Pipe and Heat Pipe Shell ( $d_i = 2 \text{ mm}$ and $f = 30 \text{ Hz}$ ) ...	87
Table 4-3 Comparison of Sector Heat Pipe and Sector Heat Pipe Shell ( $Q = 75 \text{ W}$ , $f = 15 \text{ Hz}$ ).....	92
Table 4-4 Comparisons of Calculated and Experimental Lengthwise Temperature Distributions of a Single Heat Pipe ( $d_i = 1.5 \text{ mm}$ , $Q = 250 \text{ W}$ , $\frac{\omega^2 \bar{Z}_a}{g} = 1881$ ) .....	105
Table 4-5 Comparisons of Calculated and Experimental Lengthwise Temperature Distributions of a Single Heat Pipe ( $d_i = 2.0 \text{ mm}$ , $Q = 280 \text{ W}$ , $\frac{\omega^2 \bar{Z}_a}{g} = 1881$ ).....	106

## LIST OF FIGURES

FIGURE	PAGE
Figure 1.1 Perkins Tube [1] .....	1
Figure 1.2 Diagram of a Gravity Assisted Wickless Heat Pipe (Two Phase Closed Thermo-Siphon) [2] .....	2
Figure 1.3 The Gay's Device [1].....	3
Figure 1.4 Dipiction of a Conventional Capillary Driven Heat Pipe [2].....	4
Figure 1.5 Basic Heat Pipe Regions [1].....	5
Figure 1.6 Working Fluids and Temperature Ranges [1] .....	7
Figure 1.7 Wick Structures [1].....	9
Figure 1.8 Conventional Annular Heat Pipe [2].....	10
Figure 1.9 Concentric Annular Heat Pipe [2].....	11
Figure 1.10 Depiction of a Flat Plate Heat Pipe [2].....	12
Figure 1.11 Depiction of a Gas Loaded Variable Conductance Heat Pipe [2].....	13
Figure 1.12 Diagram of a Capillary Pumped Loop Heat Pipe [2] .....	14
Figure 1.13 Diagram of a Rotating Heat Pipe [2].....	15
Figure 1.14 Diagram of an Axially Reciprocating Heat Pipe [9] .....	16
Figure 1.15 Transpiration Cooling Turbine Blade [10].....	19
Figure 1.16 Turbine Blade Film Cooling [11].....	20
Figure 1.17 Turbine Blade Convection Cooling [12].....	21
Figure 1.18 Depiction of Radially Rotating Heat Pipes being Utilized in a Turbine Blade .....	22
Figure 1.19 Depiction of Heat Pipe Utilization with Air Cooling in Turbine Blade [13]	24
Figure 1.20 Depiction of a Radially Rotating Heat Pipe with a Tilt Angle [14] .....	25

Figure 1.21 Depiction of a Possible Configuration for the use of Radially Rotating Heat Pipes Cooling for a Turbine Disk .....	26
Figure 2.1 Representation of a Typical Turbine Disk.....	28
Figure 2.2 Hidden Line View of the Heat Pipes in a Turbine Disk.....	29
Figure 2.3 Turbine Disk Enlarged View.....	29
Figure 2.4 Dissected View of Sector Heat Pipe.....	30
Figure 2.5 Depiction of a Radially Rotating Heat Pipe .....	31
Figure 2.6 Depiction of a Differential Control Volume in the Condensate [16] [17] .....	33
Figure 2.7 Depiction of a Control Volume at the Liquid-Vapor Interface [16] [17].....	35
Figure 2.8 Representation of a Differential Control Volume in the Condensate Film [16] [17].....	39
Figure 2.9 Representation of a Vapor Thermal Balance in the Condenser Section [16] [17].....	47
Figure 2.10 Representation of the Overall Thermal Balance in the Condenser Section [16] [17].....	49
Figure 2.11 Maximum Temperature Decreases across the Liquid Film for Sodium as the Working Fluid ( $T_v = 1100K$ , $Q=200W$ ) .....	55
Figure 2.12 Maximum Temperature Decreases across the Liquid Film for Sodium as the Working Fluid ( $d_i/L = 0.025$ , $Q = 200W$ ) .....	56
Figure 2.13 Lengthwise Vapor Temperature Drop of the Heat Pipe at Different Rotating Speeds ( $d_i/L = 0.025$ , $Q = 200W$ ) .....	57
Figure 2.14 Lengthwise Vapor Temperature Drop of the Heat Pipe at Different Heat Pipe Dimensionless Sizes ( $Q = 200W$ , $\omega^2 \bar{Z}_a/g = 6.00 \times 10^4$ ) .....	58
Figure 2.15 Vapor Temperature Decreases along the Heat Pipe Length at Different Heat Inputs.....	59
Figure 2.16 Ratio of the Vapor Temperature Decreases to the Total Temperature Decrease, due to the Centripetal Force ( $T_v = 1100K$ , $Q = 200W$ ) .....	60

Figure 2.17 Entrainment Limitations as a Function of Rotational Speeds .....	61
Figure 3.1 Depiction of a High Speed Rotating Test Apparatus and Data Acquisition System.....	63
Figure 3.2 Schematic of High Speed Rotating Test Apparatus .....	64
Figure 3.3 Schematic of 1.5 mm Single Miniature Radially Rotating Heat Pipe.....	68
Figure 3.4 Schematic of 2 mm Single Miniature Radially Rotating Heat Pipe.....	69
Figure 3.5 Picture of a Prepared Single Radially Rotating Miniature Heat Pipe .....	72
Figure 3.6 Schematic of Sector Heat Pipe (Design 1) .....	73
Figure 3.7 Schematic of Sector Heat Pipe (Design 1) Reservoir Location.....	74
Figure 3.8 Picture of a Prepared Sector Heat Pipe (Design 1).....	77
Figure 3.9 Schematic of Sector Heat Pipe (Design 2) .....	78
Figure 3.10 Schematic of Sector Heat Pipe (Design 2), Reservoir Location.....	79
Figure 3.11 Picture of Sector Heat Pipe (Design 2) being filled .....	80
Figure 3.12 Picture of a Prepared Sector Heat Pipe (Design 2).....	82
Figure 4.1 Temperature Distributions of Single Heat Pipe and Heat Pipe Shell ( $d_i = 1.5$ mm and $f = 30Hz$ ) .....	86
Figure 4.2 Temperature Distributions of Single Heat Pipe and Heat Pipe Shell ( $d_i = 2$ mm and $f = 30Hz$ ) .....	87
Figure 4.3 Lengthwise Temperature Distributions of the Single Radially Rotating Miniature Heat Pipe with Different Heat Inputs ( $d_i = 1.5$ mm , $f = 30Hz$ ).....	89
Figure 4.4 Lengthwise Temperature Distributions of the Single Radially Rotating Miniature Heat Pipe with Different Heat Inputs ( $d_i = 2.0$ mm , $f = 30Hz$ ).....	90
Figure 4.5 Temperature Distributions of Sector Heat Pipe (Design 2) and Sector Heat Pipe Shell ( $Q = 75$ W , $f = 15$ Hz).....	91

Figure 4.6 Lengthwise Temperature Distributions of the Sector Heat Pipe with Different Heat Inputs ( $f = 30$ Hz) .....	93
Figure 4.7 Lengthwise Temperature Distribution for Different Heat Inputs ( $d_i = 1.5$ mm , $f = 30$ Hz) .....	95
Figure 4.8 Lengthwise Temperature Distribution for Different Heat Inputs ( $d_i = 2$ mm , $f = 30$ Hz) .....	96
Figure 4.9 Sector Heat Pipe (Design 2) Lengthwise Temperature Distribution ( $f = 30$ Hz).....	97
Figure 4.10 Sector Heat Pipe (Design 2) Lengthwise Temperature Distribution ( $f = 45$ Hz).....	98
Figure 4.11 Lengthwise Temperature Distributions for Sector Heat Pipe with Different Rotational Frequencies ( $Q = 75$ W).....	100
Figure 4.12 Sector Heat Pipe with Heat Input of 75 W ( $f = 15$ Hz).....	103
Figure 4.13 Sector Heat Pipe with Heat Input of 75 W ( $f = 30$ Hz) .....	103
Figure 4.14 Sector Heat Pipe with Heat Input of 75 W ( $f = 45$ Hz) .....	104
Figure 4.15 Comparisons of Calculated and Experimental Lengthwise Temperature Distributions of a Single Heat Pipe ( $d_i = 1.5$ mm).....	106
Figure 4.16 Comparisons of Calculated and Experimental Lengthwise Temperature Distributions of a Single Heat Pipe ( $d_i = 2.0$ mm).....	107
Figure 4.17 Sectional View of Empty Sector Heat Pipe.....	109
Figure 4.18 Sectional View of Sector Heat Pipe with a Conductive Solid within the Cavity .....	110
Figure 4.19 Three-dimensional Temperature Plot of Empty Sector Heat Pipe .....	112
Figure 4.20 Three-dimensional Temperature Plot of Filled Sector Heat Pipe .....	112

## LIST OF SYMBOLS

$A$	cross-sectional area, $m^2$
$a$	constant
Bo	Bond number
$c$	constant
$C_w$	empirical constant in Wallis' correlation
$d$	heat pipe diameter, $m$
$F_v$	frictional coefficient
$f$	skin-friction coefficient or rotating frequency, $Hz$
$g$	gravitational acceleration, $m/s^2$
$h_c$	heat transfer coefficient, $W/m^2 \cdot K$
$h_{fg}$	latent heat of vaporization, $J/kg$
$k$	thermal conductivity, $W/m \cdot K$
$k_p$	thermal conductivity of heat pipe wall, $W/m \cdot K$
$L$	length of the heat pipe, $m$
$L_a$	adiabatic length, $m$
$L_c$	condenser length, $m$
$L_e$	evaporator length, $m$
$L_{eff}$	effective length of the heat pipe, $m$
$L_{c,n}$	length of the heat pipe occupied by the non-condensable gas, $m$

$m$	coefficient, $1/m$
$\dot{m}$	mass flow rate, $kg/s$
$M_v$	Mach number
$p$	pressure, $N/m^2$
$Q$	heat transfer rate, W
$q^n$	heat flux, $W/m^2$
$Re$	Reynolds number
$R, r$	heat pipe radius, $m$
$T$	temperature, $K$ or $^{\circ}C$
$w$	axial velocity, $m/s$
$W$	flow rate of cooling air, $m^3/s$
$x$	axial coordinate, $m$
$z$	axial location of the heat pipe, $m$
$Z$	revolving radius of the heat pipe, $m$
$\phi$	tilt angle between the heat pipe centerline and the disk radial line, <i>degree</i>
$\theta$	rotating angle of the heat pipe, <i>degree</i>
$\Gamma$	liquid mass flow rate per unit circumferential length, $\frac{kg}{m \cdot s}$
$\delta$	thickness of liquid film, $m$
$\sigma$	surface tension, $N/m$
$\rho$	density, $kg/m^3$



$\mu$  dynamic viscosity,  $\text{kg}/\text{m}\cdot\text{s}$

$\tau$  shear stress,  $\text{N}/\text{m}^2$

$\omega$  angular velocity,  $\text{rad}/\text{s}$

$\psi$  dimensionless coefficient

### *Subscripts*

$a$  adiabatic section or average

$c$  condenser

$e$  evaporator

$ent$  entrainment

$eff$  effective

$l$  liquid phase

$p$  heat pipe wall

$v$  vapor phase

$z$  axial location of the heat pipe

$R - \delta$  liquid-vapor interface

## 1. Introduction

### 1.1 History of the Heat Pipe

A heat pipe is a device of very high thermal conductance, which has the ability to raise the heat transfer capacity where it is utilized. The concept of a heat pipe, called a thermosiphon today, is first developed by A.M. Perkins and J. Perkins in the mid-1800s. The device was originally referred to as a Perkins tube, which utilized either a single or two phased process to transfer heat from the furnace section to the boiler section. Below is an illustration of their device:

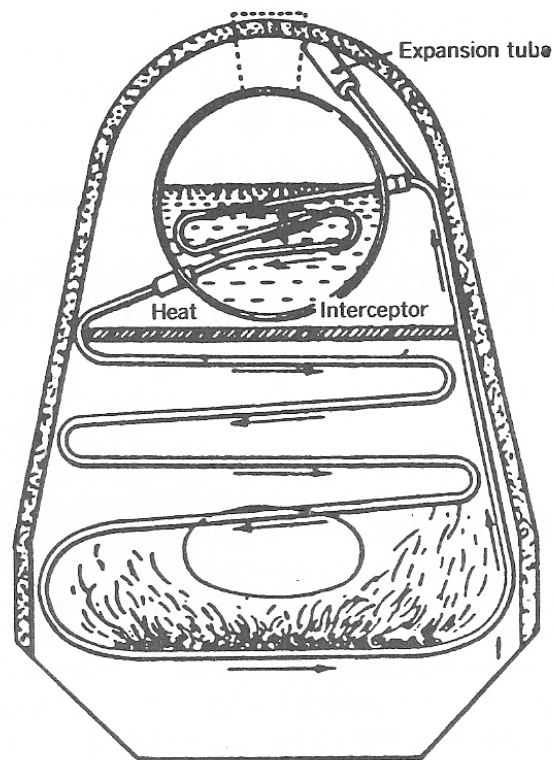


Figure 1.1 Perkins Tube [1]

A two phase closed thermo-siphon is a gravity assisted wickless heat pipe, as depicted in Figure 1.2. As can be seen in the figure, the condenser section is located above the evaporator section.

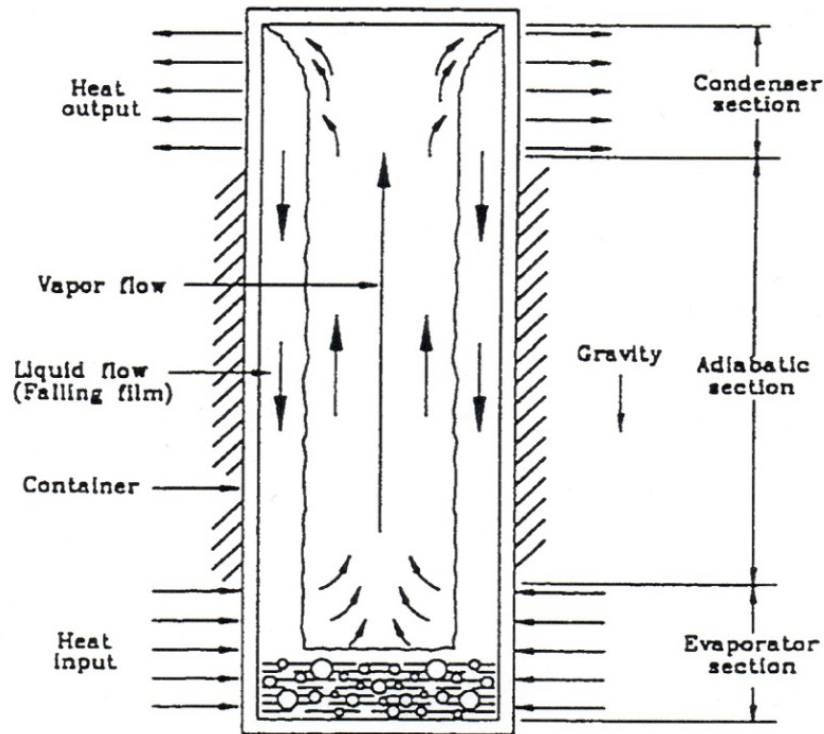


Figure 1.2 Diagram of a Gravity Assisted Wickless Heat Pipe (Two Phase Closed Thermo-Siphon) [2]

Heat is conducted through the evaporator container into the heat pipe, boiling the working fluid. The vapor ascends to the condenser section, where the vapor condenses and releases its latent heat. Gravity then draws the condensate back to the evaporator section to start the cycle over again. Because of their reliability, cost effectiveness, and high efficiency, thermo-siphons have been used in a wide variety of applications, such as intensive heat transfer in heat exchangers [3] and the de-icing of roadways [4].

The next device leading towards a heat pipe was first developed by Gay in 1929, which consisted of a number of vertical tubes that were arranged with the evaporator section below the condenser section. But it is still, as well as the Perkins tube, considered as a thermo-siphon. Figure 1.3 illustrates Gay's device.

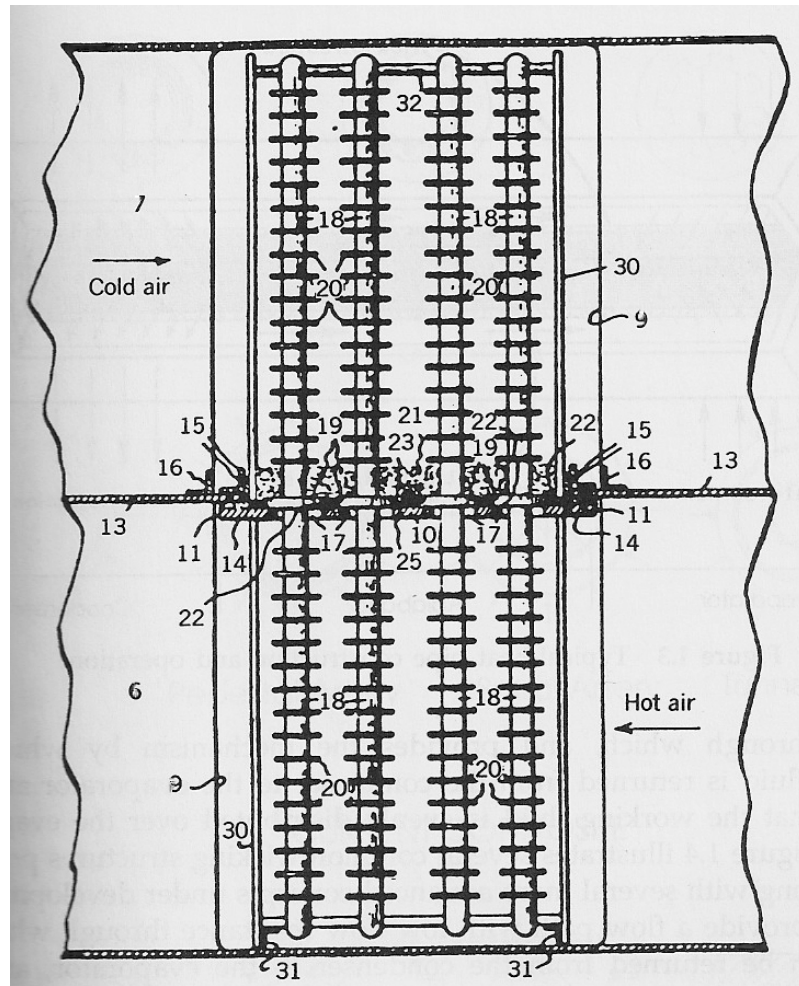


Figure 1.3 The Gay's Device [1]

As can be seen from the two preceding figures, these two devices laid down the basic concepts and paved the way towards modern day heat pipes.

The notion of the heat pipe was first introduced by R. S. Gaugler of the General Motors Corporation in 1942 [1]. George Grover at Los Alamos Laboratory also published an evaporation-condensation heat transfer device, which was, as well, named a heat pipe in 1963 [1]. Grover's heat pipe was fundamentally indistinguishable to that of the Gaugler heat pipe. However, Grover provided some degree of theoretical analysis and presented experimental results performed on stainless steel heat pipes that contained a wire mesh wick and sodium as the working fluid. Many studies have been performed and numerous types of heat pipes have been presented to the scientific community since these pioneering works were done. To date, heat pipes have been used and developed for almost all aspects of engineering and are acknowledged as an important advancement in the field of heat transfer. There are many heat pipe configurations for a wide range of applications [2]. Figure 1.4 illustrates a capillary driven heat pipe.

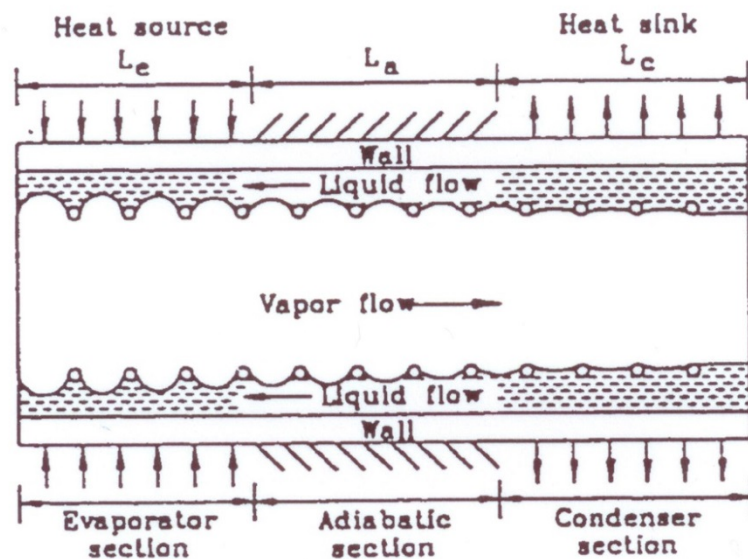


Figure 1.4 Dipiction of a Conventional Capillary Driven Heat Pipe [2]

The capillary driven heat pipe is primarily comprised of a condenser section and an evaporator section. For traditional requirements, an adiabatic section can be incorporated to separate the condenser and evaporator sections.

One of the main differences between thermo-siphons and most heat pipes can be seen in the adiabatic/isothermal section where a wick structure aids in the transport of the working fluid by means of introducing capillary forces along the walls of the heat pipe.

Figure 1.5 further illustrates the basic regions of a heat pipe and the wick structure.

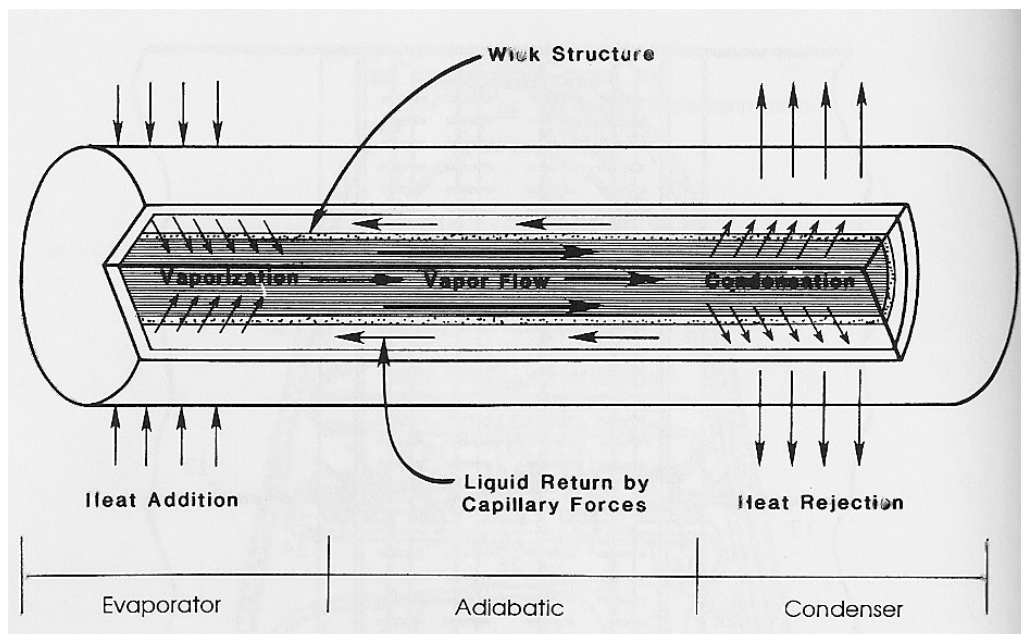


Figure 1.5 Basic Heat Pipe Regions [1]

Typical heat pipes consist of three main components: the container, a wick structure, and a working fluid. The container can be constructed from a wide range of materials, such as ceramic, metal, glass, and composites. Secondly, the wick structure can also be fabricated from a wide range of materials but must have some type of porousness to it. Typical materials for the wick include woven fiberglass, sintered metal powders, screens, wire

meshes, grooves, etc. Lastly, the working fluid (which is chosen based on the working temperature) can vary from nitrogen and helium for low temperatures (mainly used in cryogenics) to sodium and lithium for high temperature heat pipes.

Great care must be taken in choosing the proper combination of materials. For instance, one should not choose a working fluid that would be highly reactive and/or corrosive with the container material or the wick structure at the working or idle temperatures, because to do so would not only be dangerous, but would have adverse effects on the performance of the heat pipe. Also, the container material must be able to withstand the pressures associated with the saturation temperatures during startup and normal operations. Figure 1.6 is a chart with some basic working fluids and their associated working temperature ranges.

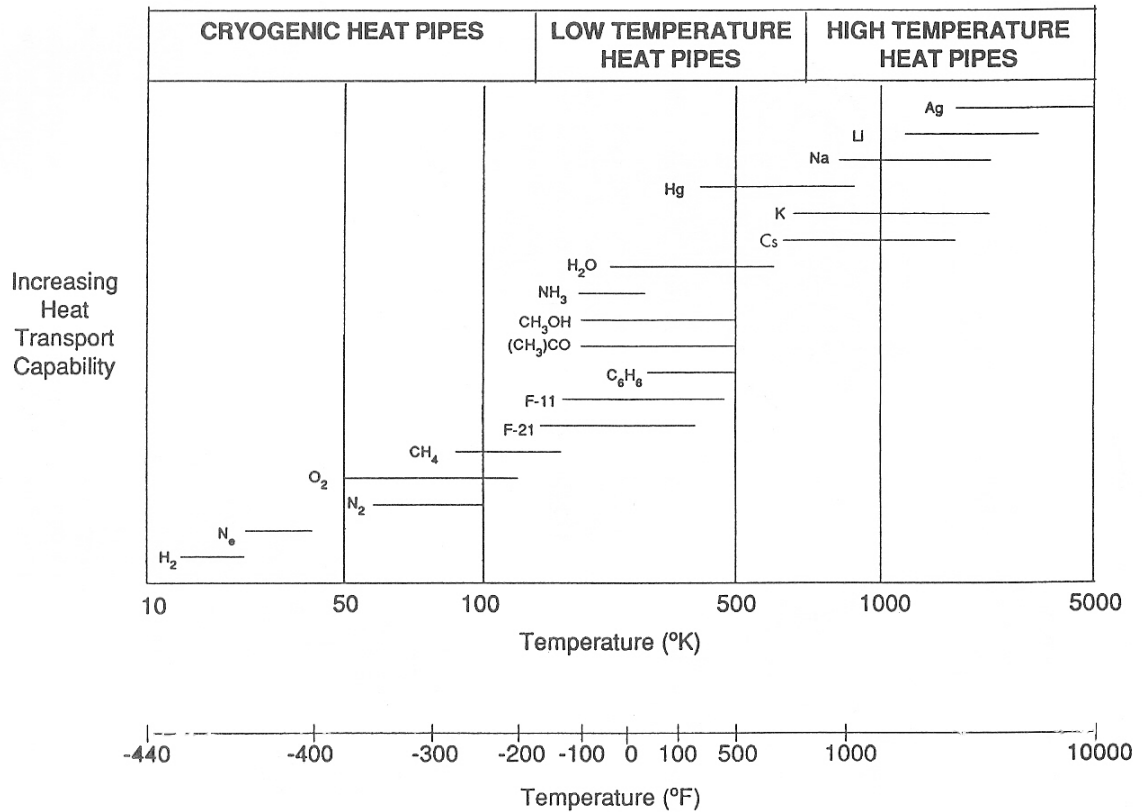


Figure 1.6 Working Fluids and Temperature Ranges [1]

The wick structure has two main functions in the operation of the heat pipe:

1. It is the transport mechanism through which the working fluid is returned to the evaporator from the condenser.
2. It also insures that the working fluid is evenly distributed over the evaporator surface.

Though the concept is simple enough, choosing a wick structure can prove to be rather difficult for two reasons:



1. An open porous structure with high permeability is desired in order to provide a low flow resistance through which the liquid can be returned to the evaporator
2. To increase capillary pumping pressure, a small pore size is desired.

This is obviously a dichotomous task, which may have an evident solution. Therefore, it is beneficial to have a wick structure that is non-homogeneous throughout; i.e., a wick structure made of several different materials or having a composite wick structure. Figure 1.7 on the following page shows some wick configurations and structures.

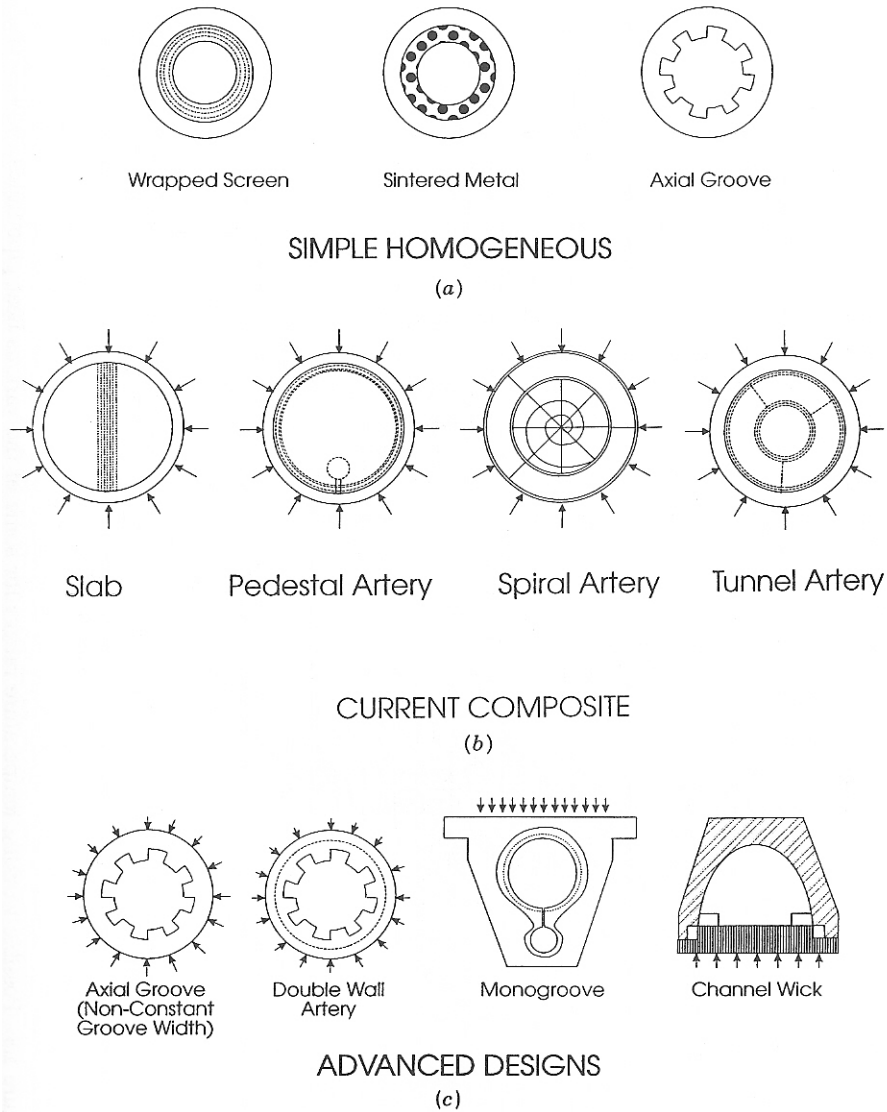


Figure 1.7 Wick Structures [1]

As is found in traditional heat pipes, a wick can be inserted into the heat pipe shell. The wick creates a capillary force which returns the condensate from the condenser section to the evaporator section of the heat pipe. When an external heat is applied, it is absorbed by the evaporator section and then the liquid in the evaporator section is concurrently heated and evaporated. The vapor travels lengthwise through the center of the heat pipe and releases its latent heat in the condenser section. The discharged latent heat is expelled to

the environment by means of convection and radiation from the outer surface of the condenser. The condensate then returns to the evaporator section through the wick structure, to complete the heat transfer cycle occurring within the heat pipe.

The annular heat pipe [1] is comparable to the standard wicked capillary driven heat pipe with the exception that the cross section of the vapor space is annular in place of circular, as shown in Figure 1.8 and Figure 1.9

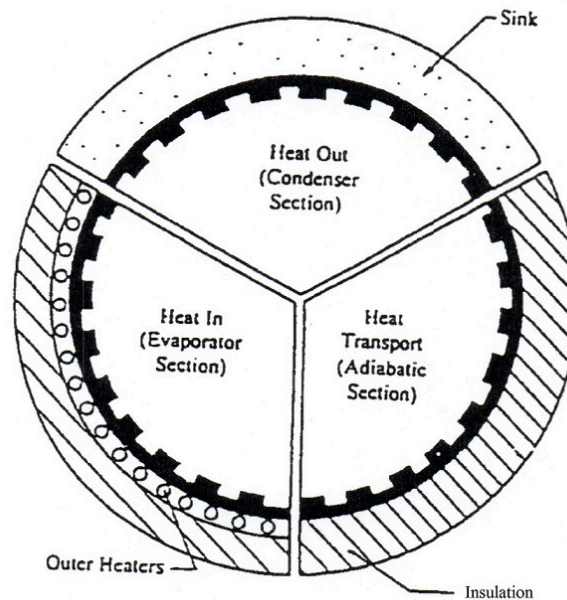


Figure 1.8 Conventional Annular Heat Pipe [2]

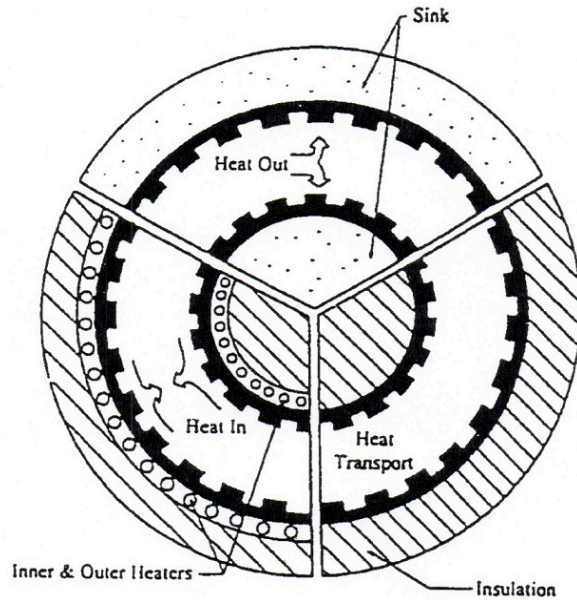


Figure 1.9 Concentric Annular Heat Pipe [2]

This design allows the engineer an area where wick material can be placed both on the inside of the outer pipe and on the outside of the inner pipe. Hence, the surface area for heat input and output can be increased significantly devoid of expanding the outer diameter of the heat pipe. The annular heat pipe has been employed as an isothermal furnace with exceptional results due to its temperature leveling abilities and fast reaction time to a cold charge [5].

The flat plate capillary driven heat pipe [1] has a rectangular shape with a minor aspect ratio, as can be seen in Figure 1.10. Additional wick blocks between the evaporator and condenser facilitate in the condensate's return, particularly when the condenser is below the evaporator in a gravity field. If the condenser is above the evaporator, the wick in the condenser section can be abandoned since the condensate on the upper plate will trickle back to the evaporator. It is possible to simplify the configuration of the flat plate heat

pipe by substituting the wick structures in the heat pipe by grooves; the grooves can create the capillary force provided by the wick structure.

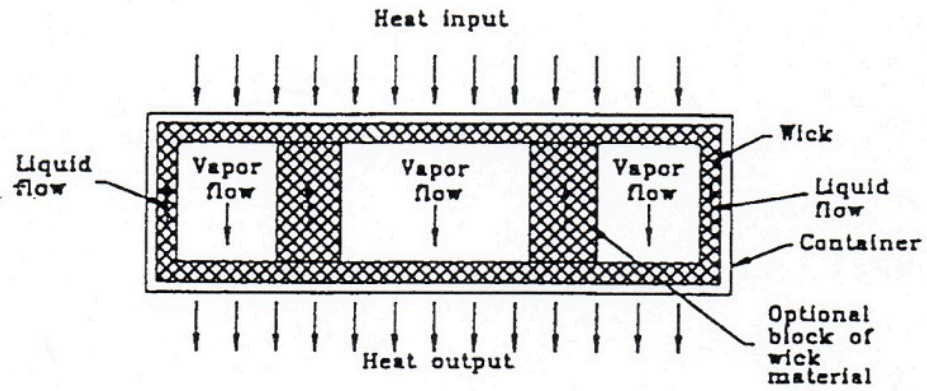


Figure 1.10 Depiction of a Flat Plate Heat Pipe [2]

The gas charged heat pipes are known as variable conductance heat pipes [1]. They are identical as the capillary driven heat pipe with the exception that a non-condensable gas is placed in the vapor space, as is shown in Figure 1.11.

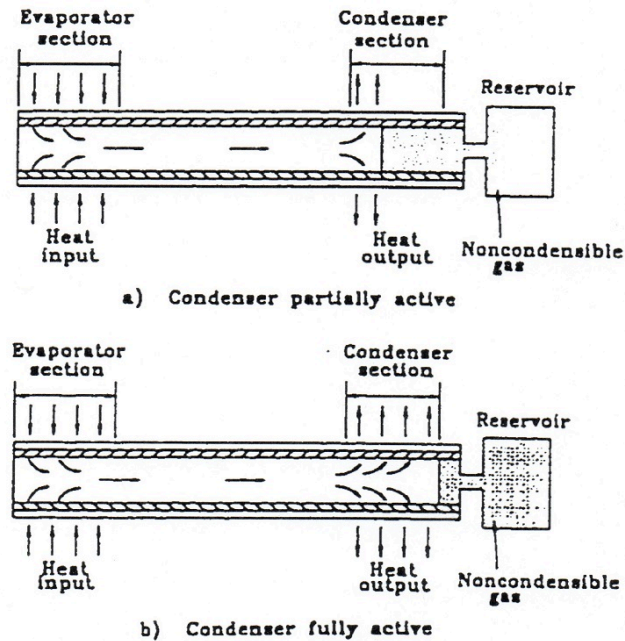


Figure 1.11 Depiction of a Gas Loaded Variable Conductance Heat Pipe [2]

Throughout operation, the gas is moved along the length of the heat pipe by the vapor of the working fluid in the condenser section [6]. Subsequently, condensation of the working fluid cannot be performed where the non-condensable gas is present, disabling a portion of the condenser and restricting it from transferring heat to the heat sink (Figure 1.11a). However, if the heat flux to the evaporator section is increased, the vapor pressure of the working fluid will be increased, which accompanies the compression of the non-condensable gas. It consecutively increases the condensing surface of condenser and allows for more heat to be transferred (Figure 1.11b). Gas loaded heat pipes can be utilized in an annular arrangement, for instance, for electric element cooling, or as an isothermal furnace.

With the advancement of miniature heat pipes, the wick structure in the heat pipe is often substituted by grooves to create the capillary force, which removes the condensate from the condenser and transports it to the evaporator. This is typically done due to the difficulties of manufacturing and installing a wick structure in a miniature heat pipe.

Figure 1.12 depicts a basic diagram of capillary pumped loop heat pipe [7].

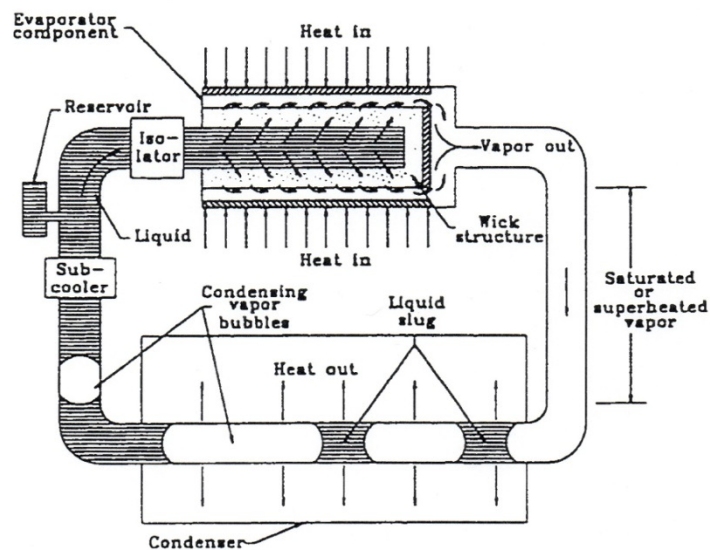


Figure 1.12 Diagram of a Capillary Pumped Loop Heat Pipe [2]

During operation, heat is applied to the evaporator section, which contains a hollowed rod of wick material crowned at one end and press fitted into an internally axially grooved tube. The heat applied to the exterior of the evaporator boils the working fluid, which then transverses the length of axially grooved channels and into the vapor header. The vapor of the working fluid traverses to the condenser, where it is initially condensed as a film on the inner wall of the pipe, and then into a liquid sludge flow. Before arriving at the evaporator, the working fluid passes through a sub-cooler, which collapses any

residual vapor bubbles and provides additional sub-cooling if necessary. The capillary pressure produced in the wick structure continuously pushes the working fluid throughout the cycle.

Rotating heat pipes can be fabricated in two different configurations [8]. First, the heat pipe can be fabricated in the shape of a disk, where two parallel disks are united at the inner and outer radii to form the vapor space, as shown in Figure 1.13.

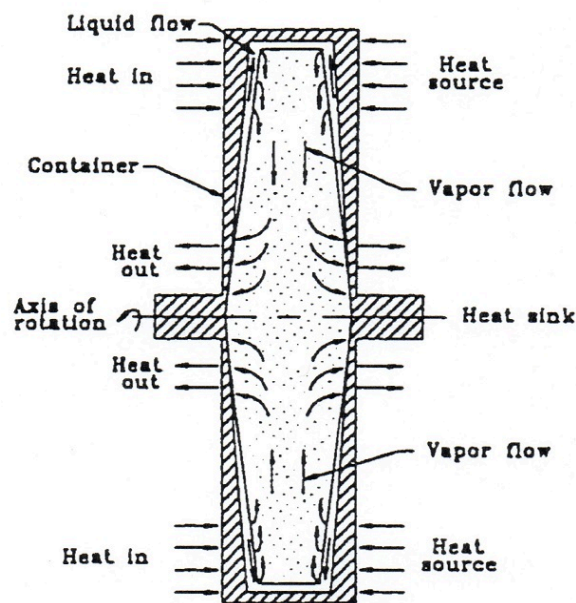


Figure 1.13 Diagram of a Rotating Heat Pipe [2]

The condensate from the condenser section is restored to the evaporator section by the centripetal force, with the aid of an interior taper. Disk-shaped heat pipes have been proposed to cool turbine disk and automobile brakes. Secondly, the heat pipe can be fabricated in the shape of a circular cylinder that can include an axial taper. The cylinder can rotate either about its own axis of symmetry or it can revolve off-axis. Consequently, capillary wicks are typically not used in rotating heat pipes. Cylindrical rotating heat



pipes can be used to cool electric motors and metal cutting tools, such as drills and end mills.

The axially reciprocating heat pipe is an innovative heat pipe design [9]. This type of heat pipe is similar in structure to the wickless two phase thermo-siphon, which has a condenser section, an evaporator section, and an amount of working fluid inside the heat pipe, which is depicted in Figure 1.14.

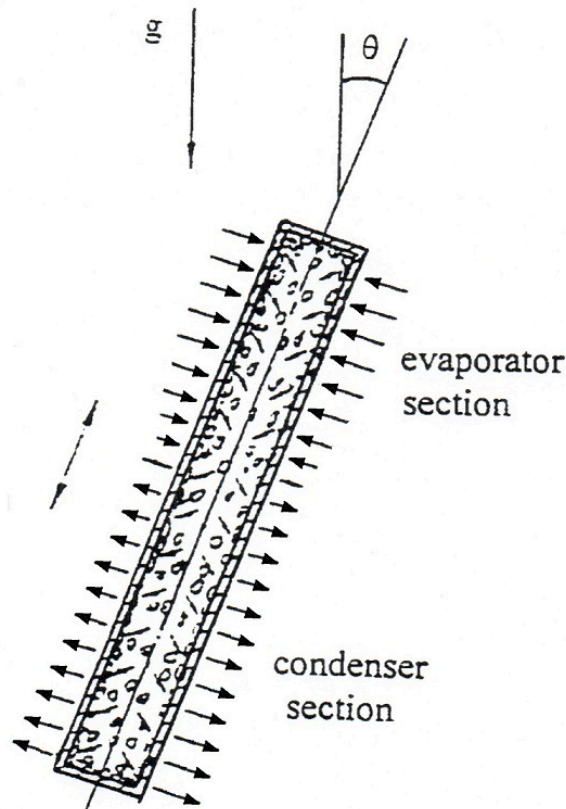


Figure 1.14 Diagram of an Axially Reciprocating Heat Pipe [9]

Nevertheless, the operational principle of the axially reciprocating heat pipe is considerably different from other heat pipes. The condensate return is achieved by a

stirring up inertia force of the axially reciprocating heat pipe. The condensate splatter and impingement inside the reciprocating heat pipe guarantees the condensate supply to the evaporator section. As displayed in Figure 1.14, the lower section of the heat pipe functions as the condenser and the upper section acts as an evaporator. Heat is conducted through the heat pipe wall into the evaporator section, where the heat is absorbed by the working liquid through evaporation. The vapor then flows down to the condenser section, where the vapor condenses and discharges the latent heat onto the interior surface of the heat pipe. Concurrently, the impinging effect of the working fluid inside the heat pipe causes a portion of the heat input to be carried from the evaporator to condenser section by the liquid working fluid. The latent heat from the vapor and the heat carried by the working fluid are conducted through the heat pipe's condenser wall to the exterior surface of the heat pipe, where the heat is removed from the surface by the cooling medium, such as air or cooling oil. The condensate is then returned by the stirring up inertia force caused by the axially reciprocating motion of the heat pipe. The axially reciprocating heat pipe can also be fabricated into different shapes, such as an annular shape.

The varieties of the heat pipes are not limited to those pointed out above. With further research into heat pipes, many new heat pipes can be created. Initially heat pipes were mainly applied to satellites; the first use was the case of two heat pipes that were used to reduce the temperature differences between the various transponders in a satellite (GEOS-B). But heat pipes have branched out from the space field and are now being used in a wide range of applications, from electronics and engine cooling to air conditioning and heat exchangers.

## 1.2 Turbine Blade and Disk Cooling

Designing turbines for either aerospace or power production is a daunting task for any heat transfer scientist or engineer. Turbine designers are continuously pursuing better ways to convert the stored chemical energy in the fuel into useful work with maximum efficiency. Based on thermodynamic principles, one way to improve thermal efficiency is to increase the turbine inlet temperature and pressure, which results in turbines being designed to work with inlet temperatures of 1500-1700 K, making the operating environment of the turbine blades and disks very hostile. Generally, these temperatures are exceeding the capabilities of standard materials for safe and long-life operation of the turbine.

Three techniques are typically considered by a turbine designer to overcome these difficulties. One approach is to develop more advanced and innovative surface coatings that have the ability to resist this adverse environment, while being as non-thermally conductive as possible in order to protect the blade and disk. This approach has been used for many years and is very convenient and advantageous. However, the advancement with new coatings is generally slow due to the fact that new surface coatings must be subjected to the impingement of high temperature gases and the vibration of turbines, thus making it challenging for the coating to adhere to the blade surface. Another method, which is primarily used on turbine blades, is the air cooling method. This technique is a conventional and effective method of cooling the turbine blade. The practice is seen in three varieties:

### A. Transpiration or porous cooling

Transpiration or porous cooling involves the use of porous materials; the cooling air is driven through the turbine blade surface to form an insulating film, as shown in Figure 1.15.

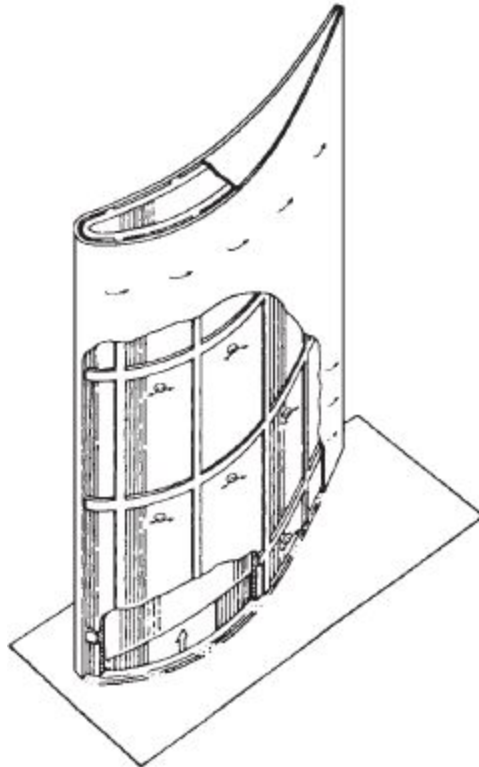


Figure 1.15 Transpiration Cooling Turbine Blade [10]

This technique, though effective, is easily neutralized due to pore blockage and material oxidation.

### B. Film Cooling

Film cooling is accomplished by having the cooling air flow through the inner channels of the blade and out through passages in the blade surface and trailing

edge. The cooling air is inserted into the boundary layer of the high temperature gases on the blade surfaces, as shown in Figure 1.16.

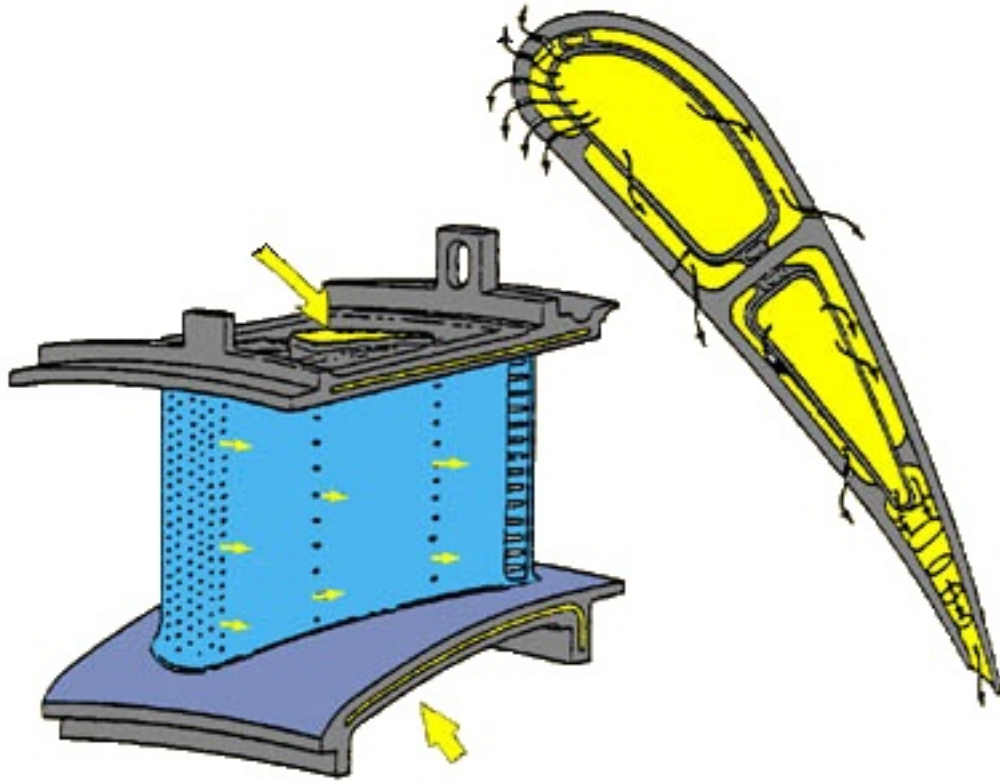


Figure 1.16 Turbine Blade Film Cooling [11]

This provides a protective layer to the turbine blade surface, while the temperature gradient in the cross-sectional area of the blade decreases significantly. Conversely, film cooling requires a large amount of cooling air, and adversely influences the thermodynamic and aerodynamic performance of the turbine.

### C. Convection Cooling

Convection cooling is one of the earlier techniques used to cool turbine blades and involves having cooling air from the compressor flow into inner channels in

the turbine blade from the blade root and flow out through the top of the turbine blade. The discharged cooling air is then mixed with the principal gas flow of the next stage. This has been proven to be an effective cooling technique since the cooling air can remove heat that is stored within the turbine blades through convection, as depicted in Figure 1.17.

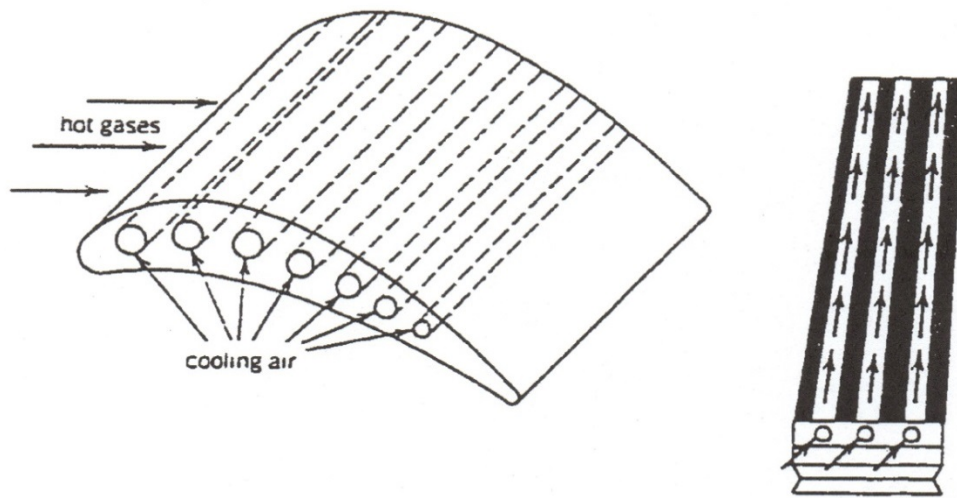


Figure 1.17 Turbine Blade Convection Cooling [12]

However, the narrow air passages typically become obstructed over time and the flow rate of the cooling air becomes reduced, this is most prevalent at the blade trailing edge. Consequently, the cooling influence at the trailing edge will be reduced, and the temperature at the trailing edge will become considerably greater than that of other regions in the turbine blade.

Another possible technique for turbine blade cooling is the use of heat pipes [13], which can possibly provide an effective means of cooling or redistributing the high heat fluxes. Since heat pipes have an operational characteristic of high thermal conductance, and the

ability to create an isothermal surface of low thermal impedance, they can be utilized in the turbine blades and disks as a cooling device, as depicted in Figure 1.18.

### Radially Rotating Heat Pipes

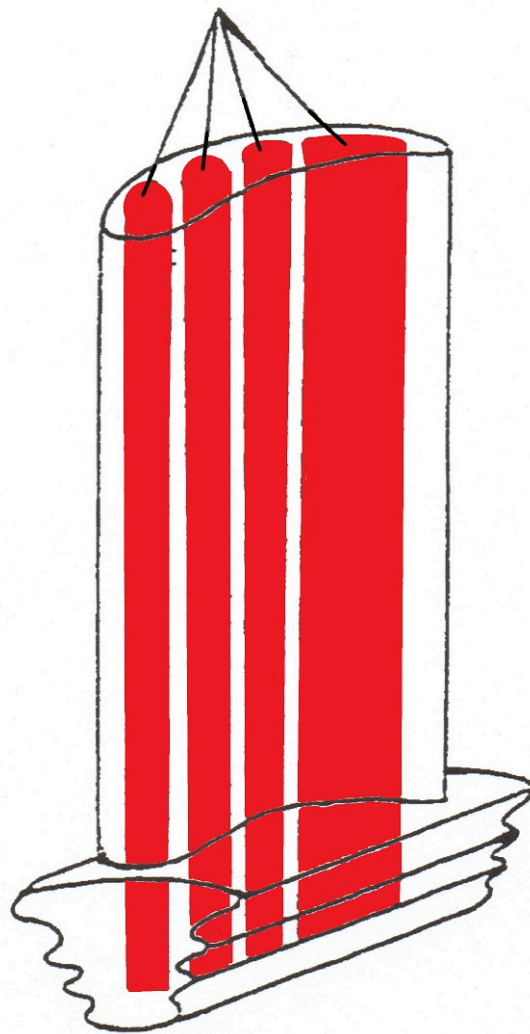


Figure 1.18 Depiction of Radially Rotating Heat Pipes being Utilized in a Turbine Blade

### **1.3 Application of Radially Rotating Miniature Heat Pipes to the Turbine Blade and Disk**

To have better thermal efficiency and the ability to operate at higher combustion temperatures, turbine blade and disk cooling is vital. Although air cooling techniques are effective and convenient, the coolant flow in the turbine blades and disk affects the thermodynamic and aerodynamic performance of the turbine. Concurrently, air cooling is accompanied by other difficulties.

- A. Air cooling techniques requires approximately 2% of the total air flow from the compressor to cool the high temperature components, which results in a decrease in the over-all efficiency of the turbine.
- B. Due to the narrow space of the turbine blade trailing edge, flow resistance of the cooling air increases, and the flow rate of cooling air reduces in the blade trailing edge, causing the temperature gradient over the cross-sectional area of the blade to increase.
- C. Air cooling usefulness, in the turbine blade tip, is reduced as its temperature increases, creating a general temperature rise of the entire turbine blade and thus resulting in a significant temperature gradient between the turbine blade base and tip.

A reduction of the temperature gradient in turbine blade and disk could be accomplished by combining the air cooling techniques stated previously with radially rotating miniature heat pipes. This could be done by installing a radially rotating miniature heat pipe in the blade trailing edge, as shown in Figure 1.19.



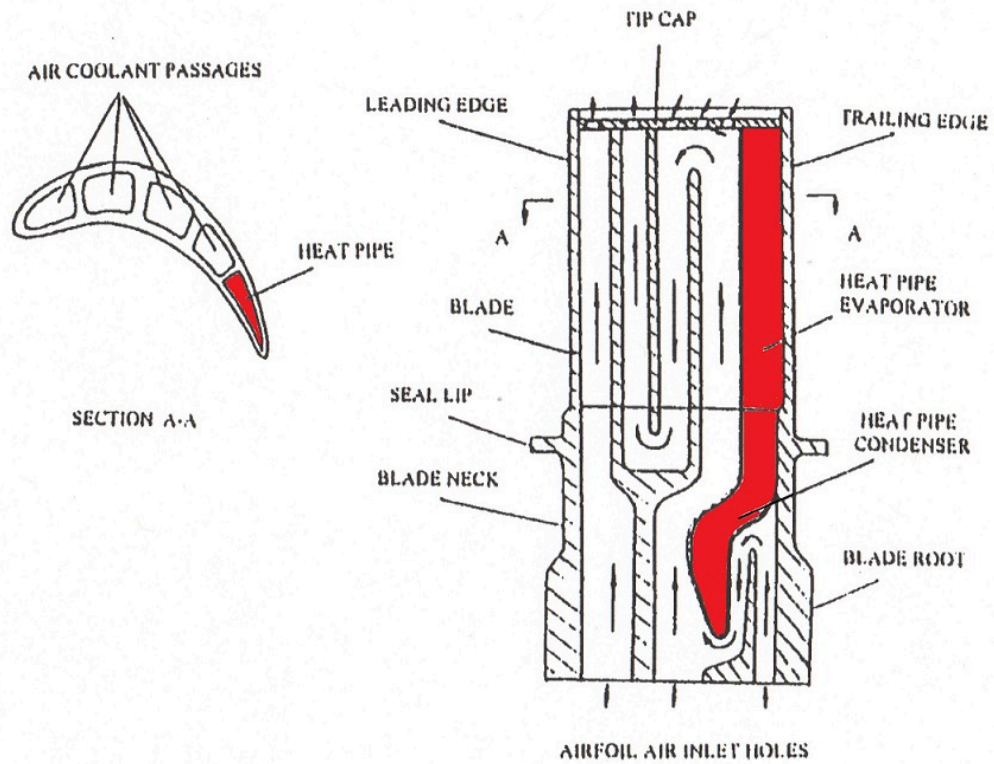


Figure 1.19 Depiction of Heat Pipe Utilization with Air Cooling in Turbine Blade [13]

The radially rotating heat pipe is a wickless heat pipe that consists of a certain amount of working fluid vacuum-packed within the container, as depicted in Figure 1.20.

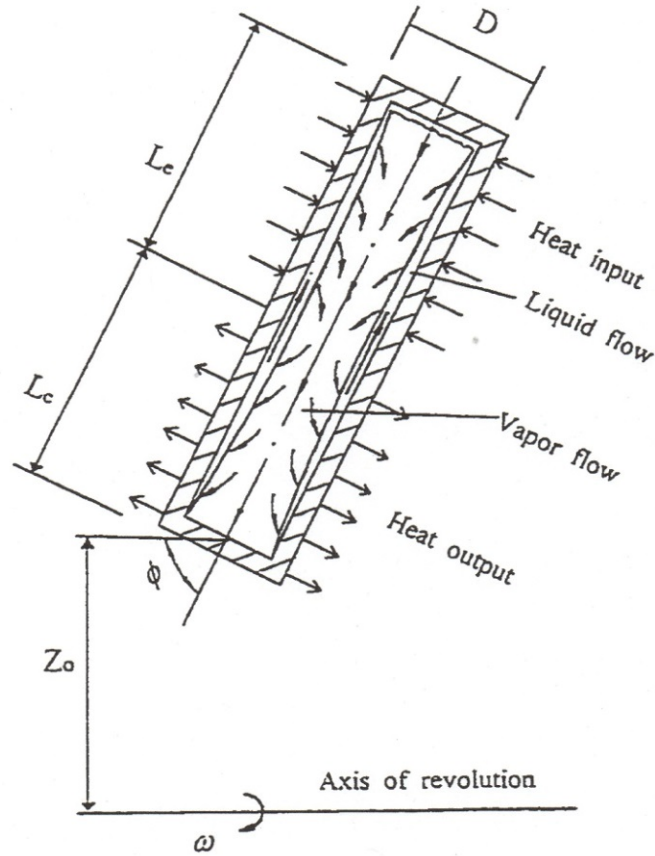


Figure 1.20 Depiction of a Radially Rotating Heat Pipe with a Tilt Angle [14]

The liquid condensate from the condenser is returned to the evaporator by utilizing the centripetal force generated by the rotating motion of the heat pipe. The thermal energy in the turbine blades would be transferred from the evaporator section to the condenser section, where the energy would then be dissipated by the cooling air convection. Due to the high thermal conductance of the radially rotating miniature heat pipe, the temperature gradients over the cross-sectional areas of the blade and between the blade base and tip would be greatly reduced utilizing the cooling technique.

In addition to the high-temperature working condition of a turbine blade, the upper portion of a turbine disk would operate at higher temperatures due to the turbine blades

being directly attached to the disk rim. Therefore, utilizing the radially rotating heat pipes in the disk would similarly enhance the cooling abilities of the turbine blades, as shown in Figure 1.21 [15].

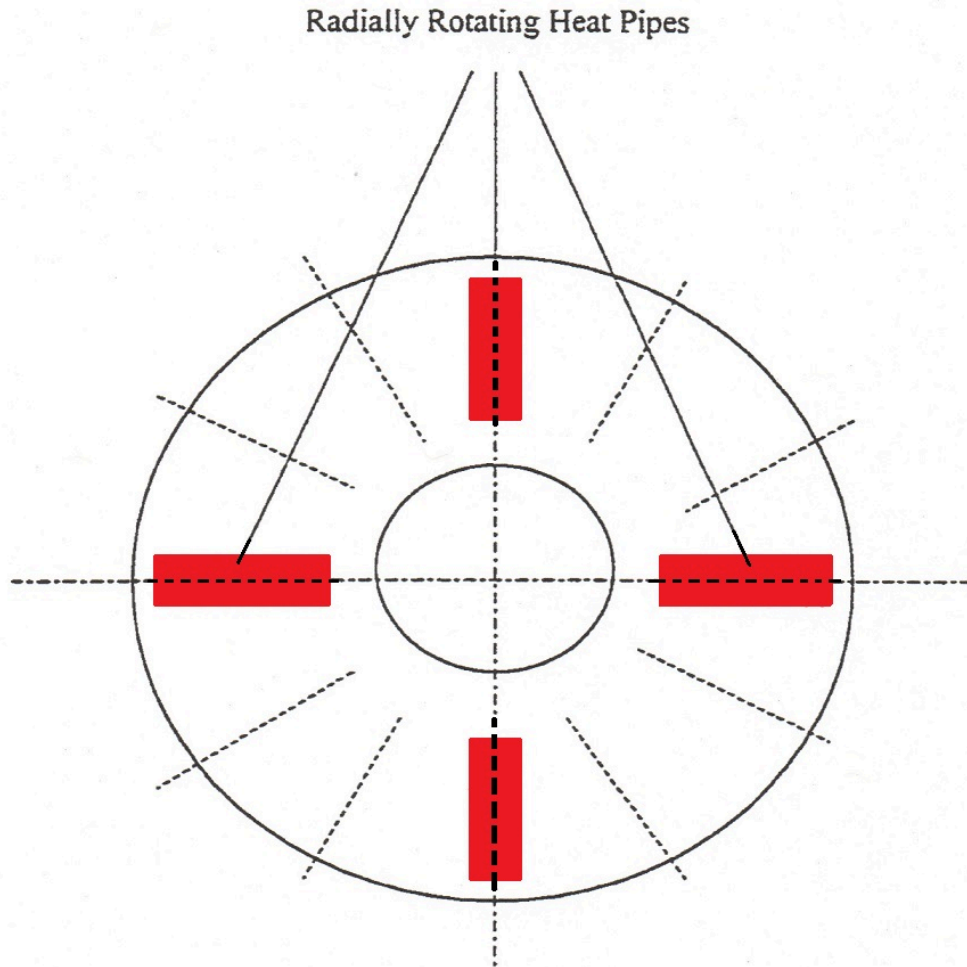


Figure 1.21 Depiction of a Possible Configuration for the use of Radially Rotating Heat Pipes Cooling for a Turbine Disk

#### **1.4 Objectives of this Study**

Radially rotating miniature heat pipes could become a significant part of the turbine blade and disk cooling techniques. In addition, the heat transfer phenomena and the two-phase flow in radially rotating miniature heat pipes is very complex. To date, in-depth studies regarding the heat transfer mechanisms in this new heat pipe are insufficient and the fluid flow situations inside the heat pipe, as well as the design criteria, are not entirely comprehended. Also, the use of discrete heat pipes may increase the cost of the turbine blade or disk because of the large number of heat pipes involved.

Therefore, the objectives of this Ph.D. dissertation are as follows:

- I. Design and fabricate two sector heat pipes each with four interconnected heat pipe branches.
- II. Identify the performance characteristics of the heat pipe under low- and high-temperature and rotating conditions, and validate the reliability of the heat pipe as well the compatibility of the working fluid with the heat pipe shell.
- III. Experimentally study the fabricated specimens of interconnected heat pipes to determine the feasibility of the interconnected rotating heat pipe sharing a common reservoir.
- IV. Investigate the liquid distribution among the four interconnected heat pipe branches.

## 2. Analysis of the Performance of a Single Radially Rotating Miniature Heat Pipe Derived from a Sector of the Turbine Disk

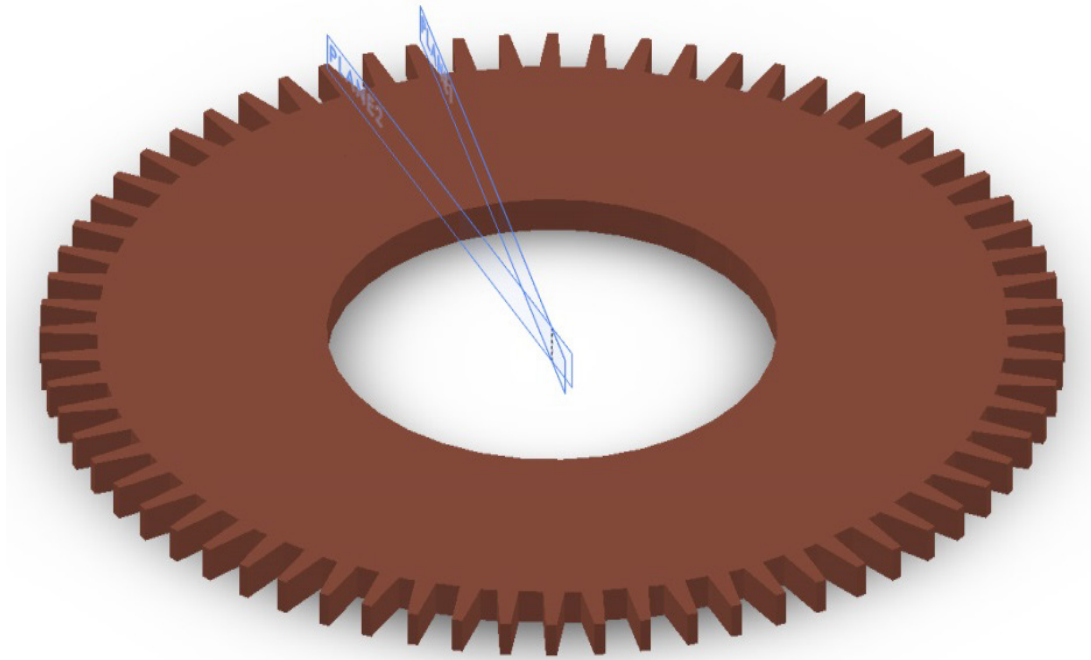


Figure 2.1 Representation of a Typical Turbine Disk

As can be seen from the figure above (Figure 2.1), a turbine disk with about 72 blades attached is rotationally symmetrical, which allows for a simplification of the sector heat pipe analysis. The simplification starts by dissecting the disk with two planes separated apart by  $10^\circ$  (or by  $5^\circ$  for a single dovetail), as shown in Figure 2.1, Figure 2.2, and Figure 2.3.

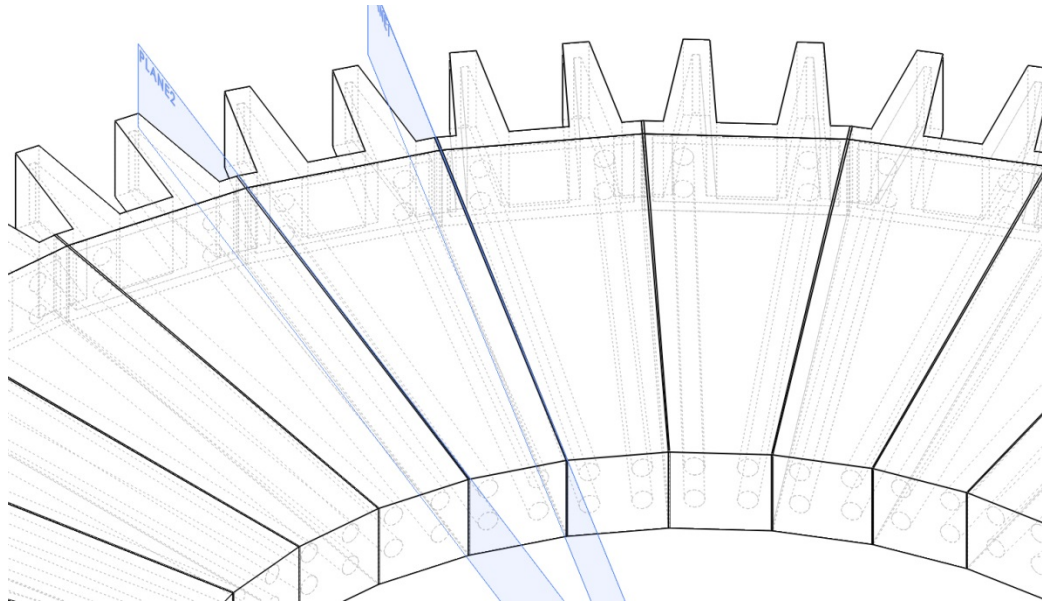


Figure 2.2 Hidden Line View of the Heat Pipes in a Turbine Disk

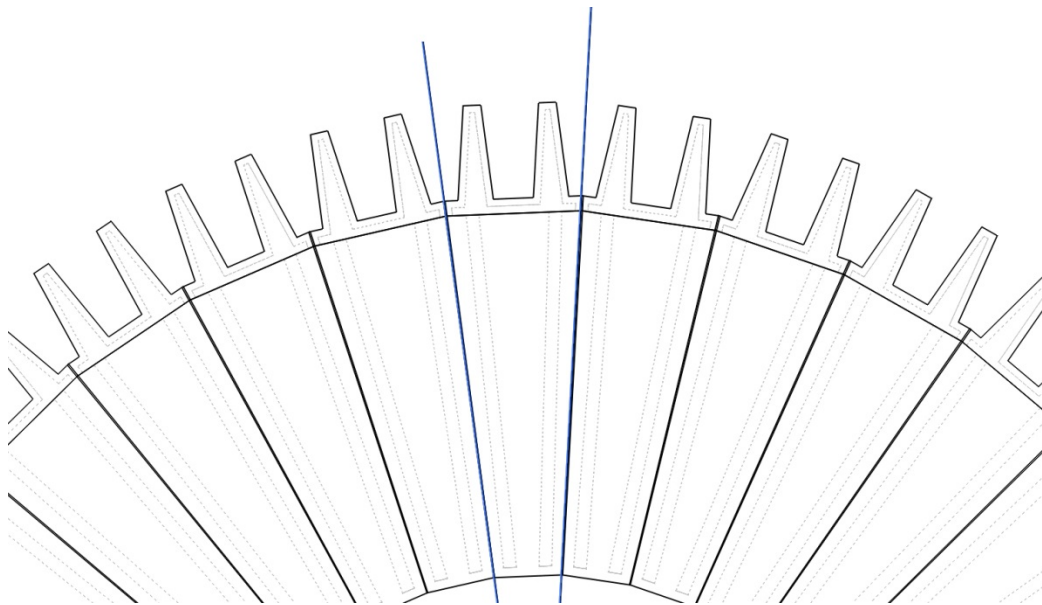


Figure 2.3 Turbine Disk Enlarged View

Once this is done, it can be seen from Figure 2.2 and Figure 2.3 that the sector heat pipe being studied is formed, with four lengthwise singular heat pipes connected with a common reservoir located in the dovetail section.

Further simplification can be accomplished with two perpendicular planes, cutting the sector heat pipe into quadrants. As shown in the figure below, Figure 2.4

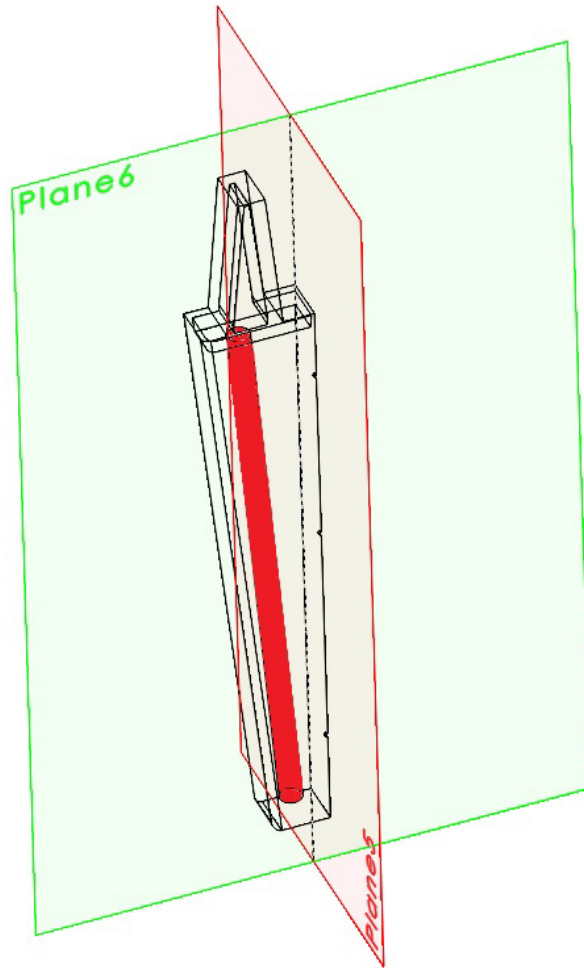


Figure 2.4 Dissected View of Sector Heat Pipe

After this dissection of the sector heat pipe is done, what is left is a single heat pipe, which will be the focus of the following analysis.

## 2.1 Analytical Solution for the Liquid Film Distribution in the Condenser Section of a Single Heat Pipe

As discussed in the previous chapter, a wickless radially rotating heat pipe operates by rotating about the axis of revolution and is comprised of an air-evacuated hollow container with an amount of working fluid sealed within the container. Before the sector heat pipe can be applied to the turbine disk the fundamental transport phenomena related to various heat transfer limitations must be fully understood. Figure 2.5 is a schematic that illustrates a single radially rotating heat pipe and its interior working conditions.

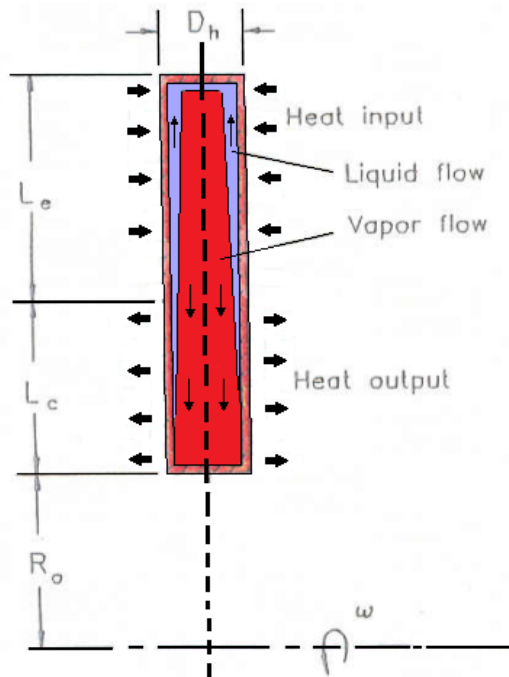


Figure 2.5 Depiction of a Radially Rotating Heat Pipe

Assumptions for the general thin-film condensation analysis are as follows:

1. The condensate is film-wise.
2. Liquid sub-cooling of the working fluid is negligible.



3. Convective effects of the working fluid are negligible.
4. The vapor space radius is much larger than the liquid film thickness.
5. Temperature gradients and circumferential velocity are negligible.
6. The vapor pressure is uniform over the cross-sectional area of the heat pipe.
7. In the presence of a large body force, the thermo-capillary flow effects are negligible.

However, since the size of the heat pipe in this study is very small, the curvature effect of the wall on the liquid film distribution is required in the calculation, therefore a cylindrical coordinate system will be employed in this study. For the analysis a cylindrical differential control volume in the liquid condensate film of a single radially rotating heat pipe is schematically shown in Figure 2.6 [13] [16] [17].

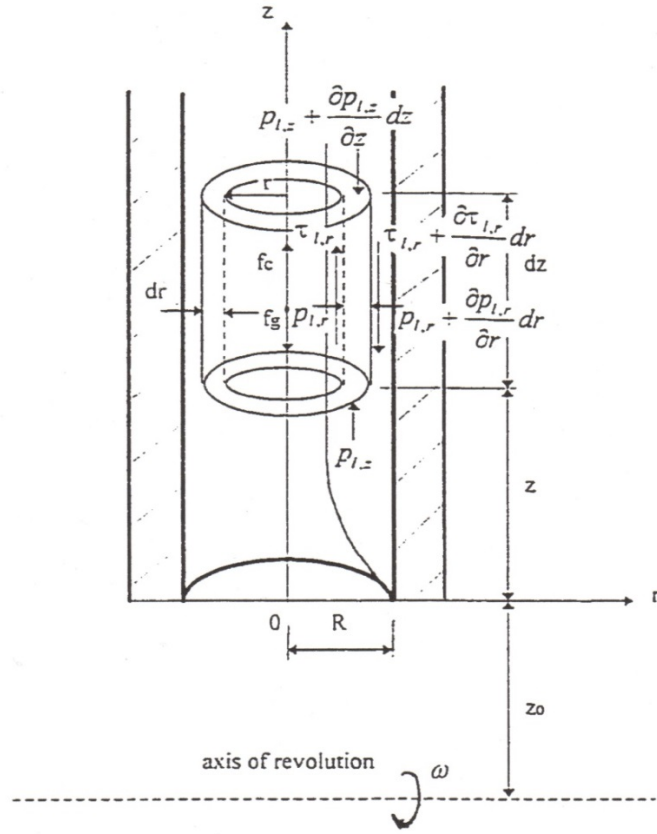


Figure 2.6 Depiction of a Differential Control Volume in the Condensate [16] [17]

In the schematic, the liquid centripetal force and gravitational force are [16] [17]

$f_c = 2\pi\rho_l\omega^2 Zdrdz$  and  $f_g = 2\pi\rho_l grdrdz \cos\theta$ , respectively. Equating all forces to

zero in  $z$  direction results in the following differential equation:

$$\begin{aligned}
 p_{l,z} 2\pi r dr - \left( p_{l,z} + \frac{\partial p_{l,z}}{\partial z} dz \right) 2\pi r dr + \tau_{l,r} 2\pi r dr dz - \left( \tau_{l,r} + \frac{\partial \tau_{l,r}}{\partial r} dr \right) (2\pi + dr) dz \\
 + \rho_l (\omega^2 Z - g \cos \theta) 2\pi r dr dz = 0
 \end{aligned} \tag{2.1}$$

where  $\theta$  is the rotating angle of the heat pipe and  $Z \approx z_0 + z$ , is the revolving radius of the control volume.

Since  $r \gg dr$  and  $2\pi r + dr \approx 2\pi r$ , Equation (2.1) can be simplified into

$$\frac{\partial \tau_{l,r}}{\partial r} + \frac{\partial p_{l,z}}{\partial z} - \rho_l (\omega^2 Z - g \cos \theta) = 0 \quad (2.2)$$

And when equating the force balance in  $r$  direction to zero, we have

$$p_{l,r} 2\pi r dz - \left( p_{l,r} + \frac{\partial p_{l,r}}{\partial r} dr \right) (2\pi r + dr) dz = 0 \quad (2.3)$$

The equation can be simplified by neglecting higher order infinitesimals,

$$\frac{\partial p_{l,r}}{\partial r} = 0 \quad (2.4)$$

After simplifying Equation (2.4) it is shown that the pressure of the liquid film is a function of  $z$  only. By considering the momentum equations in both the  $z$  and  $r$  directions, the shear stress and pressure at the liquid film surface can be studied by using the interface control volume shown in Figure 2.7.

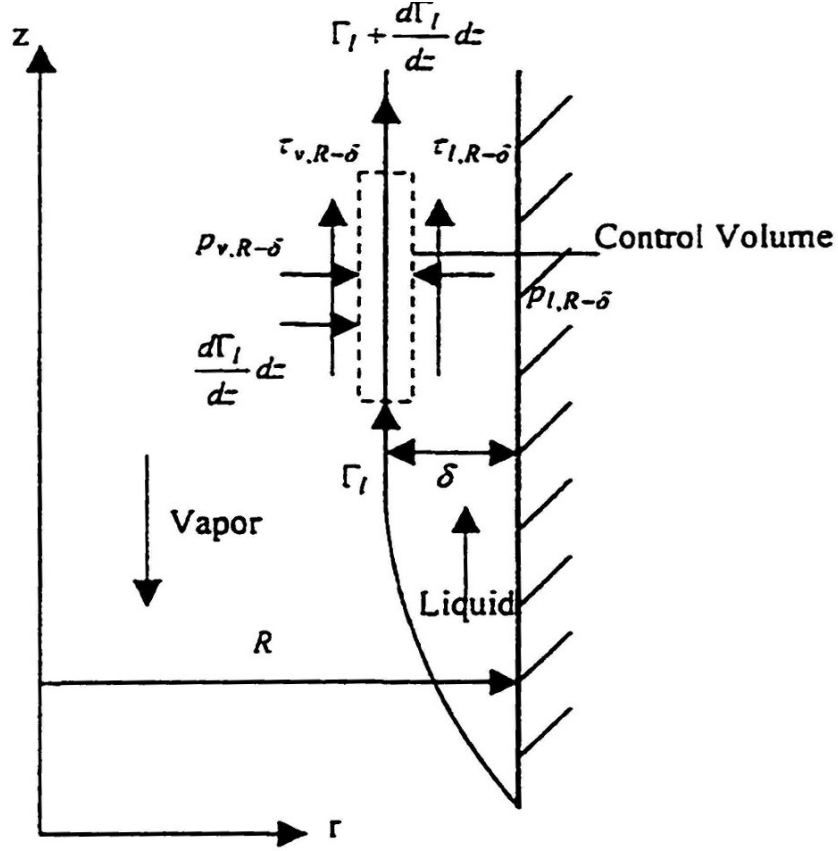


Figure 2.7 Depiction of a Control Volume at the Liquid-Vapor Interface [16] [17]

Then the following equations are obtained

$$\tau_{l,R-\delta} 2\pi r dz = -\tau_{v,R-\delta} 2\pi r dz - (\bar{w}_v + w_{l,R-\delta}) \frac{d\Gamma_l}{dz} 2\pi r dz \quad (2.5)$$

$$p_{v,R-\delta} 2\pi r dz - p_{l,R-\delta} (2\pi r + dr) dz + (\bar{w}_v + w_{l,R-\delta}) \frac{d\Gamma_l}{dz} 2\pi r dz = 0 \quad (2.6)$$

Where  $\tau_{l,R-\delta}$  and  $\tau_{v,R-\delta}$  are the shear stresses of the liquid film and the vapor at the liquid-vapor interface due to the counter-current liquid and vapor flows.  $\bar{w}_v$  is the average vapor velocity and  $w_{l,R-\delta}$  is the liquid velocity at the liquid film surface.  $\Gamma_l$  is the liquid mass flow rate per unit circumferential length and  $\delta$  is the thickness of the thin liquid film, as shown in Figure 2.7.

Realizing that  $\frac{d\Gamma_l}{dz}$  is very small and can be ignored, Equations (2.5) and (2.6) can be simplified as follows:

$$\tau_{l,R-\delta} = -\tau_{v,R-\delta} \quad (2.7)$$

$$P_{l,R-\delta} = P_{v,R-\delta} \quad (2.8)$$

Due to the very small cross-sectional area of the miniature heat pipe, it can be assumed that the vapor pressure over the cross section is uniformed. And with Equations (2.4) and (2.8) we get,

$$p_l(z) = p_v(z) \quad (2.9)$$

Equation (2.9) shows that the pressures of the vapor and liquid in the  $r$  direction, in the condenser section, are equal, and vary only in  $z$  direction. Therefore, Equation (2.2) can be simplified as:

$$\frac{\partial \tau_{l,r}}{\partial r} + \frac{dp_v}{dz} - \rho_l(\omega^2 Z - g \cos \theta) = 0 \quad (2.10)$$

The boundary equations for Equation (2.10) are

$$w_l = 0 \quad \text{at } r = R \quad (2.11)$$

$$\mu_l \frac{\partial w_l}{\partial r} = -\tau_{l,R-\delta} = \tau_{v,R-\delta} \quad \text{at } r = R - \delta \quad (2.12)$$

Integrating Equation (2.10) in the  $r$  direction yields the following equation:

$$-\tau_{l,r} = \frac{dp_v}{dz} r - \rho_l(\omega^2 Z - g \cos \theta)r + c_l \quad (2.13)$$

And for a Newtonian fluid, this equation becomes

$$\tau_{l,r} = -\mu_l \frac{dw_l}{dr} \quad (2.14)$$

Substituting Equation (2.14) into Equation (2.13) and integrating it in the  $r$  direction yields

$$w_l = \frac{1}{\mu_l} \left[ \frac{dp_v}{dz} - \rho_l (\omega^2 Z - g \cos \theta) \right] \frac{r^2}{2} + \frac{c_1}{\mu_l} r + c_2 \quad (2.15)$$

After applying the boundary conditions (2.11) and (2.12), we have

$$w_l = \frac{1}{\mu_l} \left[ \frac{1}{2} (R^2 - r^2) - (R - r)(R - \delta) \right] \left[ \rho_l (\omega^2 Z - g \cos \theta) - \frac{dp_v}{dz} \right] - \frac{1}{\mu_l} \tau_{v,R-\delta} (R - r) \quad (2.16)$$

Once the velocity distribution is determined, the liquid mass flow rate per unit circumferential length,  $\Gamma_l$ , can be evaluated through the following integral:

$$\Gamma_l = \frac{\dot{m}_l}{\pi D} = \frac{1}{2\pi R} \int_{R-\delta}^R \rho_l w_l 2\pi r dr \quad (2.17)$$

For a radially rotating miniature heat pipe with a high rotational speed, the liquid film thickness,  $\delta$ , is much smaller than the heat pipe radius,  $R$ . Therefore,  $r$  and  $R$  can be considered equal and can be negated in Equation (2.17). Then, by substituting Equation (2.16) into Equation (2.17) and integrating will yield

$$\Gamma_l \approx \frac{\rho_l}{\mu_l} \left[ \rho_l (\omega^2 Z - g \cos \theta) - \frac{dp_v}{dz} \right] \frac{\delta^3}{3} - \frac{\rho_l}{\mu_l} \tau_{v,R-\delta} \frac{\delta^2}{2} \quad (2.18)$$

Based on the energy balance, and by neglecting the change in sensible heat, the following relation can be used to evaluate the mass flow rate.

$$\Gamma_l = \int_0^z \frac{q_c''}{h_{fg}} dz = \frac{\bar{q}_c''}{h_{fg}} z \quad (2.19)$$

Where  $q_c$  is the heat flux and  $\bar{q}_c''$  is the average heat flux in the condenser section. By substituting Equation (2.19) into Equation (2.18), a solution for the liquid film thickness is obtained

$$-\frac{\rho_l h_{fg}}{3\mu_l \bar{q}_c'' z} \left[ \rho_l (\omega^2 Z - g \cos \theta) - \frac{dp_v}{dz} \right] \delta^3 + \frac{\rho_l h_{fg} \tau_{v,R-\delta}}{2\mu_l \bar{q}_c'' z} \delta^2 + 1 = 0 \quad (2.20)$$

After using Equation (2.20) to evaluate the liquid film thickness, the temperature drop,  $\Delta T_l$ , across the liquid film can be calculated by

$$\Delta T_l = \frac{R \bar{q}_c'' \ln \frac{R}{R-\delta}}{k_l} \cong \frac{\bar{q}_c'' \delta}{k_l} \quad (2.21)$$

The local Nusselt number,  $Nu_z$ , and local heat transfer coefficient,  $h_z$ , in the condenser section are defined, respectively by,

$$Nu_z = \frac{h_z z}{k_l} \cong \frac{z}{\delta} \quad (2.22)$$

$$h_z = \frac{\bar{q}_c''}{\Delta T_l} \cong \frac{k_l}{\delta} \quad (2.23)$$

Where  $k_l$ , in Equations (2.22) and (2.23), is the heat conductivity of the liquid film.

## 2.2 General Solution of the Liquid Film Distribution in the Condenser Section with Consideration of the Tilt Angle

The basic assumptions established in section 2.1 for the mathematical model continue to apply here [16] [17]. Typically, the tilt angle,  $\phi$ , of a single heat pipe should be close to  $90^\circ$ , as shown in Figure 2.8.

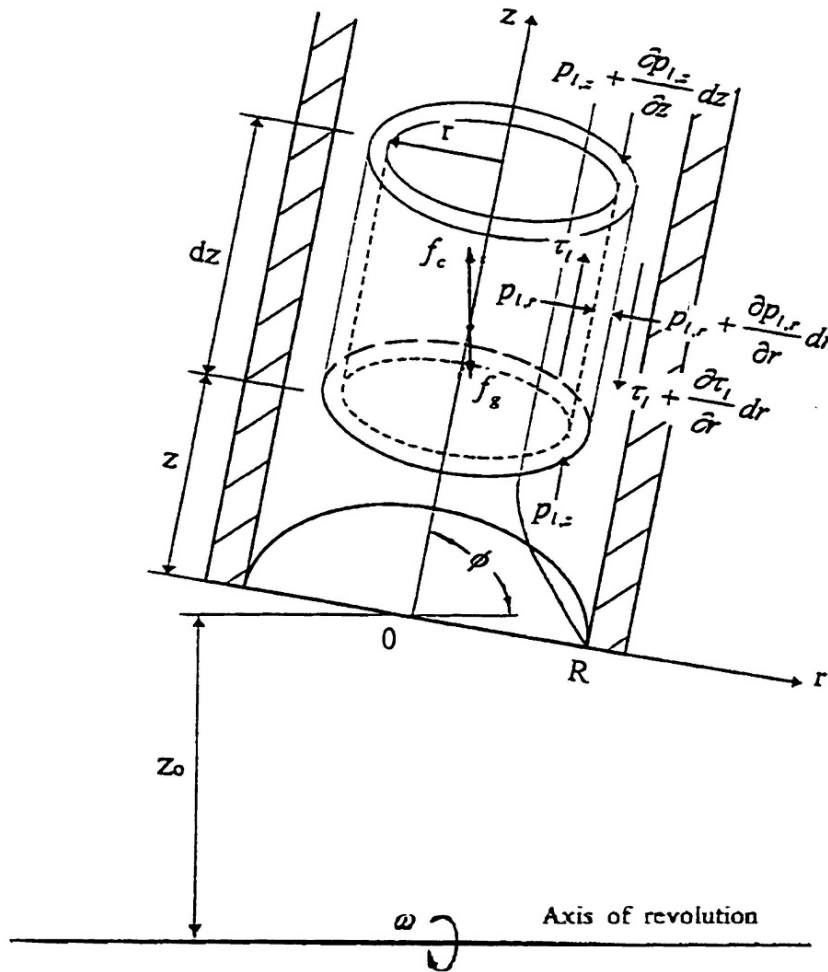


Figure 2.8 Representation of a Differential Control Volume in the Condensate Film [16] [17]



Equating forces to zero in the  $z$  direction gives

$$p_l 2\pi r dr - \left( p_l + \frac{\partial p_l}{\partial z} dz \right) 2\pi r dr + \tau_l 2\pi r dz - 2\pi (r + dr) dz \left( \tau_l + \frac{\partial \tau_l}{\partial r} dr \right) + \rho_l (\omega^2 \bar{Z} - g \cos \theta) \sin(\phi) 2\pi r dr dz = 0 \quad (2.24)$$

Where,  $z_0$  is the revolving radius of the coordinate origin and  $\bar{Z} = z_0 + z \sin \phi$  is the revolving radius of the control volume.

Noting that  $r \gg dr$ ,

$$2\pi (r + dr) dz = 2\pi r dz + 2\pi r dr dz \approx 2\pi r dz \quad (2.25)$$

Inserting Equation (2.25) in Equation (2.24) yields

$$p_l 2\pi r dr - \left( p_l + \frac{\partial p_l}{\partial z} dz \right) 2\pi r dr + \tau_l 2\pi r dz - 2\pi r dz \left( \tau_l + \frac{\partial \tau_l}{\partial r} dr \right) + \rho_l (\omega^2 \bar{Z} - g \cos \theta) \sin(\phi) 2\pi r dr dz = 0 \quad (2.26)$$

Simplifying Equation (2.26) and rearranging, gives

$$\frac{\partial \tau_l}{\partial r} = -\frac{\partial p_l}{\partial z} + \rho_l (\omega^2 \bar{Z} - g \cos \theta) \sin \phi \quad (2.27)$$

Equating forces to zero in the  $r$  direction would give

$$p_l 2\pi r dz - \left( p_l + \frac{\partial p_l}{\partial r} dr \right) 2\pi (r + dr) dz - \rho_l (\omega^2 \bar{Z} - g \cos \theta) \cos(\phi) 2\pi r dr dz = 0 \quad (2.28)$$

Equation (2.28) can be simplified and rearranged to give

$$\frac{\partial p_l}{\partial r} = -\rho_l (\omega^2 \bar{Z} - g \cos \theta) \cos \phi \quad (2.29)$$

Integrating Equation (2.29) from  $r$  to  $R - \delta$  gives

$$p_{l,R-\delta} - p_l = -\rho_l (\omega^2 \bar{Z} - g \cos \theta) \cos(\phi) (r - R + \delta) \quad (2.30)$$

Hence

$$p_l = p_{l,R-\delta} + \rho_l (\omega^2 \bar{Z} - g \cos \theta) \cos \phi (r - R + \delta) \quad (2.31)$$

Differentiating Equation (2.31) with respect to  $z$  yields

$$\frac{\partial p_l}{\partial z} = \frac{\partial p_{l,R-\delta}}{\partial z} + \rho_l \omega^2 \sin(\phi) \cos(\phi) (r - R + \delta) + \rho_l (\omega^2 \bar{Z} - g \cos \theta) \cos(\phi) \frac{d\delta}{dz} \quad (2.32)$$

It can be assumed that the liquid pressure at the liquid-vapor interface is equal to the vapor pressure, which yields

$$p_{l,R-\delta} = p_v \quad (2.33)$$

Substituting Equation (2.33) into Equation (2.32) provides

$$\frac{\partial p_l}{\partial z} = \frac{\partial p_v}{\partial z} + \rho_l \omega^2 \sin(\phi) \cos(\phi) (r - R + \delta) + \rho_l (\omega^2 \bar{Z} - g \cos \theta) \cos(\phi) \frac{d\delta}{dz} \quad (2.34)$$

Inserting Equation (2.34) into Equation (2.27), we have

$$\begin{aligned} \frac{\partial \tau_l}{\partial r} = & -\frac{\partial p_v}{\partial z} - \rho_l \omega^2 \sin(\phi) \cos(\phi) (r - R + \delta) \\ & + \rho_l (\omega^2 \bar{Z} - g \cos \theta) \left( \sin \phi - \cos(\phi) \frac{d\delta}{dz} \right) \end{aligned} \quad (2.35)$$

Considering that  $\frac{d\delta}{dz}$  is very small,

$$\sin \phi - \cos(\phi) \frac{d\delta}{dz} \approx \sin \phi \quad (2.36)$$

Substituting Equation (2.36) into Equation (2.35) and integrating gives

$$\begin{aligned} \tau_l = & \left[ -\frac{\partial p_v}{\partial z} r + \rho_l (\omega^2 \bar{Z} - g \cos \theta) \sin \phi \right] r \\ & - \rho_l \omega^2 \sin(\phi) \cos(\phi) \left[ \frac{r^2}{2} - (R - \delta) r \right] + c_1 \end{aligned} \quad (2.37)$$

Noting that,  $\tau_l = -\mu_l \frac{dw_l}{dr}$ , and replacing  $\tau_l$  with this relation in Equation (2.37) and

integrating, will yield

$$w_l = \frac{1}{2\mu_l} \left[ \frac{\partial p_v}{\partial z} - \rho_l (\omega^2 \bar{Z} - g \cos \theta) \sin \phi \right] r^2 + \frac{\rho_l}{\mu_l} \omega^2 \sin(\phi) \cos(\phi) \left[ \frac{r^3}{6} - \frac{1}{2} (R - \delta) r^2 \right] - \frac{c_1}{\mu_l} r + c_2 \quad (2.38)$$

The constants of integration in the above equation can be determined by using the following boundary conditions:

$$\tau_{l,R-\delta} = -\tau_{v,R-\delta} - (\bar{w}_v + w_{l,R-\delta}) \frac{d\Gamma_l}{dz} \quad \text{at } r = R - \delta \quad (2.39)$$

$$w_l = 0 \quad \text{at } r = R \quad (2.40)$$

Considering that  $\frac{d\Gamma_l}{dz}$  is very small and negligible, Equation (2.40) can be simplified to

$$\tau_{l,R-\delta} = -\tau_{v,R-\delta} \quad \text{at } r = R - \delta \quad (2.41)$$

Once the constants of integration in Equation (2.38) are determined by using the boundary conditions, the velocity of liquid in the  $z$  direction can be obtained

$$w_l = \frac{1}{\mu_l} \left[ \frac{\partial p_v}{\partial z} - \rho_l (\omega^2 \bar{Z} - g \cos \theta) \sin \phi \right] \left[ (R - \delta)(R - r) - \frac{1}{2} (R^2 - r^2) \right] - \frac{1}{\mu_l} \tau_{v,R-\delta} (R - r) - \frac{\rho_l}{\mu_l} \omega^2 \sin(\phi) \cos(\phi) \left[ \frac{1}{2} (R - \delta)^2 (R - r) - \frac{1}{2} (R - \delta)(R^2 - r^2) + \frac{1}{6} (R^3 - r^3) \right] \quad (2.42)$$

The liquid mass flow rate per unit circumferential length,  $\Gamma_l$ , is given by

$$\Gamma_l = \frac{\dot{m}_l}{\pi D} = \frac{1}{2\pi R} \int_{R-\delta}^R \rho_l w_l 2\pi r dr \quad (2.43)$$

This is expanded to give

$$= \frac{\rho_l}{\mu_l R} \left\{ \begin{array}{l} \left[ \frac{\partial p_v}{\partial z} - \rho_l (\omega^2 \bar{Z} - g \cos \theta) \sin \phi \right] \left( -\frac{1}{3} R \delta^3 + \frac{5}{24} \delta^4 \right) \\ -\tau_{v,R-\delta} \left( \frac{1}{2} R \delta^2 - \frac{1}{3} \delta^3 \right) \\ -\rho_l \omega^2 \sin(\phi) \cos(\phi) \left( \frac{1}{8} R \delta^4 - \frac{3}{40} \delta^5 \right) \end{array} \right\} \quad (2.44)$$

By use of the energy balance  $\Gamma_l$  can also be evaluated by the following relation

$$\Gamma_l = \int_0^z \frac{q_c''}{h_{fg}} dz = \frac{\bar{q}_c}{h_{fg}} z \quad (2.45)$$

Inserting Equation (2.45) into Equation (2.44) gives

$$\frac{\bar{q}_c'' z}{h_{fg}} = \frac{\rho_l}{\mu_l R} \left\{ \begin{array}{l} \left[ \frac{\partial p_v}{\partial z} - \rho_l (\omega^2 \bar{Z} - g \cos \theta) \sin \phi \right] \left( -\frac{1}{3} R \delta^3 + \frac{5}{24} \delta^4 \right) \\ -\tau_{v,R-\delta} \left( \frac{1}{2} R \delta^2 - \frac{1}{3} \delta^3 \right) \\ -\rho_l \omega^2 \sin(\phi) \cos(\phi) \left( \frac{1}{8} R \delta^4 - \frac{3}{40} \delta^5 \right) \end{array} \right\} \quad (2.46)$$

Rearranging Equation (2.46) gives the general solution for the liquid film thickness

$$\begin{aligned} & -\frac{3h_{fg}}{40\mu_l R \bar{q}_c'' z} \rho_l^2 \omega^2 \sin(\phi) \cos(\phi) \delta^5 + \frac{5h_{fg}\rho_l}{24\mu_l R \bar{q}_c'' z} \left[ \rho_l (\omega^2 \bar{Z} - g \cos \theta) \sin \phi - \frac{\partial p_v}{\partial z} \right] \delta^4 - \frac{h_{fg}\rho_l}{3\mu_l R \bar{q}_c'' z} \delta^3 \\ & + \frac{h_{fg}}{8\mu_l R \bar{q}_c'' z} \rho_l^2 \omega^2 \sin(\phi) \cos(\phi) \delta^4 - \frac{h_{fg}\rho_l}{3\mu_l \bar{q}_c'' z} \left[ \rho_l (\omega^2 \bar{Z} - g \cos \theta) \sin \phi - \frac{\partial p_v}{\partial z} \right] \delta^3 \\ & + \frac{h_{fg}\rho_l}{2\mu_l \bar{q}_c'' z} \tau_{v,R-\delta} \delta^2 + 1 = 0 \end{aligned} \quad (2.47)$$

It can be assumed that  $\delta \ll R$ , then by substituting  $r \cong R$  into Equation (2.44), it can be simplified as

$$\Gamma_l = \frac{\dot{m}_l}{\pi D} \cong \int_{R-\delta}^R \rho_l w_l dr$$

$$= \frac{\rho_l}{\mu_l} \left\{ \begin{array}{l} -\rho_l \omega^2 \sin(\phi) \cos(\phi) \frac{\delta^4}{8} \\ - \left[ \frac{\partial p_v}{\partial z} - \rho_l (\omega^2 \bar{Z} - g \cos \theta) \sin \phi \right] \frac{\delta^3}{3} \\ - \tau_{v,R-\delta} \frac{\delta^2}{2} \end{array} \right\} \quad (2.48)$$

Inserting Equation (2.45) into Equation (2.48) and reordering it, a simplified version of Equation (2.47) is obtained

$$\frac{h_{fg}}{8\mu_l \bar{q}_c'' z} \rho_l^2 \omega^2 \sin(\phi) \cos(\phi) \delta^4 - \frac{h_{fg} \rho_l}{3\mu_l \bar{q}_c'' z} \left[ \rho_l (\omega^2 \bar{Z} - g \cos \theta) \sin \phi - \frac{\partial p_v}{\partial z} \right] \delta^3$$

$$+ \frac{h_{fg} \rho_l}{2\mu_l \bar{q}_c'' z} \tau_{v,R-\delta} \delta^2 + 1 = 0 \quad (2.49)$$

Equation (2.49) is similar to the liquid film thickness over a plane geometry with a tilt angle [18], if  $R \gg \delta$ , then the cylindrical surface can be treated as a plane surface.

Hence, Equation (2.49) as well can be used for the calculation of liquid film thickness for a plane geometry with a tilt angle.

If the tilt angle,  $\phi$ , is fixed to  $90^\circ$ , then the equation for the liquid film thickness can be simplified further to give

$$- \frac{h_{fg} \rho_l}{3\mu_l \bar{q}_c'' z} \left[ \rho_l (\omega^2 \bar{Z} - g \cos \theta) \sin \phi - \frac{\partial p_v}{\partial z} \right] \delta^3 + \frac{h_{fg} \rho_l}{2\mu_l \bar{q}_c'' z} \tau_{v,R-\delta} \delta^2 + 1 = 0 \quad (2.50)$$

Equation (2.50) and Equation (2.20) are identical because they are the equation of the liquid film thickness for a cylindrical heat pipe with  $\phi = 90^\circ$ .

When comparing Equations (2.49) and (2.47), it is evident that Equation (2.49) can be obtained from Equation (2.47) if the first, second and third terms on the left-hand side of Equation (2.47) are dropped. Similarly, Equation (2.50) is obtained from Equation (2.49) with  $\phi = 90^\circ$ . These cases show that Equations (2.49), (2.20) and (2.50) are three special circumstances of Equation (2.47). By way of deduction, Equation (2.47) is the general relation for liquid film distributions in radially rotating heat pipes.

After the liquid film thickness,  $\delta$ , is determined from the equations for the liquid film thickness, the temperature drop across liquid film thickness is

$$\Delta T_l = T_\delta - T_p = \frac{R\bar{q}_c'' \ln \frac{R}{R-\delta}}{k_l} \quad (2.51)$$

If the temperature distribution of the liquid film is linear, then the temperature drop across the liquid film can be expressed as

$$\Delta T_l = T_\delta - T_p = \frac{\bar{q}_c'' \delta}{k_l} \quad (2.52)$$

The local Nusselt number,  $Nu_z$ , and local heat transfer coefficient,  $h_z$ , in the condenser section can be the same as Equations (2.22) and (2.23), respectively.

### **2.3 Axial Vapor Flow Analysis along the Single Heat Pipe Length**

In the preceding analytical solutions for the liquid film distributions on the single heat pipe wall, both the vapor pressure gradient along the heat pipe and the shear stress at the liquid vapor interface are present. To complete the analysis, solutions for the vapor flow within the cavity must be obtained [16] [17]. Additionally, the centripetal force may contribute to the vapor temperature drop along the heat pipe length and must be addressed. In some outlying circumstances, this temperature drop may present a heat transfer limitation for the performance of the single heat pipe and possibly the sector heat pipe. Consequently, it is necessary to obtain the temperature drop along the single heat pipe length. If a one-dimensional, laminar, and incompressible vapor flow along the heat pipe length under the steady-state operating condition is considered, as shown in Figure 2.9,

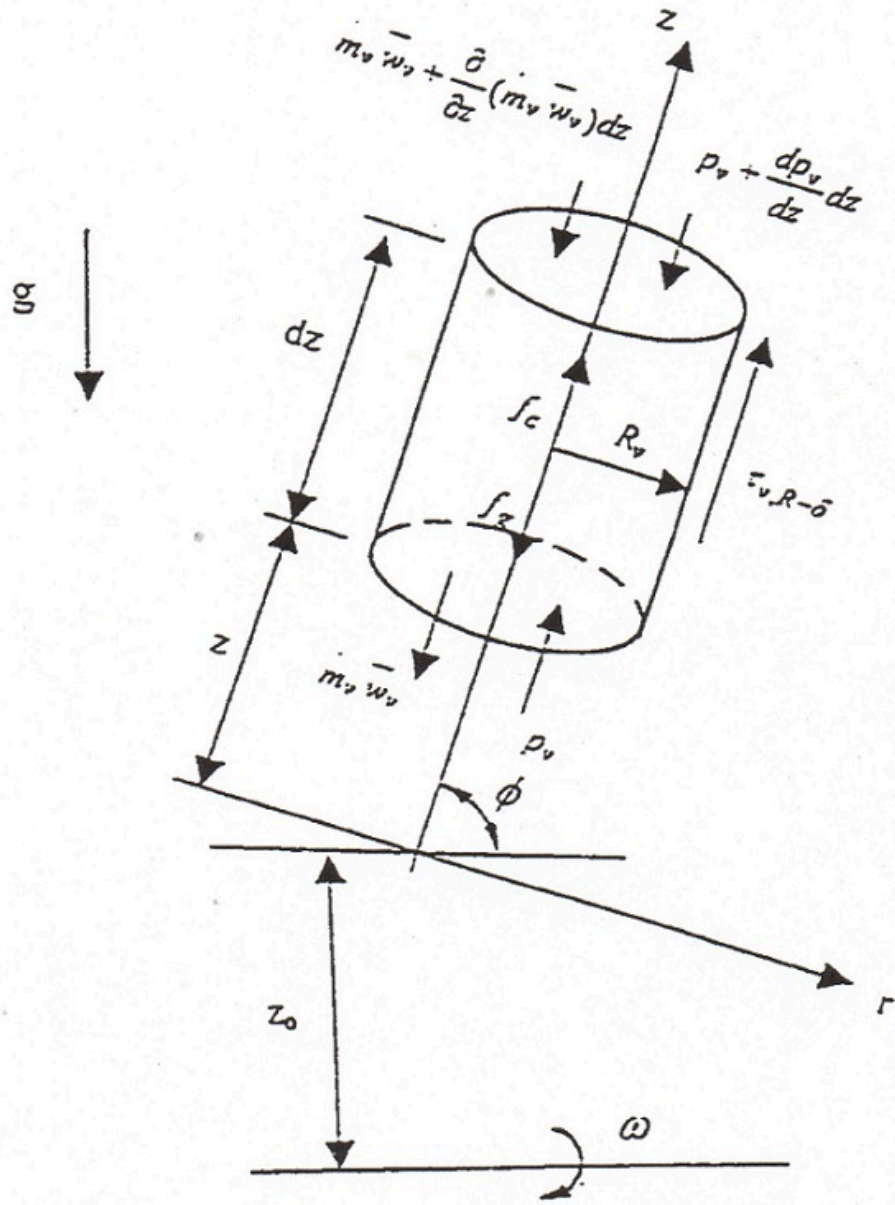


Figure 2.9 Representation of a Vapor Thermal Balance in the Condenser Section [16] [17]

where  $f_g = \rho_v g \pi R_v^2 \sin(\phi) \cos(\theta) dz$  is the gravitational force of the vapor, and  $f_c = \rho_v \omega^2 Z \pi R_v^2 \sin(\phi) dz$  is the centripetal force of the vapor. Then the momentum equation for the vapor flow is



$$\begin{aligned}
p_v \pi R_v^2 \sin \phi - \left( p_v + \frac{dp_v}{dz} dz \right) \pi R_v^2 \sin(\phi) + \tau_{v,R_v} 2\pi R_v dz + \rho_v (\omega^2 \bar{Z} - g \cos \theta) \pi R_v^2 \sin(\phi) dz \\
= \dot{m}_v \bar{w}_v - \left[ \dot{m}_v \bar{w}_v + \frac{d}{dz} (\dot{m}_v \bar{w}_v) dz \right]
\end{aligned} \tag{2.53}$$

Equation (2.53) can be simplified to give

$$\frac{dp_v}{dz} = \frac{2}{R_v \sin \phi} \tau_{v,R_v} + \rho_v (\omega^2 \bar{Z} - g \cos \theta) - \frac{d}{dz} (\dot{m}_v \bar{w}_v) \frac{1}{\pi R_v^2 \sin \phi} \tag{2.54}$$

Noting that the shear stress of the vapor flow is

$$\tau_{v,R_v} = \frac{1}{2} f \rho_v \bar{w}_v^2 = f \left( \frac{2 \bar{w}_v R_v \rho_v}{\mu_v} \right) \left( \frac{\mu_v}{2 \bar{w}_v R_v \rho_v} \right) \frac{1}{2} \rho_v \bar{w}_v^2 = (f \text{Re})_v \frac{\mu_v \bar{w}_v}{4 R_v} \tag{2.55}$$

Where  $\dot{m}_v$  is the vapor mass flow rate,  $\bar{w}_v$  is the average vapor velocity over the heat pipe cross-sectional area,  $f$  is the laminar vapor skin-friction coefficient, and  $R_v = R - \delta$  is the vapor space radius within the heat pipe.

By performing an overall thermal balance in the condenser section, as shown in Figure

2.10

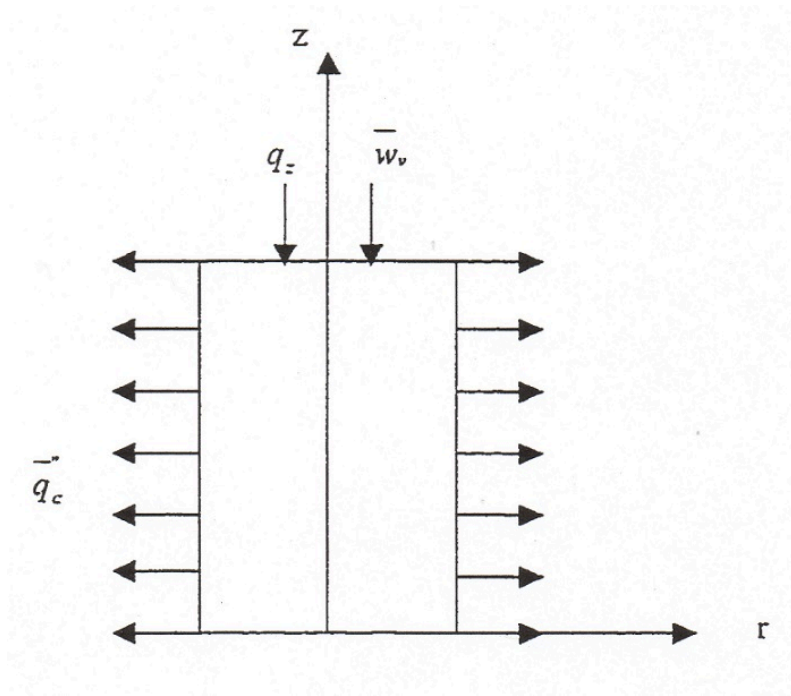


Figure 2.10 Representation of the Overall Thermal Balance in the Condenser Section [16] [17]

Will yield

$$\dot{m}_v = \frac{2\pi R_v \bar{q}_c'' z}{h_{fg}} = \pi R_v^2 \rho_v \bar{w}_v \quad (2.56)$$

Consequently,  $\bar{w}_v = \frac{2\bar{q}_c'' z}{R_v \rho_v h_{fg}}$ . And by substituting it into Equation (2.55) will yield

$$\tau_{v,R_v} = (f \text{Re})_v \frac{\mu_v \bar{q}_c'' z}{2R_v^2 \rho_v h_{fg}} \quad (2.57)$$

Noting that

$$\frac{d(\dot{m}_v \bar{w}_v)}{dz} = 2\pi R_v^2 \rho_v \bar{w}_v \frac{d\bar{w}_v}{dz} = \frac{8\pi \bar{q}_c''^2 z}{\rho_v h_{fg}^2} \quad (2.58)$$

After substituting Equations (2.57) and (2.58) into Equation (2.54), will yield

$$\frac{dp_v}{dz} = (f \text{ Re})_v \frac{\mu_l \bar{q}_c'' z}{R_v^3 \rho_v h_{fg} \sin \phi} + \rho_l (\omega^2 \bar{Z} - g \cos \theta) - \frac{8 \bar{q}_c''^2 z}{\rho_v R_v^2 h_{fg}^2 \sin \phi} \quad (2.59)$$

Generally, the above equations are valid when the following two conditions are satisfied, those being the vapor Mach number and Reynolds number:

$$M_v = \frac{Q}{A_v \rho_v h_{fg} \sqrt{\gamma_v R_g T_v}} \leq 0.3 \quad (2.60)$$

$$\text{Re}_v = \frac{2R_v Q}{A_v \mu_v h_{fg}} \leq 2300 \quad (2.61)$$

Where  $\gamma_v$  is the vapor specific heat ratio,  $R_g$  is the gas constant of the vapor, and  $A_v$  is the cross-sectional area of the vapor space [19]. These two conditions are typically satisfied for high-temperature single heat pipes having a small diameter and operating at steady-state.

Presuming that the heat fluxes along the evaporator (input) and the condenser (removal) are constant, the axial mass flow rate of vapor can be found by a mass and energy balance during steady-state conditions [2].

$$\dot{m}_v = \frac{q_z}{h_{fg}} = \begin{cases} \frac{Q_c z}{L_c h_{fg}} & 0 \leq z \leq L_c \\ \frac{Q_c}{h_{fg}} & L_c \leq z \leq L_c + L_a \\ \frac{L - z}{L - (L_c + L_a)} \frac{Q_c}{h_{fg}} & L_c + L_a \leq z \leq L \end{cases} \quad (2.62)$$

Where  $q_z$  is the axial heat transfer rate of the vapor within the cavity.

Substituting Equation (2.62) into Equation (2.56) and reordering it gives,

$$\bar{q}_c'' z = \frac{\dot{m}_v h_{fg}}{2\pi R_v} = \begin{cases} \frac{Q_c z}{2\pi R_v L_c} & 0 \leq z \leq L_c \\ \frac{Q_c}{L_c h_{fg}} \frac{h_{fg}}{2\pi R_v} & L_c \leq z \leq L_c + L_a \\ \frac{Q_c}{h_{fg}} \frac{h_{fg}}{2\pi R_v} \frac{L-z}{L-(L_c+L_a)h_{fg}} & L_c + L_a \leq z \leq L \end{cases} \quad (2.63)$$

Inserting Equation (2.63) into Equation (2.59) and integrating it along the heat pipe length (from 0 to  $L$ ), the vapor pressure drop along the single heat pipe is given by

$$\begin{aligned} \Delta p_v &= \int_0^L \frac{dp_v}{dz} dz \\ &= \frac{1}{\sin \phi} \int_0^L (f \operatorname{Re})_v \frac{\mu_v \bar{q}_c'' z}{R_v^3 \rho_v h_{fg}} dz + \int_0^L \rho_v (\omega^2 \bar{Z} - g \cos \theta) dz - \frac{1}{\sin \phi} \int_0^L \frac{8 \bar{q}_c''^2 z}{\rho_v R_v^2 h_{fg}^2} dz \end{aligned} \quad (2.64)$$

Subsequently, the vapor momentum is very small and can be negligible. Then the vapor pressure drop along the heat pipe can be simplified as

$$\begin{aligned} \Delta p_v &= \frac{1}{\sin \phi} F_v Q_c \left( \frac{L_c + 2L_a + L_e}{2} \right) + \rho_v \omega^2 L \left( z_0 + \frac{L}{2} \sin \phi \right) - \rho_v L g \cos \theta \\ &= \frac{1}{\sin \phi} F_v L_{eff} Q_c + \rho_v \omega^2 L \bar{Z}_a - \rho_v L g \cos \theta \end{aligned} \quad (2.65)$$

Where  $L$  is the single heat pipe length,  $L_{eff} = \frac{1}{2}(L_c + 2L_a + L_e)$  is the effective length of a

single heat pipe,  $F_v = \frac{(f \operatorname{Re})_v \mu_v}{2\pi R_v^4 \rho_v h_{fg}}$  is the vapor frictional coefficient,  $\bar{Z}_a = z_0 + \frac{1}{2} L \sin \phi$  is

the average revolving radius of the heat pipe, and  $Q_c = Q_e = \pi D L_c \bar{q}_c''$  is the total heat transfer rate at the condenser or evaporator section at steady-state.

As discussed earlier, the vapor Reynolds number is generally less than 2300. However, with an increase in the total heat flux,  $Q$ , the Mach number could become greater than 0.3 when the heat pipe operating temperature is relatively low. In this circumstance, the vapor compressibility should be taken into account. Fashioned upon the bulk fluid properties, the ratio of the drag coefficient for a compressible flow,  $f_{v,c}$ , to that of an incompressible flow,  $f_{v,i}$ , at the same vapor Reynolds number can be rectified by the following equation [19]:

$$\frac{f_{v,c}}{f_{v,i}} = \left(1 + \frac{\gamma_v - 1}{2} M_v^2\right)^{-\frac{1}{2}} \quad (2.66)$$

By inserting Equation (2.65) into the relation for the vapor frictional coefficient, a modified vapor friction coefficient is attained:

$$F_v = \frac{(f \text{ Re})_v \mu_v}{2\pi R_v^4 \rho_v h_{fg}} \left(1 + \frac{\gamma_v + 1}{2} M_v^2\right)^{-\frac{1}{2}} \quad (2.67)$$

It should be realized that the vapor pressure drop caused by gravity is very minor and can be neglected. Hence, the vapor pressure drop along a single heat pipe length becomes

$$\Delta p_v = \frac{F_v L_{eff}}{\sin \phi} Q_c + \rho_v \omega^2 L \bar{Z}_a \quad (2.68)$$

The Clapeyron equation that establishes a relation between the saturated temperature to the saturated pressure is

$$\Delta p_v = \frac{h_{fg} \rho_v}{T_v} \Delta T_v \quad (2.69)$$

Using this relation in Equation (2.68), the vapor temperature drop along the heat pipe length becomes

$$\Delta T_v = \frac{T_v}{h_{fg}\rho_v} \Delta p_v = \frac{T_v L_{eff} F_v}{\rho_v h_{fg} \sin \phi} Q_c + \frac{T_v}{h_{fg}} \omega^2 L \bar{Z}_a = \Delta T_{v,f} + \Delta T_{v,c} \quad (2.70)$$

Then changing to a dimensionless form, the temperature drop of the vapor along a single heat pipe length is given by

$$\frac{\Delta T_v}{T_v} = \frac{L_{eff} F_v}{\rho_v h_{fg} \sin \phi} Q_c + \frac{\omega^2 L \bar{Z}_a}{h_{fg}} = \frac{\Delta T_{v,f}}{T_v} + \frac{\Delta T_{v,c}}{T_v} = \Delta T_f + \Delta T_c \quad (2.71)$$

Where  $T_v$  is the operating temperature of a single heat pipe,  $\Delta T_v$  is the total vapor temperature drop along the heat pipe length,  $\Delta T_c$  is the dimensionless temperature drop due to the vapor centripetal force, and  $\Delta T_f$  is the dimensionless temperature drop due to friction at the liquid-vapor interface.

## 2.4 Analytical Results for the Heat Transfer Limitations and Temperature Drop in a Single Heat Pipe

The temperature decline across the liquid film or along the heat pipe length is a crucial criterion for designing radially rotating miniature heat pipes with high operating temperatures and rotational speeds. In order to justify the feasibility of the turbine disk cooling application, analytical results are exhibited for a single radially rotating miniature heat pipe working under high heat flux and high rotational speed conditions. The limits of geometric dimensions, heat fluxes, dimensionless centripetal force, and rotational speed are given in the table below, Table 2-1.

$1mm \leq d_i \leq 3mm$	$L = 80mm$
$40W \leq Q \leq 200W$	$L_c = L_e = 40mm$
$6.26 \leq \frac{\omega^2 \bar{Z}_a}{g} \leq 6.26 \times 10^5$	$L_a = 0$
$10Hz \leq f \leq 60Hz$	$\phi = 90^0$

Table 2-1 Parameters of Testing and Heat Pipes

It should be noted that these limits are only approximations to the turbine disk cooling conditions, and not to be confused with real-world design values [20]. It is evident from Equations (2.47) through (2.71) that the liquid film thickness, the temperature drop across the liquid film, and the vapor temperature drop along the heat pipe length are chiefly a function of shear stress, heat flux, liquid and vapor centripetal forces, liquid and vapor thermo-physical properties, heat pipe size, and the heat pipe operating temperature. Consequently, the functioning of a heat pipe depends on the heat load in the evaporator

and the cooling conditions in the condenser. Typically, the operating temperature,  $T_v$ , will increase if the flow rate of the cooling air is decreased or the heat input is increased. Figure 2.11 demonstrates the maximum temperature drops across the liquid film versus the dimensionless centripetal forces,  $\frac{\omega^2 \bar{Z}_a}{g}$ , with sodium as the working fluid.

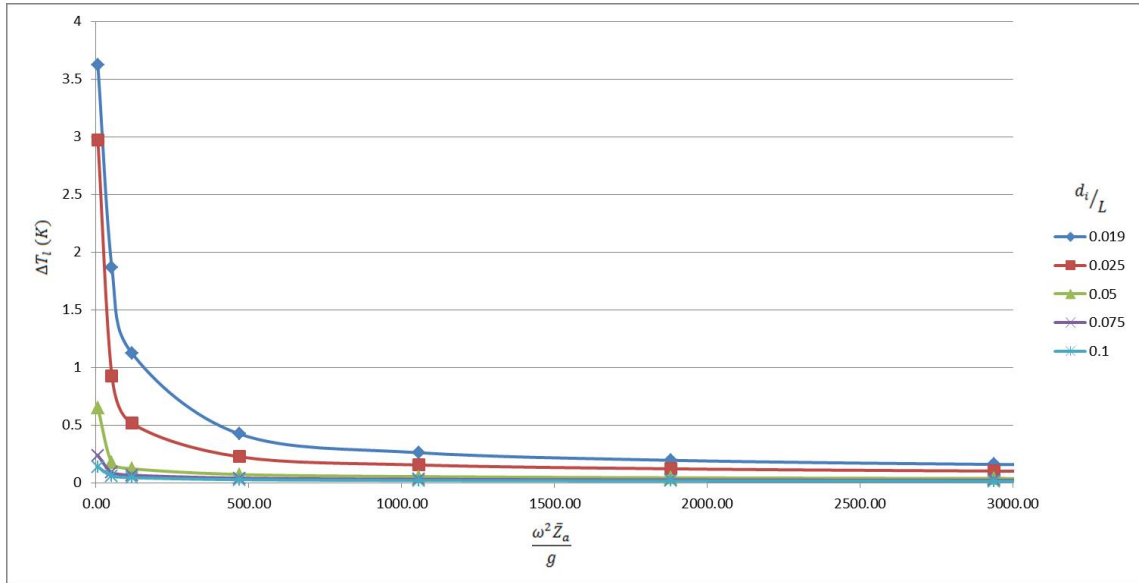


Figure 2.11 Maximum Temperature Decreases across the Liquid Film for Sodium as the Working Fluid ( $T_v = 1100K$ ,  $Q=200W$ )

The total heat input,  $Q$ , and the working temperature,  $T_v$ , are maintained constant at 200 W and 1100 K, respectively. The dimensionless geometric parameter,  $\frac{d_i}{L}$ , is handled as a variable. For the results exhibited in Figure 2.12,  $\frac{d_i}{L}$  is maintained constant, and the operating temperature is varied.



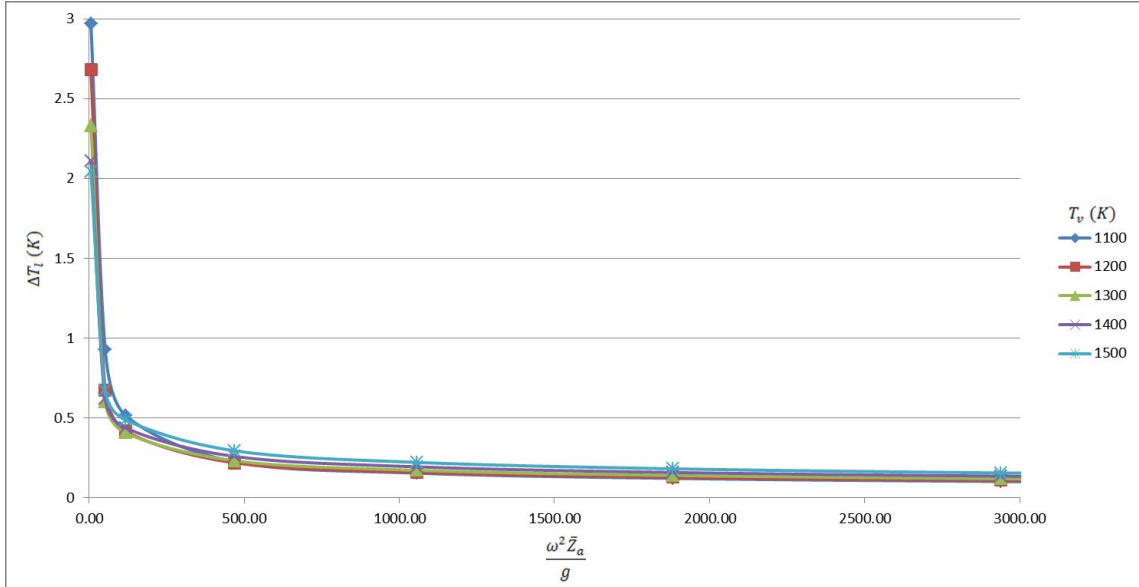


Figure 2.12 Maximum Temperature Decreases across the Liquid Film for Sodium as the Working Fluid ( $d_i/L = 0.025, Q = 200W$ )

It is perceived from Figure 2.11 and Figure 2.12 that at a relatively high rotational speed

or a large revolving radius  $\frac{\omega^2 \bar{Z}_a}{g} > 150$  creates the maximum temperature drop across

the liquid film to be negligible. Nonetheless, a low heat pipe operating temperature or a small heat pipe diameter may increase the temperature drop. However, under normal turbine working conditions, the maximum temperature drop is still much less than 1 K.

This necessitates that the normally encountered condenser limitation for a low temperature heat pipe would never be a significant problem for a high temperature heat pipe studied in this dissertation.

Calculations are then performed for the lengthwise vapor temperature drop of the heat pipe with sodium as the working fluid. Figure 2.13 depicts vapor temperature drop as a function of dimensionless centripetal forces at different operating temperatures.

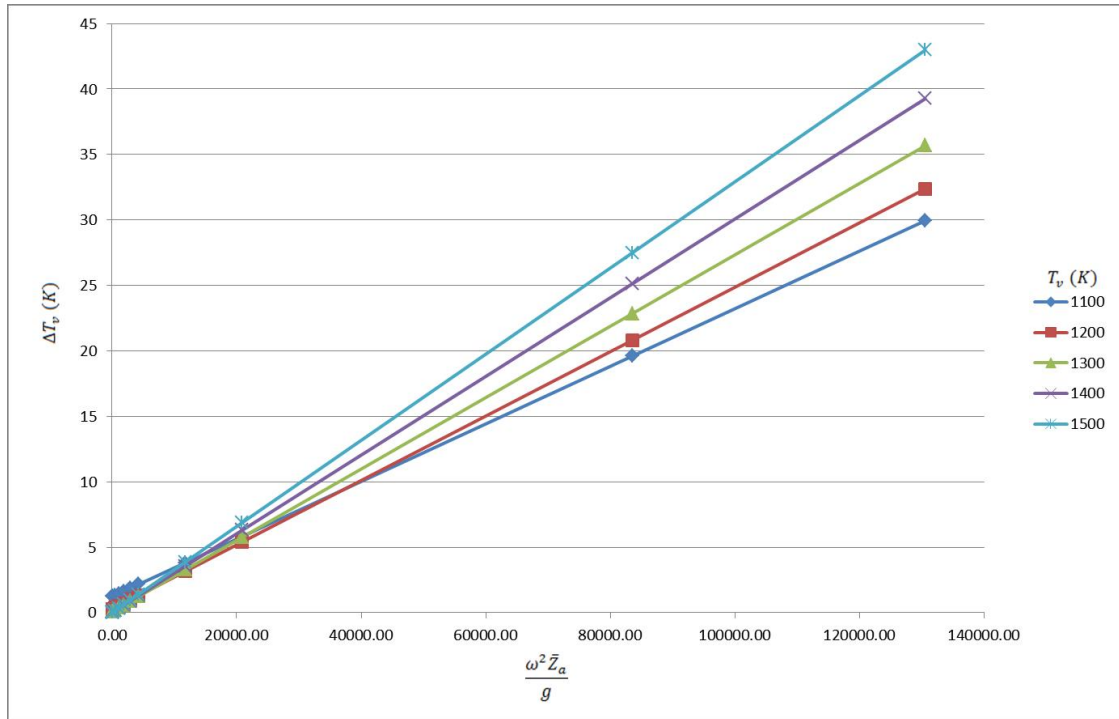


Figure 2.13 Lengthwise Vapor Temperature Drop of the Heat Pipe at Different Rotating Speeds  
 $(d_i/L = 0.025, Q = 200W)$

The total heat input and the dimensionless heat pipe geometric parameter are maintained constant ( $Q = 200W$  and  $\frac{d_i}{L} = 0.025$ ). It is evident from the figure that the vapor temperature drop increases with an increase in the operating temperature or in the centripetal force. For the high temperature heat pipes studied in this dissertation, this temperature drop is comparatively minor compared to the average heat pipe operating temperature.

The vapor temperature drop would increase slightly as the dimensionless heat pipe size is decreased, as shown in Figure 2.14.

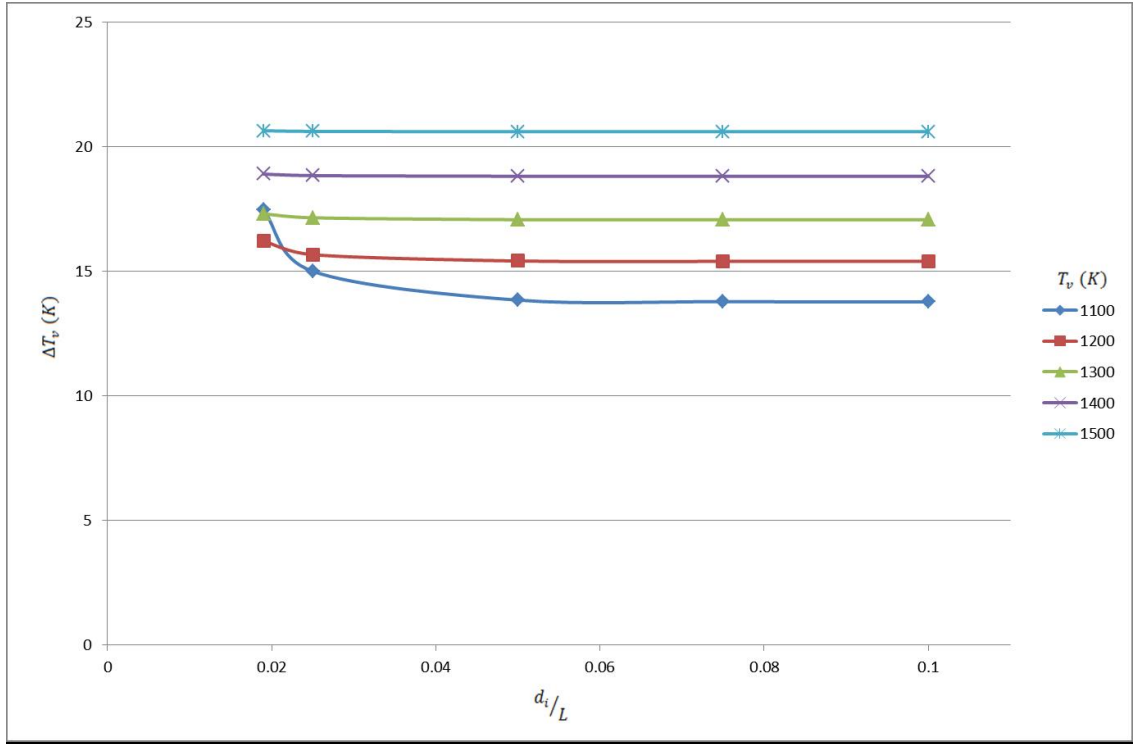


Figure 2.14 Lengthwise Vapor Temperature Drop of the Heat Pipe at Different Heat Pipe Dimensionless Sizes ( $Q = 200W$ ,  $\omega^2 \bar{Z}_a / g = 6.00 \times 10^4$ )

When the heat pipe diameter is decreased, at a specified operating temperature, the vapor temperature drop is increased due to higher friction at the liquid-vapor interface. It has been observed that when the operating temperature of the heat pipe is less than 1100 K, the vapor temperature drop for the miniature heat pipe with  $\frac{d_i}{L} = 0.0125$  will increase abruptly. Though, for a single heat pipe with a  $\frac{d_i}{L}$  greater than 0.02 or with  $d_i$  greater than 1.5 mm, the influence of the heat pipe size on the vapor temperature drop is comparatively minor.

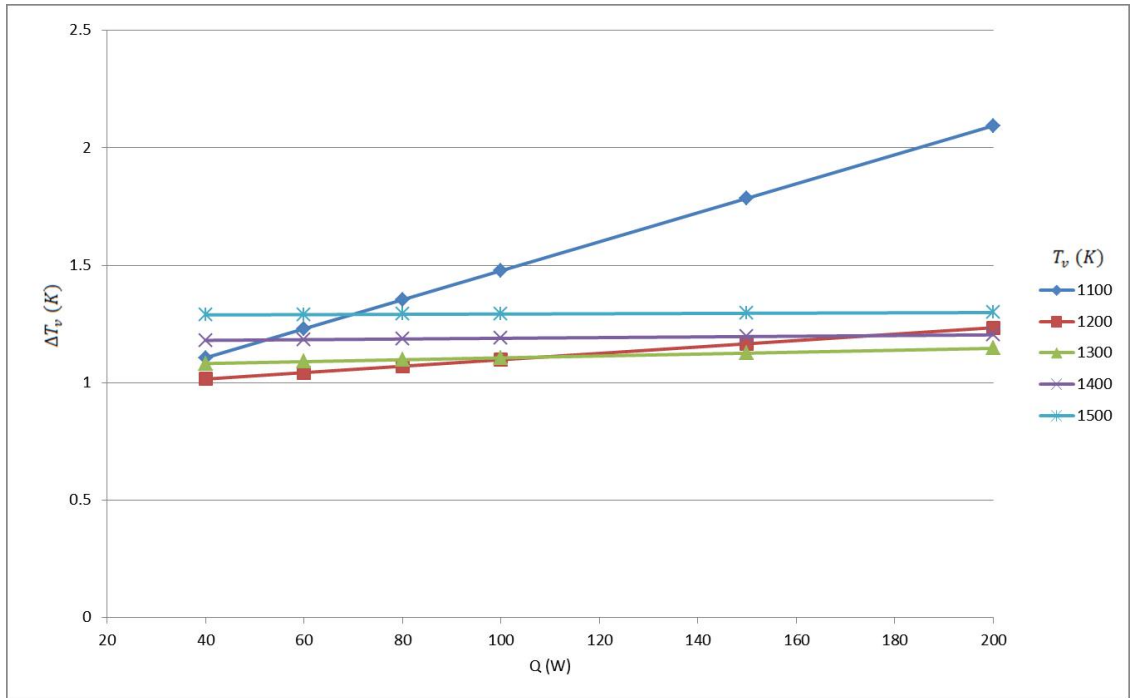


Figure 2.15 Vapor Temperature Decreases along the Heat Pipe Length at Different Heat Inputs  
 $(d_i/L = 0.025, \omega^2 \bar{Z}_a/g = 470)$

Figure 2.15 illustrates how the lengthwise vapor temperature drop of the heat pipe is influenced by the heat input. Generally, when the operating temperature of the heat pipe is relatively high, the influence of the heat input on the vapor temperature drop is comparatively minor. Nevertheless, the vapor temperature drop, for a relatively low operating temperature, is substantially increased when the heat input is high.

Conferring to Equation (2.71), contributions from the friction at the liquid-vapor interface and the vapor centripetal force in the heat pipe cause the total vapor temperature drop in the heat pipe. Figure 2.16 illustrates the contribution of the centripetal force as the ratio of the vapor temperature drop caused by the vapor centripetal force to the total vapor temperature drop.

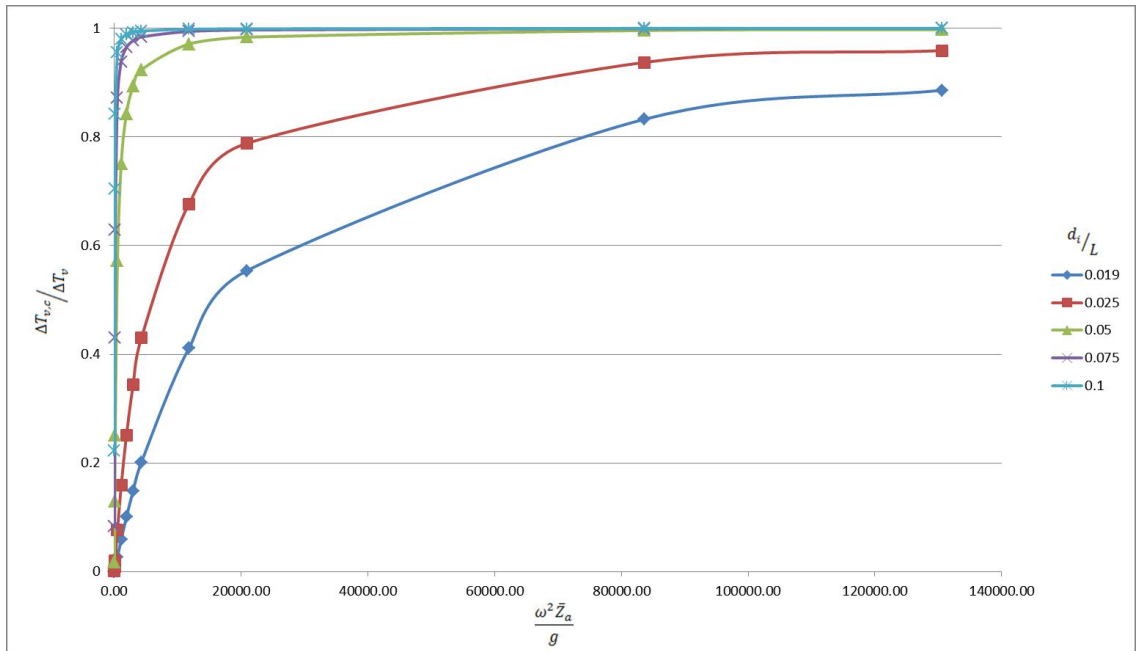


Figure 2.16 Ratio of the Vapor Temperature Decreases to the Total Temperature Decrease, due to the Centripetal Force ( $T_v = 1100K$ ,  $Q = 200W$ )

At low rotational speeds, the influence of the centripetal force is comparatively minor, but at high rotational speeds, the influence of the centripetal force becomes a dominant factor. This is particularly evident for single heat pipes having a comparatively large diameter.

As demonstrated by the preceding analytical solutions, the vapor temperature drop along the heat pipe length may pose a heat transfer limitation when a single heat pipe has a very small diameter, with a relatively low operating temperature level and a high rotational speed. Conversely, for single miniature heat pipes having a diameter of approximately 1.5 to 2 mm, the heat transfer limitation has not been observed at normal rotational speeds and normal operating temperatures. This denotes that radially rotating miniature heat pipes are viable for use in turbine disk cooling applications.

The entrainment limit is caused by the interaction between the counter-current vapor and liquid flows that takes place at the liquid-vapor interface. This limit can be of key concern when the heat flux is high and the heat pipe dimensionless sizes are minute. In this scenario, the shear stresses at the liquid-vapor interface hinder the return of liquid from the condenser to the evaporator section. When this occurs, the heat pipe is said to have reached the entrainment limit. An ample review of the entrainment limit for two-phased closed thermo-siphons is given by Faghri [2] and Peterson [21]. An assortment of correlations for the evaluation of this limit is also included in the literature. For contemporaneous single wickless rotating heat pipes, the mechanism of the entrainment limit should be parallel to that of the thermo-siphons with the gravitational force being substituted with the rotational centripetal force. Figure 2.17 illustrates the entrainment limits for the same single heat pipe examined previously at different rotational speeds.

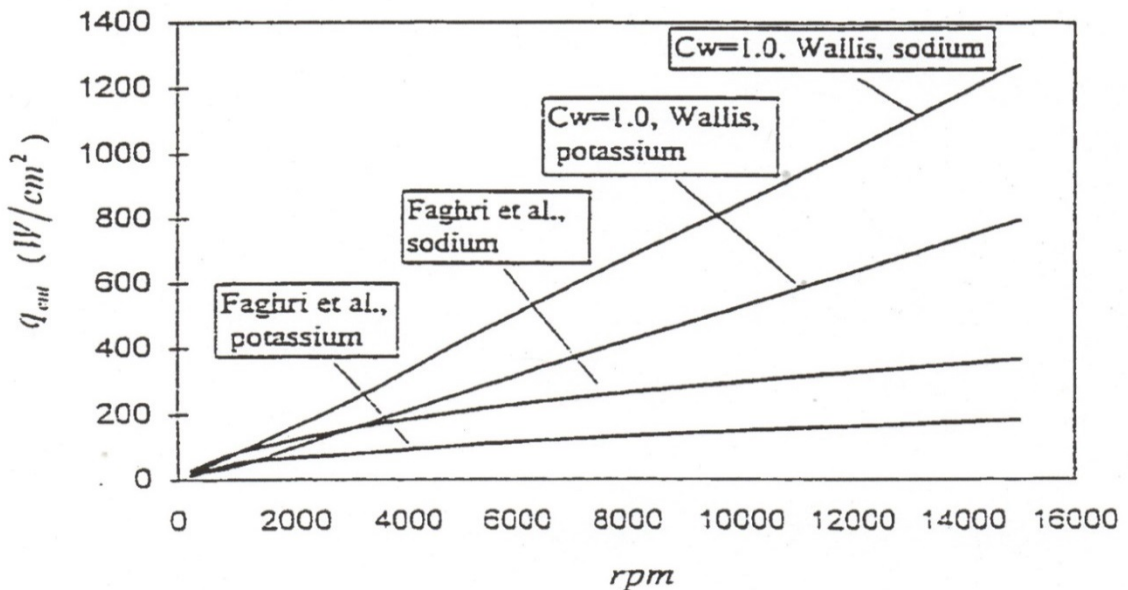


Figure 2.17 Entrainment Limitations as a Function of Rotational Speeds  
 ( $T_{ref} = 1073K$  for sodium and  $T_{ref} = 937K$  for potassium) [2]

The calculation was created based on the Wallis' correlation [2]

$$\frac{Q_{ent}}{A} = \frac{C_w^2 h_{fg} \sqrt{(r_0 + z) \omega^2 D (\rho_l - \rho_v) \rho_v}}{\left[1 + (\rho_v / \rho_l)^{1/4}\right]^2} \quad (2.72)$$

Along with the correlation from Faghri et al. [4]

$$\frac{Q_{ent}}{A} = \left(\frac{\rho_l}{\rho_v}\right)^{0.14} \left(\tanh^2 Bo^{\frac{1}{4}}\right) h_{fg} \left[(r_0 + z) \omega^2 \sigma (\rho_l - \rho_v)\right]^{1/4} \left[\rho_l^{-1/4} + \rho_v^{-1/4}\right]^2 \quad (2.73)$$

The result applies to potassium and sodium as the working fluids. For the single rotating heat pipes with a miniature dimensionless size,  $d_i/L = 0.0125$ , the entrainment limit is exceedingly sensitive to the rotational speed and can be of concern when the rotational speed is significantly slow. Conversely, when the rotational speed is reasonably high, the entrainment limit is enlarged to more than  $100 \frac{W}{cm^2}$ , which is suitable for turbo-machinery applications. The values of the entrainment limit that have been calculated by the Wallis' correlation are approximately those found in Faghri et al. [4], when the rotational speed is low. However, large deviations are observed with both working fluids at high rotational speeds. A comparable development was observed by Faghri [2] for thermo-siphons.

### 3. Experimental Testing Procedures

#### 3.1 High Speed Rotating Test Apparatus

To verify the abovementioned analytical results, a high speed test apparatus and a data acquisition system were fabricated. The data acquisition system is depicted in Figure 3.1.

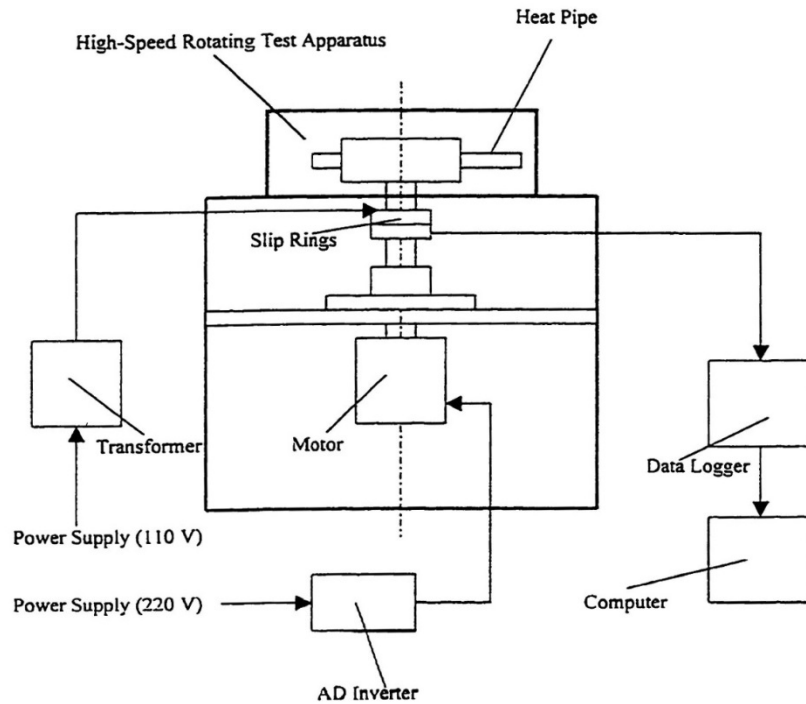


Figure 3.1 Depiction of a High Speed Rotating Test Apparatus and Data Acquisition System

The revolution range of the rotating test apparatus is adjustable from 0 to 3,600 rpm and is controlled by an AC inverter. The electric heater used to heat the heat pipes was adjusted by a transformer from 0 to 120 V, which was supplied by a two-channel slip ring. The lengthwise temperature distributions of the heat pipe were measured by five thermocouples and connected to a data acquisition system through a 5-channel slip ring. A numbered schematic of the high speed rotating test apparatus is shown in Figure 3.2.



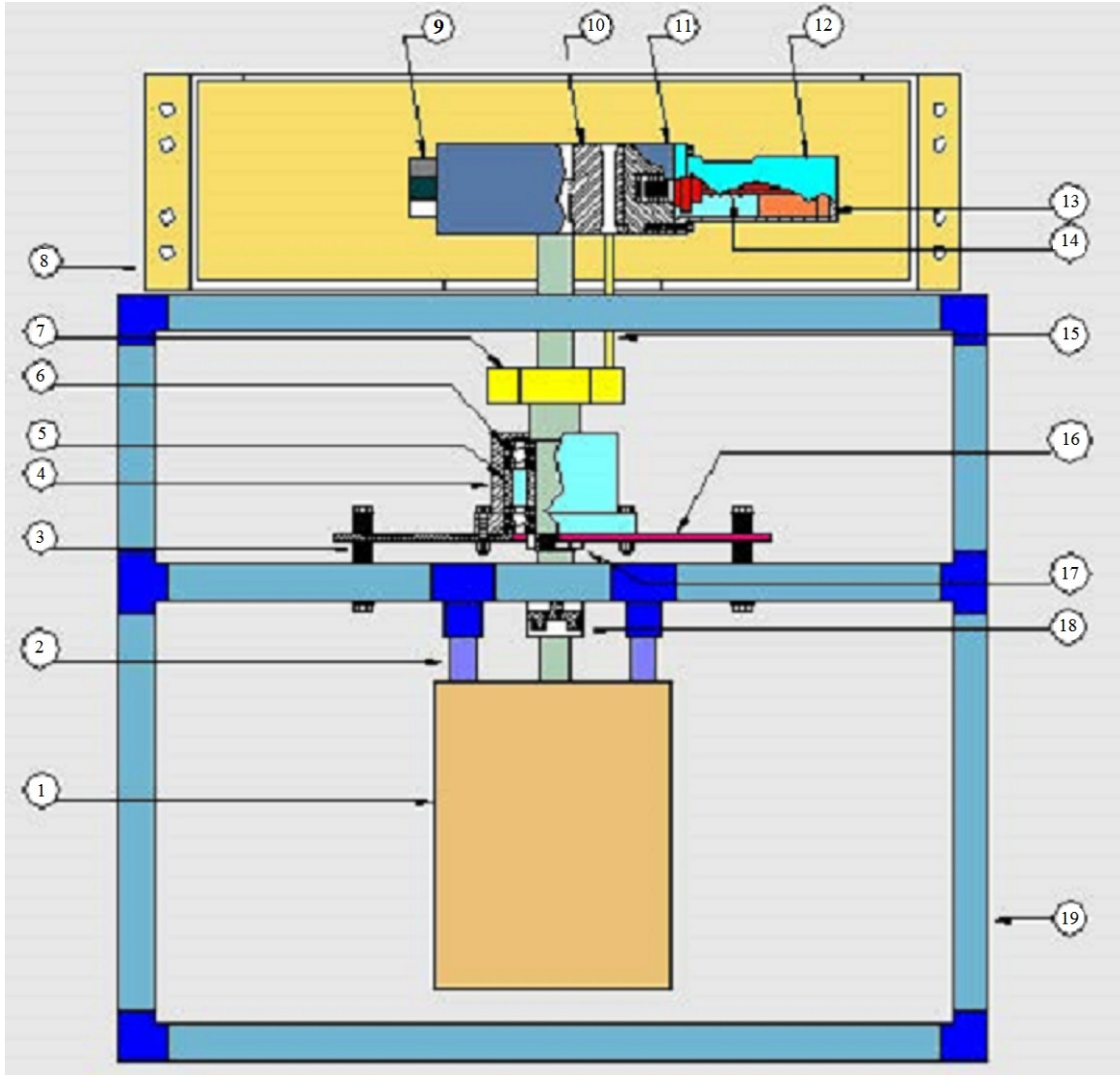


Figure 3.2 Schematic of High Speed Rotating Test Apparatus

The high speed rotating test apparatus consists of the following components:

1. The motor, which rotates the shaft
  - a. Has a capacity of 1 horsepower
  - b. Motor speed can be varied from 0 to 3,600 rpm.
2. Support Bars

- a. Mounted to the frame (19) and transfers the weight of the motor (1) to the frame (19)
3. Springs
- a. Used for vibration dampening and self-balancing
  - b. Four Sets were used and they transfer the weight of the motor to the frame (19)
4. Bearing House
- a. Houses the bearings (5) & (6)
  - b. Transfers weight of the motor to the frame (19)
5. Ball Bearing
- a. Two ball bearings were used to affix the position of the shaft (5) & (6)
6. Ball Bearings
7. Slip Rings
- a. Two slip ring assemblies were used and mounted to the shaft
    - 1. Used to supply electrical current from the power transformer to the heater of the heat pipe (15)
    - 2. Used to connect the thermocouples on the heat pipe (14) to the data acquisition device
8. Safety Shell
- a. Used to protect the user in the event of heat pipe attachment failure
9. Counter Weight
- a. Mounted opposite to heat pipe (14), for balancing
10. Inner Cylinder

- a. Mounted to the shaft and used to mount the outer cylinder (11)
- b. Used to connect the thermocouples and heater

#### 11. Outer Cylinder

- a. Mounted to the inner cylinder (10) with two attachment bolts
- b. Used to mount the heat pipe (14) and heat pipe cap (12)

#### 12. Heat Pipe Cap

- a. Used to control the flow rate of cooling air in the condenser section of the heat pipe
- b. Also used to protect the heater of the heat pipe

#### 13. Heater

- a. Used to heat the heat pipe

#### 14. Heat Pipe

#### 15. Electrical Wires

- a. Consists of the thermocouple wires and the heater wires

#### 16. Supporting Plate

- a. Supports bearing housing
- b. Dampens vibrations in the shaft

#### 17. Bearing Nut

- a. Locks the bearings in place

#### 18. Flexible Coupling

- a. Used to dampen the vibration of the rotor and to connect the shaft with the motor (1).

#### 19. Frame

Upgrades to the High Speed Rotating Test Apparatus were made to insure safety and reliability during operation and are as follows:

1. Ballistic Shielding between the rotor housing and the user.
2. All wires were wrapped with insulating material.
3. A thermocouple was added to the rotor housing to measure the rotor housing air temperature.
4. The AD Inverter was mounted to the Test Apparatus and grounded.
5. Extra electrical grounding points were added to the Test Apparatus.
6. The high voltage wires were wrapped in conduit and attached with stress relievers.
7. Inline fuses were added to all electrical sources.
8. Higher accuracy volt and current meters were implemented.
9. All thermocouple and probe ends were tinned.

The data acquisition system was also upgraded to a system that would support National Instruments LabView. Figures of the Labview block diagram and graphical user interface are given in Appendix B.

### 3.2 Single Radially Rotating Miniature Heat Pipes

The single radially rotating miniature heat pipes were fabricated from 304W stainless steel and filled with sodium. A 304W stainless steel shell with sodium as the working fluid was chosen due to the well documented compatibility found in the literature.

Two single radially rotating miniature heat pipes were designed to operate at a vapor temperature of approximately  $800^{\circ}\text{C}$  in the experiment. One consisted of an inner diameter of 1.5 mm and a length of 82 mm, as shown in Figure 3.3.

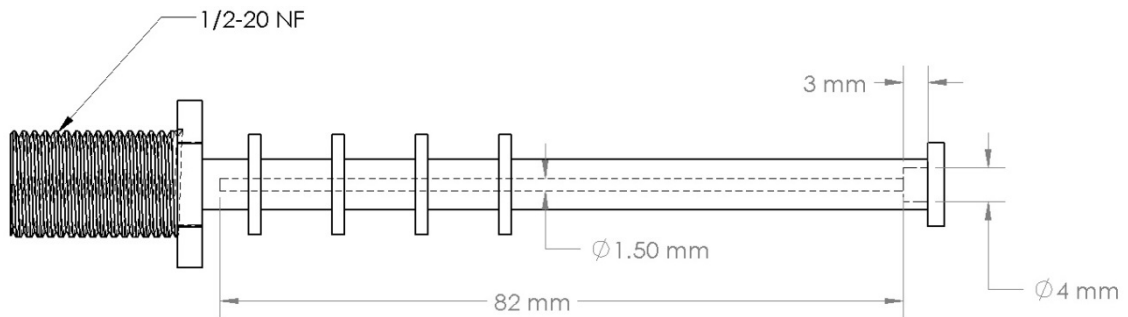


Figure 3.3 Schematic of 1.5 mm Single Miniature Radially Rotating Heat Pipe<sup>1</sup>

The other consisted of an inner diameter of 2 mm and a length of 80 mm, as shown in Figure 3.4. To assist in the sodium charging of these heat pipes, a reservoir of 4 mm in diameter and 3 mm in length for the 1.5 mm heat pipe and 5 mm in length for the 2 mm heat pipe was designed at the top of the evaporator section. An end cap was welded at the end of the reservoir of the evaporator section and a filling tube with an inner diameter of 2.1 mm was welded into the end cap.

<sup>1</sup> Full manufacturing drawings are located in the appendix.

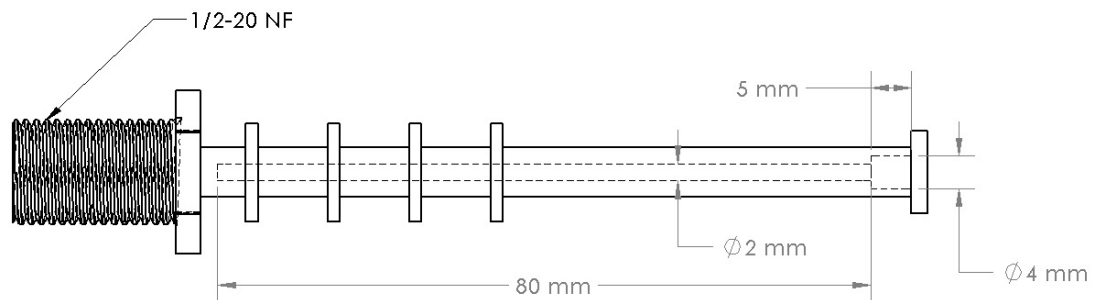


Figure 3.4 Schematic of 2 mm Single Miniature Radially Rotating Heat Pipe<sup>2</sup>

The two single radially rotating miniature heat pipes had identical outer diameters of 6 mm and the lengths of the evaporator and condenser sections were identical as well, at 40 mm. Four fins were constructed on the outer exterior of the condenser section in order to enhance the convective heat transfer of the condenser section. The heat pipes, heater caps, and filling tube were all fabricated from Type 304W stainless steel. A screw threading was machined at the heat pipe root in order to attach the heat pipe onto the outer cylinder of the high speed rotating test apparatus. All of the heat pipe components were carefully fitted and cleaned according to standardized procedures. The heat pipes, end caps, and filling tube were all degreased with 1,1,1-trichloroethane, afterwards rinsed in tap water, subsequently rinsed in methanol and then allowed to air dry. The welding process of the heat pipes, end caps and filling tubes were conducted under argon gas in order to prohibit oxidation during welding.

The sodium charging of the single radially rotating miniature heat pipes was administered by Thermacore Inc., PA. The filling method was as follows:

1. The sodium was introduced into the heat pipes in an argon filled glovebox.

<sup>2</sup> Full manufacturing drawings are located in the appendix.

2. The unsealed ends of the heat pipes were attached to a vacuum pump.
3. While pumped to a level of high vacuum, the heat pipes were heated to  $100 - 200^{\circ}\text{C}$ , in order to dissipate any absorbed water and atmospheric gases.
4. The filling tubes of the heat pipes were pinched and welded while being maintained at a level of high vacuum.

For the single radially rotating miniature heat pipe with an inner diameter of 1.5 mm, the sodium charge was approximately 0.06 g. And for the single radially rotating miniature heat pipe with an inner diameter of 2 mm, the sodium charge was approximately 0.08 g. Five type K thermocouples were used to measure the lengthwise heat pipe temperature distributions; the thermocouples were calibrated by Omega Engineering Inc. to an accuracy of  $\pm 0.5^{\circ}\text{C}$ . Two of the thermocouples were mounted at the evaporator section in order to measure the temperatures of the evaporator section; the other three thermocouples were installed at the condenser section in order to measure the temperatures of the condenser section. The five thermocouple heads were set into five small surface cavities, 0.8 mm in diameter, on the heat pipe shell along the heat pipe length.

The heater for the heat pipes was constructed from the high temperature chemical set cement, OmegaBond “600”, and from a Nickel-Chromium alloy, resistance heating wire of NI80-010 or NI80-012, both purchased from Omega Engineering Inc. The method for the construction of the heater was as follows:

1. The OmegaBond “600” high temperature chemical set cement requires mixing 100 parts of the cement with 13 parts of water by weight.

2. A thin layer of the mixture was applied uniformly to the outer surface of the heat pipe.
3. The cement cures after 18-24 hours at ambient temperature or 4 hours at  $104^{\circ}\text{C}$ .
4. The Nickel-Chromium alloy resistance heating wire was wrapped around the surface of the cement, as tightly as possible without creating a short, as a heating element.
5. Another thick layer of the cement is applied to the heating element and cured.

The heater was mounted securely on the outer surface of the evaporator section of the heat pipe; layers of fiberglass insulation fabric, equating to approximately 16 mm thick, was placed between the heater and heater cap to ensure that the majority of the heat from the heater would be conveyed to the evaporator section of the heat pipe. Figure 3.5 shows a prepared single radially rotating miniature heat pipe that is ready to be tested. The same miniature heat pipes have been tested in 2000 and an importance objective of the present retest is to further validate the performance and operational life of these heat pipes. The tests here also provide the foundation for the study of the sector heat pipes.



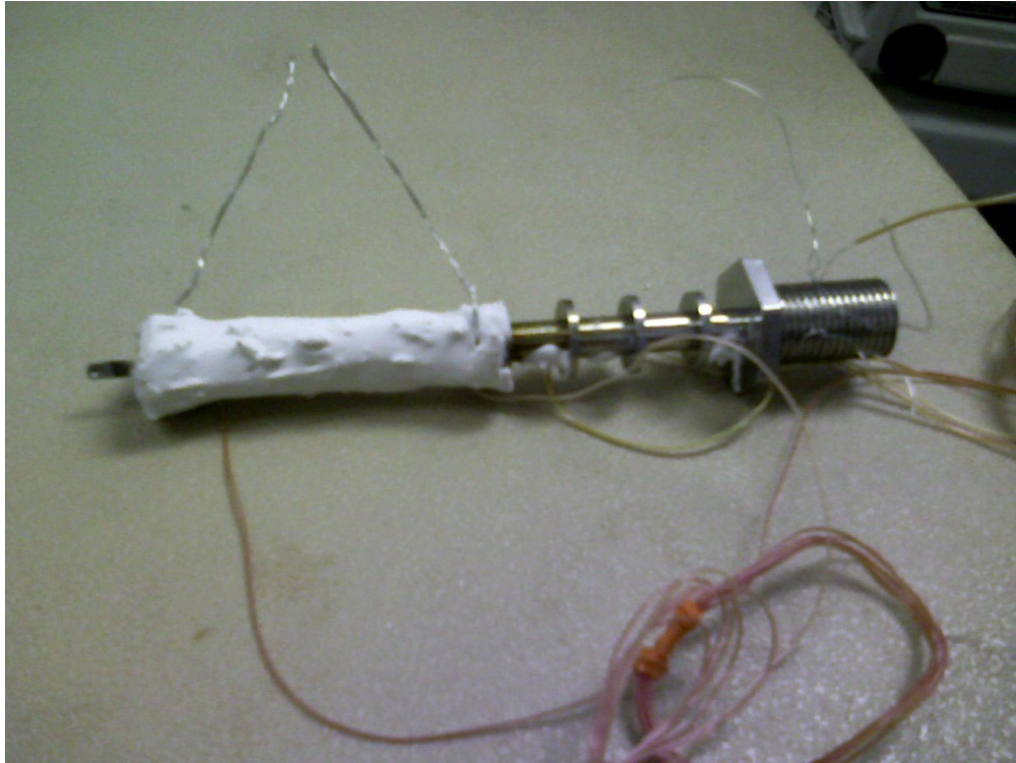


Figure 3.5 Picture of a Prepared Single Radially Rotating Miniature Heat Pipe

### 3.3 Sector Heat Pipe with Interconnected Branches (Design 1)

The sector heat pipe with interconnected branches (design 1) was fabricated from 304W stainless steel and filled with sodium. A 304W stainless steel shell with sodium as the working fluid was chosen due to the well documented compatibility found in the literature.

The sector heat pipe was designed to operate at a vapor temperature of approximately  $800\text{ }^{\circ}\text{C}$  in the experiment. The sector consisted of four single heat pipes, each with a diameter of 3 mm and a length of 85 mm, as shown in Figure 3.6.

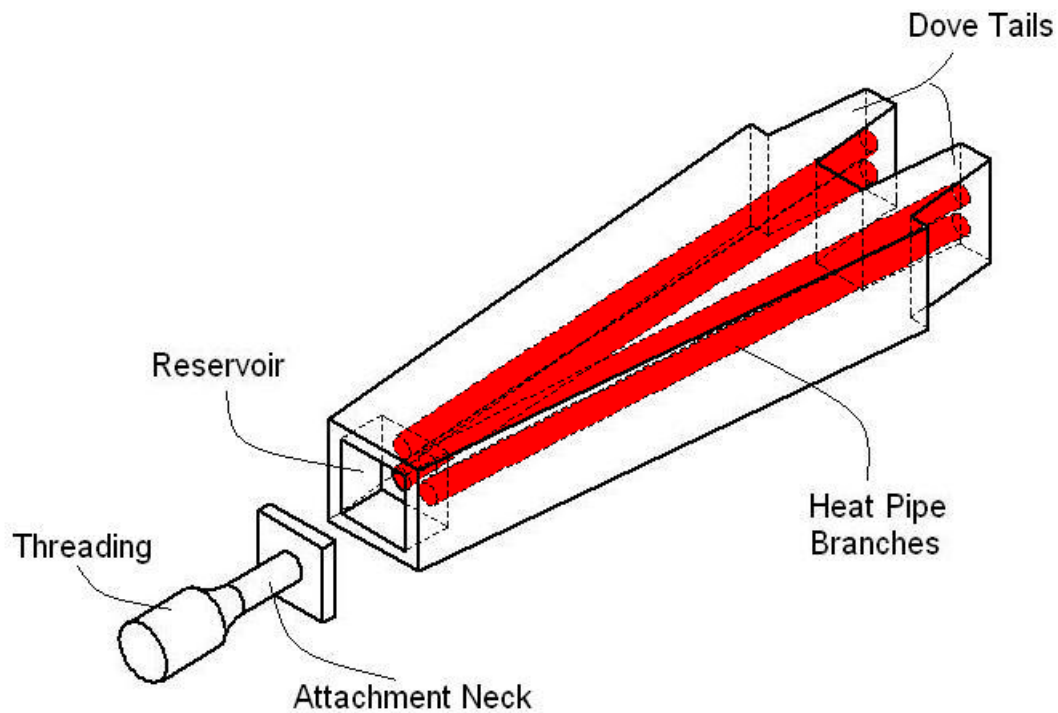


Figure 3.6 Schematic of Sector Heat Pipe (Design 1)<sup>3</sup>

<sup>3</sup> Complete manufacturing drawing are located in the appendix.

The four single heat pipes were connected with a common reservoir, located at the bottom in the condenser section, as shown in Figure 3.7.

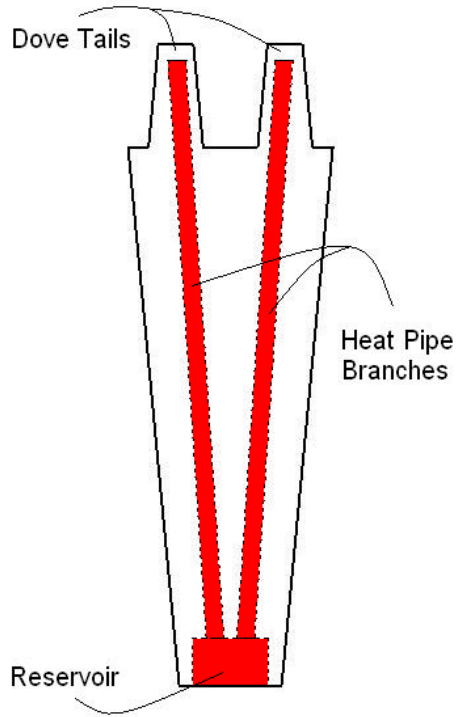


Figure 3.7 Schematic of Sector Heat Pipe (Design 1) Reservoir Location

An end cap was welded at the end of the reservoir, at the bottom of the condenser section and a filling tube with an outer diameter of 2.1 mm was welded into the side of the sector at the reservoir. The sector heat pipe, condenser cap, and filling tube were all fabricated from Type 304W stainless steel. A screw threading was machined as part of the end cap in order to attach the heat pipe onto the outer cylinder of the high speed rotating test apparatus. All of the heat pipe components were carefully fitted and cleaned according to standardized procedures. The heat pipe, end caps, and filling tube were all degreased with 1,1,1-trichloroethane, afterwards rinsed in tap water, subsequently rinsed in methanol and

then allowed to air dry. The welding process of the heat pipes, end caps and filling tubes were conducted under argon gas in order to prohibit oxidation during welding.

The sodium charging of the sector heat pipe was administered by Advanced Cooling Inc.

The filling method was as follows:

1. The sodium was introduced into the sector heat pipe in an argon filled glovebox.
2. The unsealed end of the heat pipe was attached to a vacuum pump.
3. While pumped to a level of high vacuum, the heat pipe was heated to  $100 - 200^{\circ}\text{C}$ , in order to dissipate any absorbed water and atmospheric gases.
4. The filling tube of the heat pipe was pinched and welded while being maintained at a level of high vacuum.

For the sector heat pipe with interconnected branches (design 1), the sodium charge was approximately 0.26 g. Five type K thermocouples were used to measure the lengthwise heat pipe temperature distributions; the thermocouples were calibrated by Omega Engineering Inc. to an accuracy of  $\pm 0.5^{\circ}\text{C}$ . Two of the thermocouples were mounted at the evaporator section in order to measure the temperatures of the evaporator section; the other three thermocouples were installed at the condenser section in order to measure the temperatures of the condenser section. The five thermocouple heads were set on the surface of the heat pipe shell along the heat pipe length.

The heater for the heat pipes was constructed from the high temperature chemical set cement, OmegaBond “600”, and from a Nickel-Chromium alloy, resistance heating wire of NI80-010 or NI80-012, both purchased from Omega Engineering Inc. The method for the construction of the heater was as follows:

1. The OmegaBond “600” high temperature chemical set cement requires mixing 100 parts of the cement with 13 parts of water by weight.
2. The entire surface of the heat pipe was roughened with a file.
3. A thin layer of the mixture was applied uniformly to the entire surface of the heat pipe.
4. The cement cures after 18-24 hours at ambient temperature or 4 hours at 104°C .
5. The Nickel-Chromium alloy resistance heating wire was wrapped around the dovetail portion of the heat pipe, as tightly as possible without creating a short, as a heating element.
6. Another thick layer of the cement is applied to the heating element and cured.

The heater was mounted securely to the dovetail section of the heat pipe; layers of fiberglass insulation fabric, equating to approximately 16 mm thick, was wrapped around the heater<sup>4</sup> to ensure that the majority of the heat from the heater would be conveyed to the evaporator section of the heat pipe. Figure 3.8 shows a prepared sector heat pipe (design 1) that is ready to be tested.

---

<sup>4</sup> The heater cap was not used because it was not large enough to accommodate the sector heat pipe.

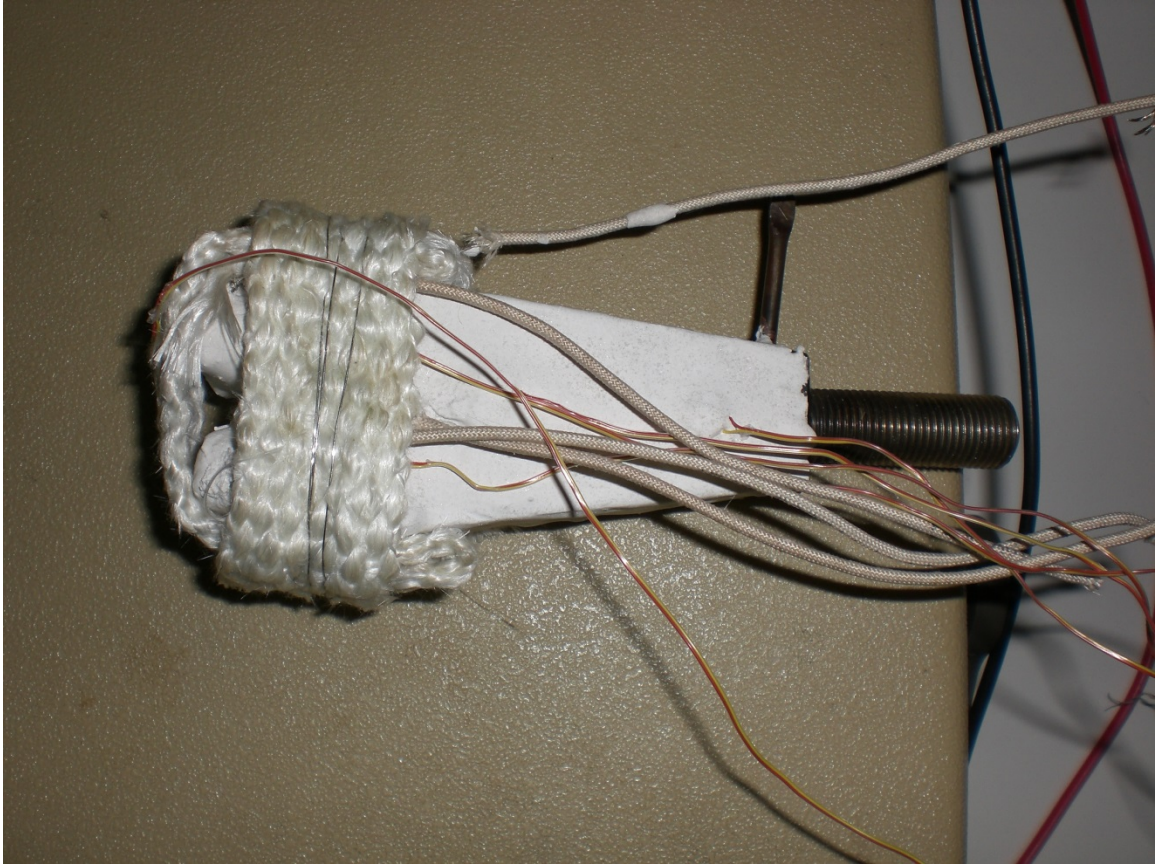


Figure 3.8 Picture of a Prepared Sector Heat Pipe (Design 1)

### 3.4 Sector Heat Pipe with Interconnected Branches (Design 2)

The sector heat pipe with interconnected branches (design 2) was fabricated from Multipurpose Copper (Alloy 110) and filled with distilled water. A Multipurpose Copper (Alloy 110) shell with distilled water as the working fluid was chosen due to the well documented compatibility found in the literature.

The sector heat pipe was designed to operate at a vapor temperature of approximately  $150^{\circ}\text{C}$  in the experiment. The sector consisted of four single heat pipes, each with a diameter of 3 mm and a length of 85 mm, as shown in Figure 3.9.

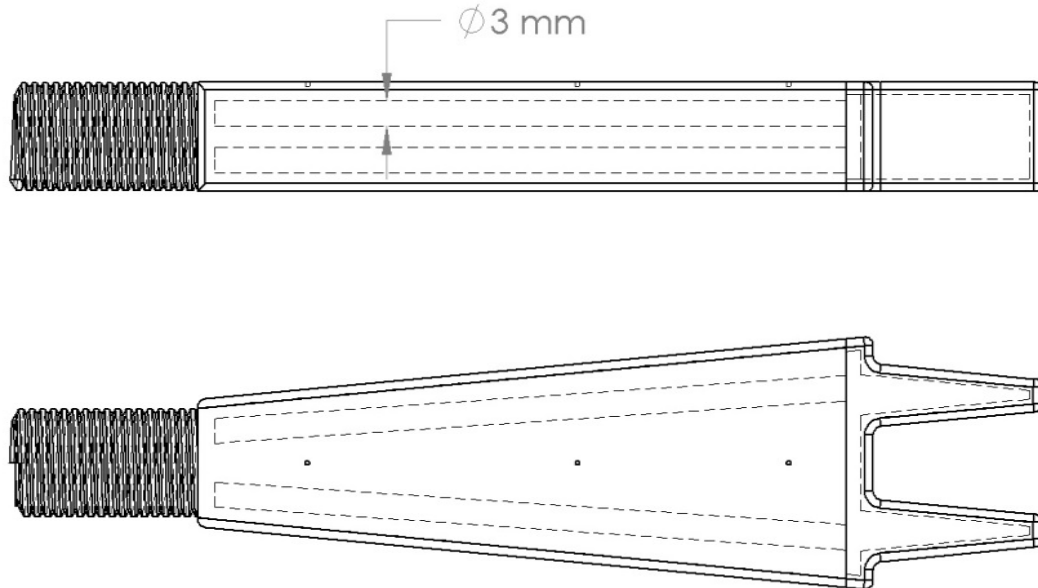


Figure 3.9 Schematic of Sector Heat Pipe (Design 2)<sup>5</sup>

The four single heat pipes were connected with a common reservoir, located at the top of the evaporator section, as shown in Figure 3.10. The sector had to be designed into two

---

<sup>5</sup> Complete manufacturing drawings are located in the appendix.

sections: the dovetail section, containing the reservoir, and a body section, containing the four heat pipes.

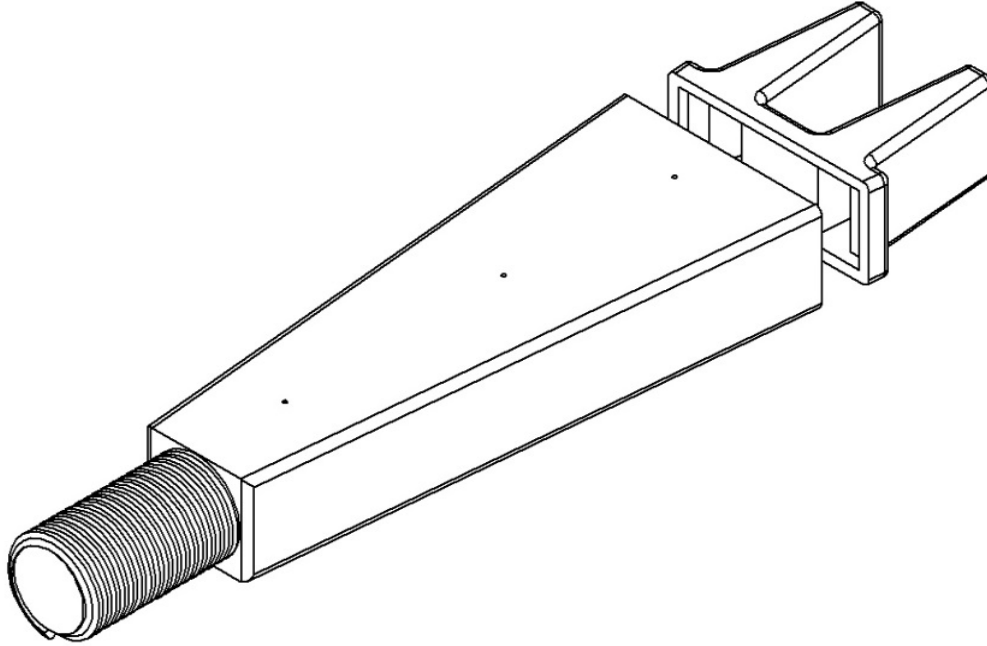


Figure 3.10 Schematic of Sector Heat Pipe (Design 2), Reservoir Location

The dovetail cap was welded at the end of the body of the evaporator section and a filling tube with an outer diameter of 2.1 mm was welded into the side of the sector at the top of the condenser. The heat pipe body, dovetail section, and filling tube were all fabricated from Multipurpose Copper (Alloy 110). A screw threading was machined as part of the heat pipe body root in order to attach the heat pipe onto the outer cylinder of the high speed rotating test apparatus. All of the heat pipe components were carefully fitted and cleaned according to standardized procedures. The heat pipe body, dovetail cap, and filling tube were all degreased with denatured alcohol and then allowed to air dry. The welding process of the heat pipe body, dovetail cap and filling tubes were conducted using rosin soldering flux in order to prohibit oxidation during welding.



The distilled water charging of the sector heat pipe was done in Florida International University's Thermal Sciences Lab. The filling method was as follows:

1. The unsealed end of the heat pipe was attached to a vacuum pump.
2. While pumped to a level of high vacuum, the heat pipe was heated to  $100 - 200^{\circ}\text{C}$ , in order to dissipate any absorbed water and atmospheric gases.
3. When a level of high vacuum was obtained, the tube leading to the vacuum pump was pinched off
4. Using a syringe, the distilled water was administered to the heat pipe.
5. The filling tube of the heat pipe was pinched and welded while being maintained at a level of high vacuum.

Figure 3.11 illustrates the filling of the heat pipe.

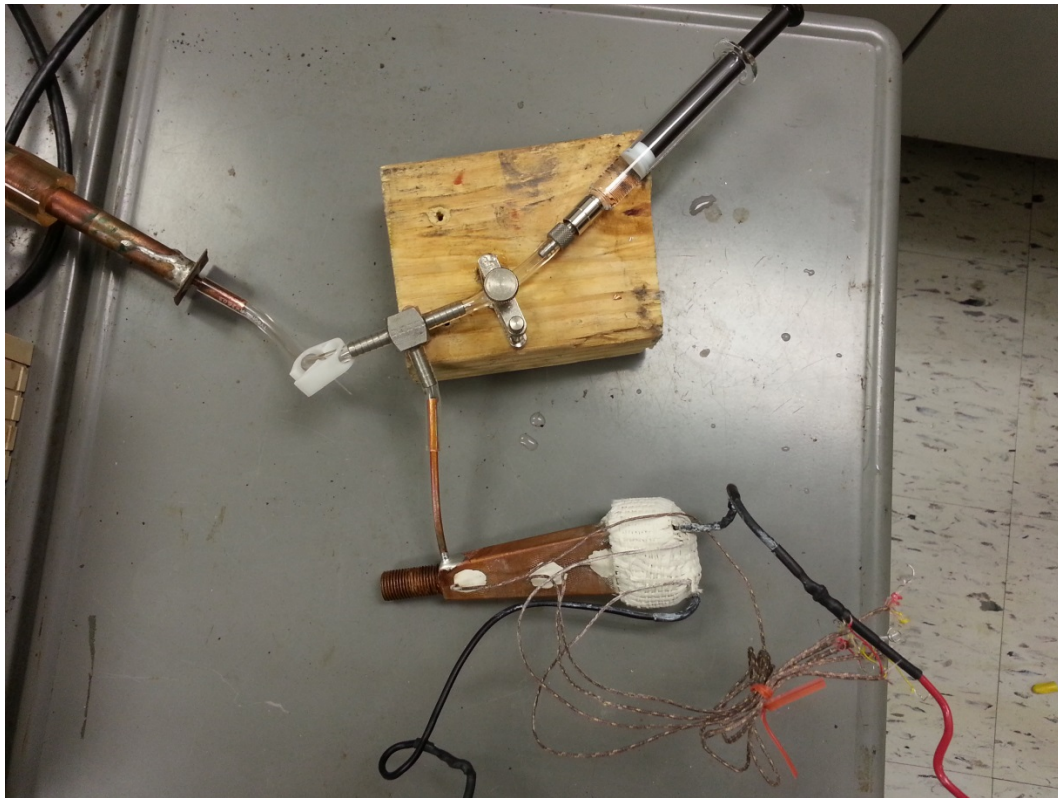


Figure 3.11 Picture of Sector Heat Pipe (Design 2) being filled

For the sector heat pipe with interconnected branches (design 2), charged with distilled water; a few fill volumes were tested: approximately, 0.7 mL for “100%” filled, 0.6 mL for “90%” filled and, 0.4 mL for “50%” fill.

Five type K thermocouples were used to measure the lengthwise heat pipe temperature distributions, the thermocouples were calibrated by Omega Engineering Inc. to an accuracy of  $\pm 0.5^{\circ}\text{C}$ . Two of the thermocouples were mounted at the dovetail section in order to measure the temperatures of the evaporator section; the other three thermocouples were installed at the condenser section in order to measure the temperatures of the condenser section. The five thermocouple heads were set on the cross-hatched surface of the heat pipe shell along the heat pipe length.

The heater for the heat pipes was constructed from the high temperature chemical set cement, OmegaBond “600”, and from a Nickel-Chromium alloy, resistance heating wire of NI80-010 or NI80-012, both purchased from Omega Engineering Inc. The method for the construction of the heater was as follows:

1. The OmegaBond “600” high temperature chemical set cement requires mixing 100 parts of the cement with 13 parts of water by weight.
2. A thin layer of the mixture was applied uniformly to the entire dovetail surface of the heat pipe.
3. The cement cures after 18-24 hours at ambient temperature or 4 hours at  $104^{\circ}\text{C}$ .
4. The Nickel-Chromium alloy resistance heating wire was wrapped around the dovetail portion of the heat pipe, as tightly as possible without creating a short, as a heating element.
5. Another thick layer of the cement is applied to the heating element and cured.

The heater was mounted securely to the dovetail section of the heat pipe; layers of wet-and-stick fiberglass insulation, equating to approximately 16 mm thick, was wrapped around the heater<sup>6</sup> to ensure that the majority of the heat from the heater would be conveyed to the evaporator section of the heat pipe. Figure 3.12 shows a prepared sector heat pipe (design 2) that is ready to be tested.

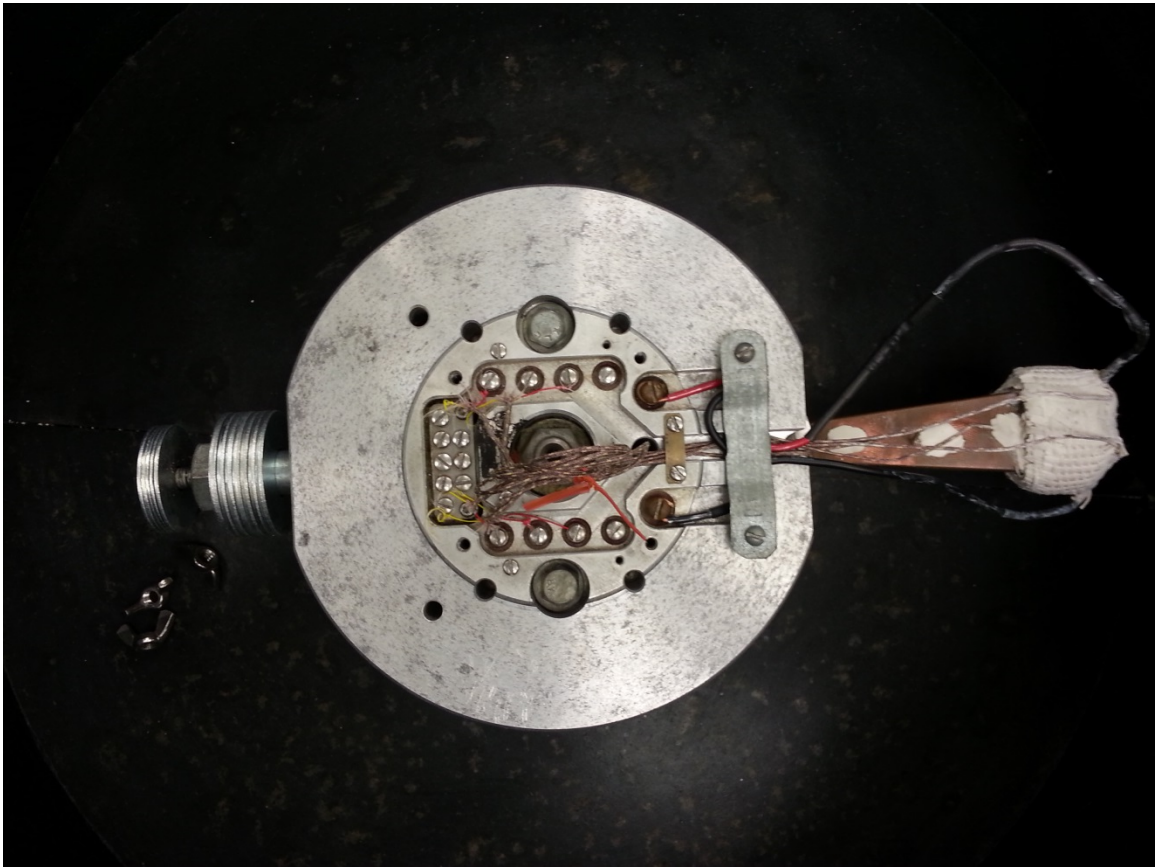


Figure 3.12 Picture of a Prepared Sector Heat Pipe (Design 2)

---

<sup>6</sup> The heater cap was not used because it was not large enough to accommodate the sector heat pipe.

#### 4. Experimental Results and Analysis

Corresponding to the preceding evaluation of the heat transfer and flow of the vapor and liquid film in the single radially rotating miniature heat pipe, it was discovered that the lengthwise temperature distribution and temperature drop for the heat pipe are functions of heat pipe length, heat pipe inner diameter, rotating speed, tilt angle, working fluid properties, cooling condition in the condenser section, and heat flux in the evaporator section. Simultaneously, other influences, such as the heat conductivity of the heat pipe container material and non-condensable gases existing in the heat pipe also have a distinct effect on the heat transfer and temperature distribution in the heat pipe.

For the experiments conducted on the radially rotating miniature heat pipes, the tilt angle,  $\phi$ , of the heat pipes was fixed at  $90^\circ$  and the rate of cooling air was fixed at 100% of the allowable rate. The arrays of geometric dimensions, heat inputs, rotating frequencies, and configurations are as follows:

1. Single Miniature Radially Rotating Heat Pipes

$$47W \leq Q \leq 325W, d_i = 1.5mm \text{ and } 2mm, L = 80mm, L_c = L_e = 40mm, L_a = 0,$$

$$470 \leq \frac{\omega^2 \bar{Z}_a}{g} \leq 1881, 30Hz \leq f \leq 60Hz$$

2. Sector Heat Pipe (Design 1)

$$47W \leq Q \leq 325W, d_i = 3mm \text{ (of each individual heat pipe)}, L = 85mm,$$

$$L_c = L_e = 40mm, L_a = 0, 470 \leq \frac{\omega^2 \bar{Z}_a}{g} \leq 1881, 30Hz \leq f \leq 60Hz$$

3. Sector Heat Pipe (Design 2)

$35W \leq Q \leq 95W$ ,  $d_i = 3$  mm (of each individual heat pipe),  $L = 85$  mm,

$$L_c = L_e = 40\text{mm}, L_a = 0, 119 \leq \frac{\omega^2 \bar{Z}_a}{g} \leq 1072, 15\text{Hz} \leq f \leq 45\text{Hz}$$

The following sub-sections present the experimental data in relation to the preceding configurations.

#### **4.1 Operating Characteristics of Radially Rotating Miniature Heat Pipes**

As stated previously, there are a number of parameters that influence the operation of radially rotating miniature heat pipes. The chief parameters are the heat pipe size, dimensionless centripetal forces, heat input in the evaporator section, and non-condensable gases in the heat pipe.

##### **1. Single Radially Rotating Heat Pipe**

To prove the heat transfer capacity of the single heat pipe, Figure 4.1, Figure 4.2, Table 4-1, and Table 4-2 are comparisons of the lengthwise temperature distributions of the single heat pipe and the lengthwise temperature distributions of a heat pipe shell (a heat pipe shell is the same heat pipe without any working fluid) with the same dimensionless centripetal forces and geometrical dimensions.

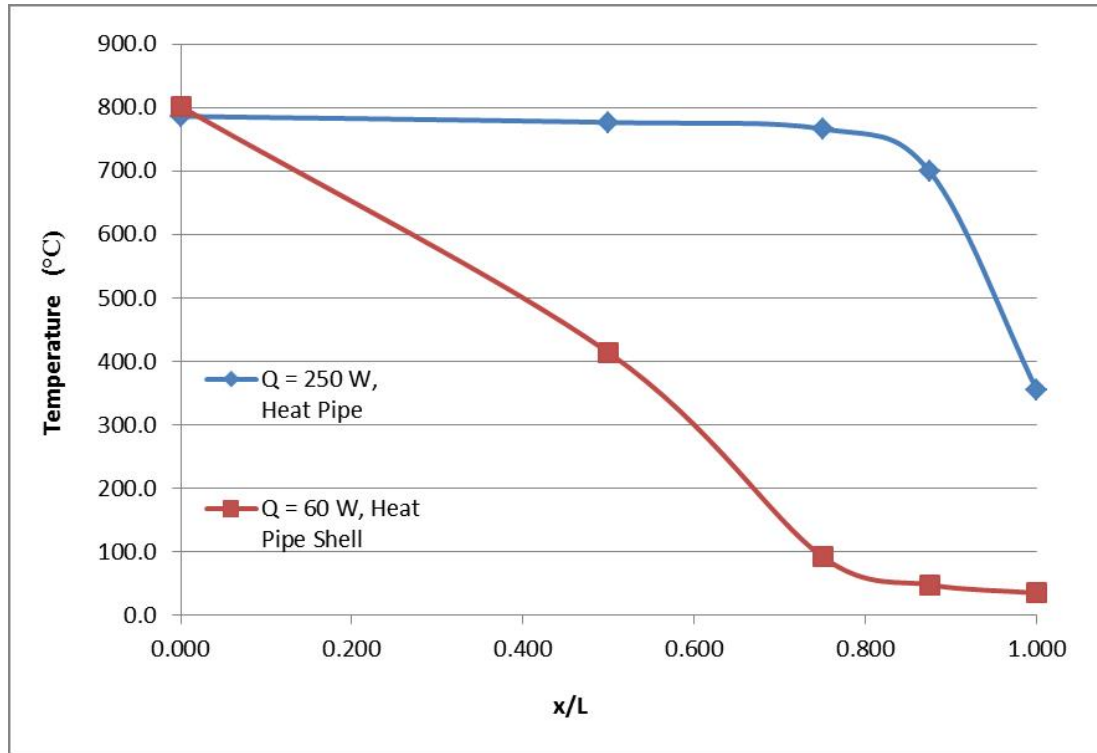


Figure 4.1 Temperature Distributions of Single Heat Pipe and Heat Pipe Shell ( $d_i = 1.5$  mm and  $f = 30$  Hz)

Table 4-1 Comparison of Heat Pipe and Heat Pipe Shell ( $d_i = 1.5$  mm and  $f = 30$  Hz)

Dimensionless Heat Pipe Length ( $x/L$ )	Temperature Distribution for Heat Pipe ( $^{\circ}C$ )	Temperature Distribution for Heat Pipe Shell ( $^{\circ}C$ )
0.0	785.1	802.3
0.50	775.7	414.2
0.75	765.6	92.4
0.875	697.8	49.5
1.0	353.6	36.7

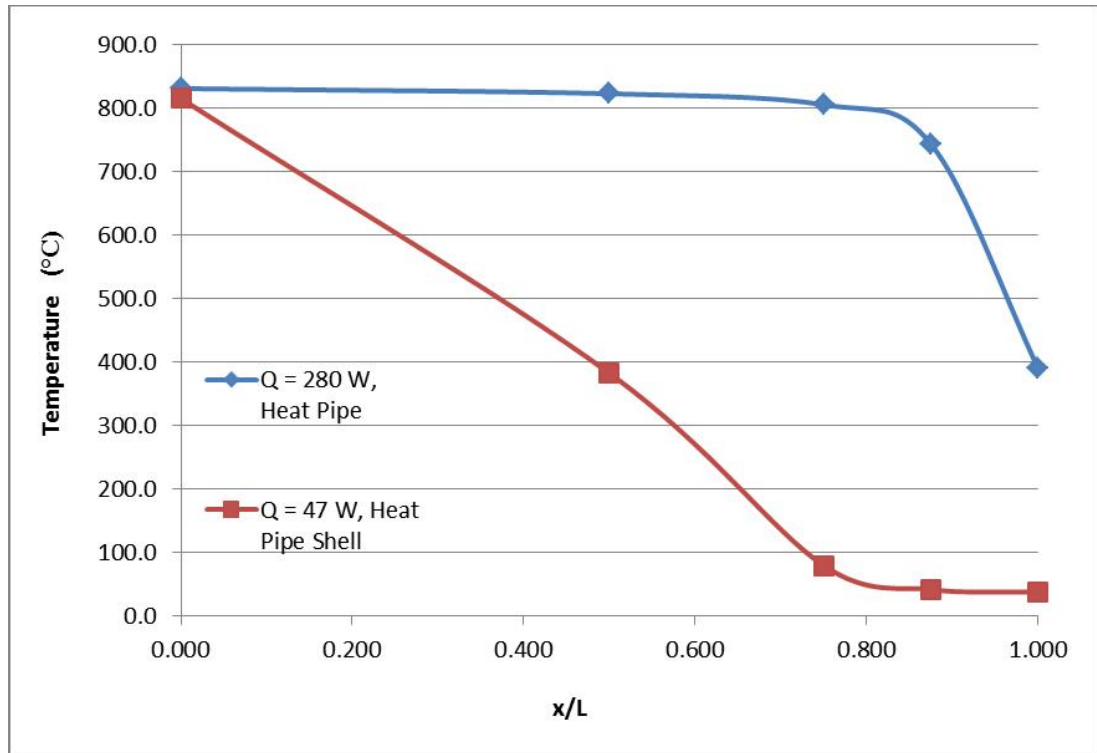


Figure 4.2 Temperature Distributions of Single Heat Pipe and Heat Pipe Shell ( $d_i = 2$  mm and  $f = 30$  Hz)

Table 4-2 Comparison of Heat Pipe and Heat Pipe Shell ( $d_i = 2$  mm and  $f = 30$  Hz)

Dimensionless Heat Pipe Length ( $x/L$ )	Temperature Distribution for Heat Pipe ( $^{\circ}C$ )	Temperature Distribution for Heat Pipe Shell ( $^{\circ}C$ )
0.0	829.3	815.7
0.50	820.5	383.3
0.75	805.7	78.7
0.875	741.3	41.7
1.0	391.3	38.3



From Figure 4.1, Figure 4.2, Table 4-1, and Table 4-2, it is clear that the heat transfer capacity of the heat pipe shell is very low; which is 60 W for the heat pipe shell with an inner diameter of 1.5 mm, and 47 W for the heat pipe with an inner diameter of 2 mm. The lengthwise temperature distribution for the shell is approximately linear and the temperature at the condenser end is nearly that of the ambient temperature. For a single heat pipe with the same dimensionless centripetal force and geometrical dimensions, significantly more heat can be transferred; which was observed to be up to 250 W for the heat pipe with an inner diameter of 1.5 mm and 280 W for the 2 mm heat pipe. If the standardized thermal conductivity of copper is taken to be  $386 \frac{W}{m \cdot ^\circ C}$ , the effective thermal conductance of the single stainless steel heat pipes is 60 – 100 times higher than that of copper. These comparisons prove that the heat transfer characteristics of the heat pipe are much better than any standard metal.

Lengthwise temperature distributions of the evaporator section and the majority of the condenser section are nearly uniform. It is apparent that the heat pipe works flawlessly in these sections; nonetheless, there occurs a large temperature gradient near the end of the condenser. This is due to the condenser end being affixed to the outer cylinder of the high speed rotating test apparatus with a screw thread, which creates a heat sink at the condenser end and allows for more heat from the condenser end to be transferred into the outer cylinder. Consequently, because of the heat transferred to the outer cylinder at the condenser end, the temperature distribution near the condenser end is lowered.

The steady-state operation of the two single radially rotating miniature high temperature heat pipes with inner diameters of 1.5 mm and 2 mm, with a dimensionless centripetal force of 470, is illustrated in Figure 4.3 and Figure 4.4.

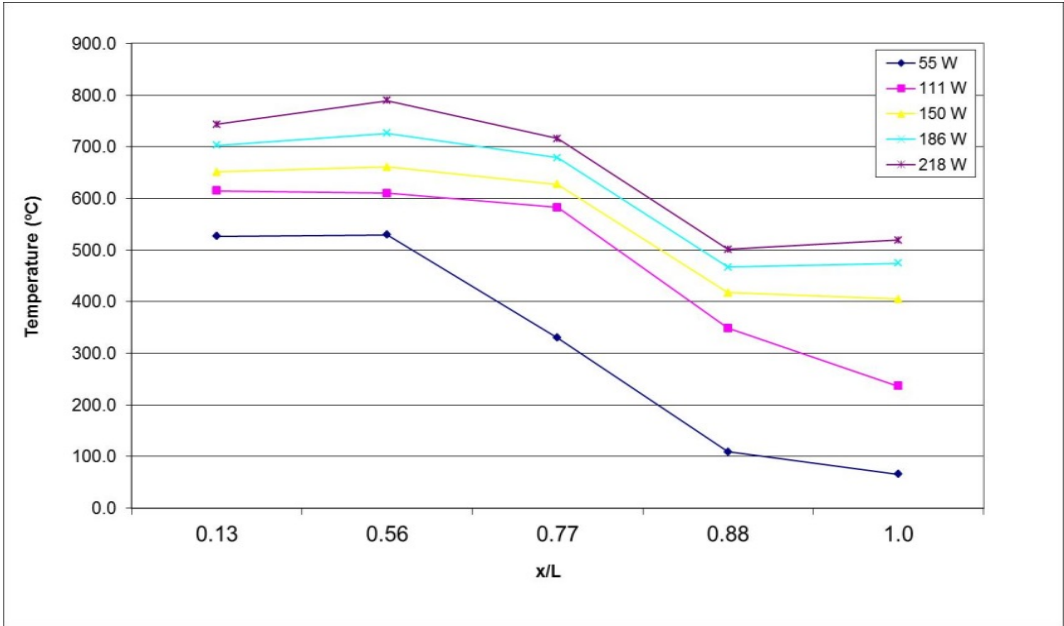


Figure 4.3 Lengthwise Temperature Distributions of the Single Radially Rotating Miniature Heat Pipe with Different Heat Inputs ( $d_i = 1.5 \text{ mm}$ ,  $f = 30 \text{ Hz}$ )

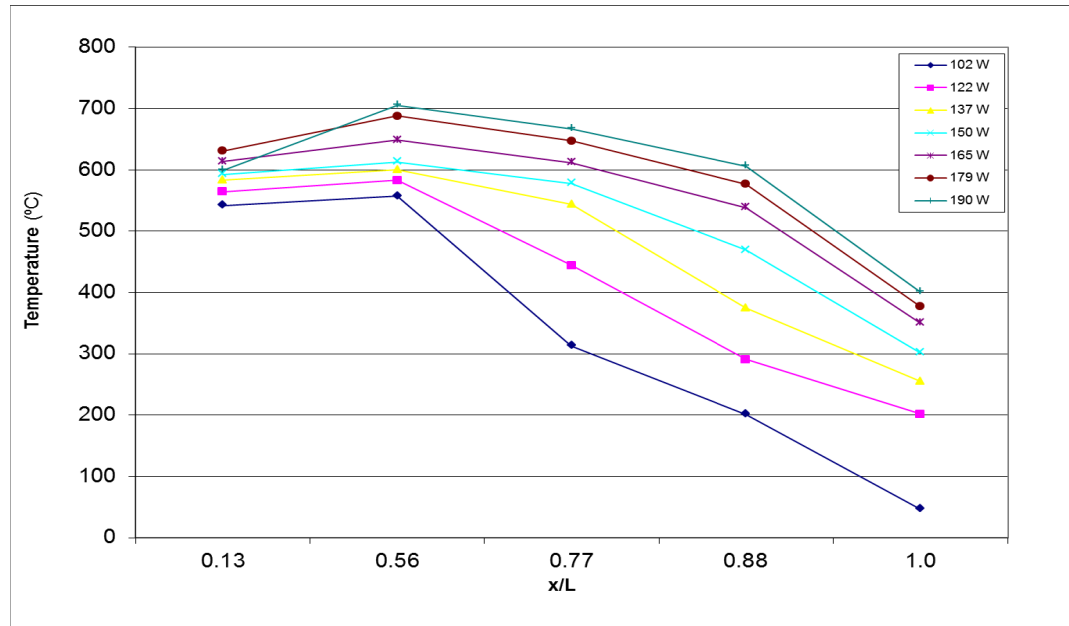


Figure 4.4 Lengthwise Temperature Distributions of the Single Radially Rotating Miniature Heat Pipe with Different Heat Inputs ( $d_i = 2.0 \text{ mm}$ ,  $f = 30 \text{ Hz}$ )

From Figure 4.3 and Figure 4.4, it is evident that the evaporator sections of the heat pipes begin working when the heat input reaches 100 W; it is also apparent from the lengthwise temperature distributions in the evaporator section that they are nearly uniform. Due to the working section in the condenser being relatively short, the temperatures along the condenser section drop sharply, this is seen because the temperatures near the condenser end are nearly that of the surrounding air temperature. By increasing the heat input, the operating temperature in the evaporator section will increase and the vapor flow rate will increase accordingly. Concurrently, the working section in the condenser will be prolonged to the condenser end, causing the lengthwise temperatures of the condenser section to increase rapidly. Once the heat input approaches approximately 250 W for the heat pipe with an inner diameter of 1.5 mm and 280

W for the heat pipe with an inner diameter of 2 mm, the lengthwise temperature distribution are nearly uniform. Nonetheless, the temperature gradient proximate to the end of the condenser section continues to remains large due to the diffuse effects of non-condensable gases and the heat sink formed from the outer cylinder.

## 2. Sector Heat Pipe (Design 2)

To prove the heat transfer capacity of the sector heat pipe, Figure 4.5 and **Error! Reference source not found.** are comparisons of the lengthwise temperature distributions of the sector heat pipe and the lengthwise distributions of a sector heat pipe shell (a heat pipe shell is the same heat pipe without any working fluid) with the same dimensionless centripetal forces and geometrical dimensions.

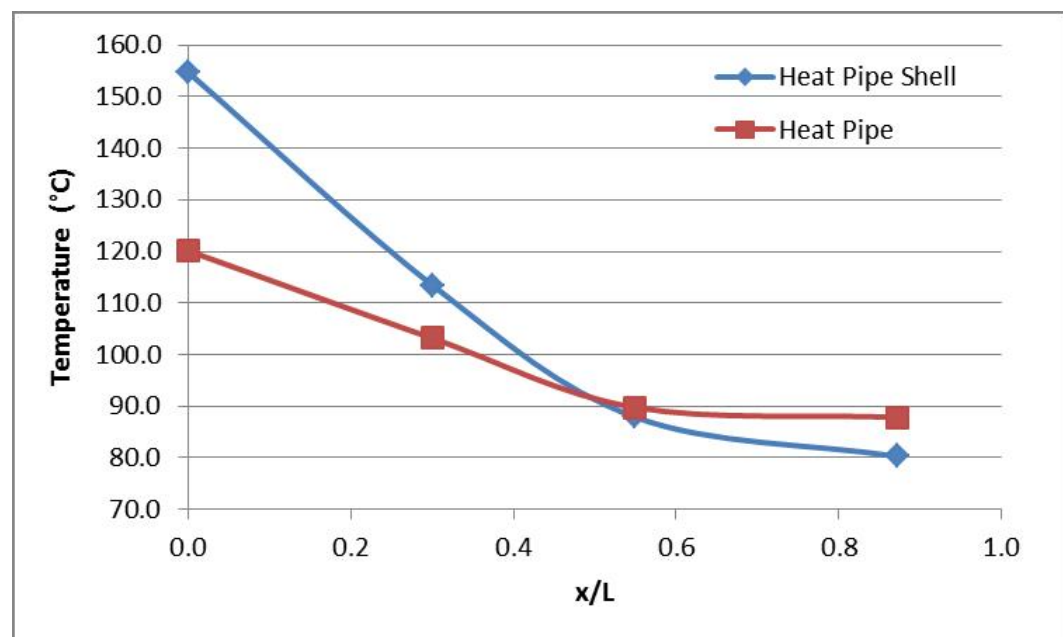


Figure 4.5 Temperature Distributions of Sector Heat Pipe (Design 2) and Sector Heat Pipe Shell ( $Q = 75 \text{ W}$ ,  $f = 15 \text{ Hz}$ )

Table 4-3 Comparison of Sector Heat Pipe and Sector Heat Pipe Shell ( $Q = 75 \text{ W}$  ,  $f = 15 \text{ Hz}$ )

Dimensionless Heat Pipe Length ( $x/L$ )	Temperature Distribution for Heat Pipe ( $^{\circ}\text{C}$ )	Temperature Distribution for Heat Pipe Shell ( $^{\circ}\text{C}$ )
0.0	120.1	154.7
0.30	103.1	113.4
0.50	89.8	87.9
0.90	87.8	80.3

From Figure 4.5 and Table 4-3, it is clear that the heat transfer capacity of the heat pipe shell is very low, which is 65 W for the heat pipe shell. The lengthwise temperature distribution for the shell is approximately linear and the temperature at the condenser end is nearly that of the ambient temperature. For the sector heat pipe with the same dimensionless centripetal force and geometrical dimensions, significantly more heat can be transferred, which was observed to be up to 75 W for the sector heat pipe.

Lengthwise temperature distributions of the evaporator section and the majority of the condenser section are nearly uniform. It is apparent that the heat pipe works flawlessly in these sections; nonetheless, there occurs a large temperature gradient near the end of the condenser. This is due to the condenser end being affixed to the outer cylinder of the high speed rotating test apparatus with a screw thread, which creates a heat sink at the condenser end and allows for more heat from the condenser end to be transferred into the outer cylinder. Consequently, because of

the heat transferred to the outer cylinder at the condenser end, the temperature distribution near the condenser end is lowered.

The steady-state operation of the sector heat pipe, with a dimensionless centripetal force of 470, is illustrated in Figure 4.6.

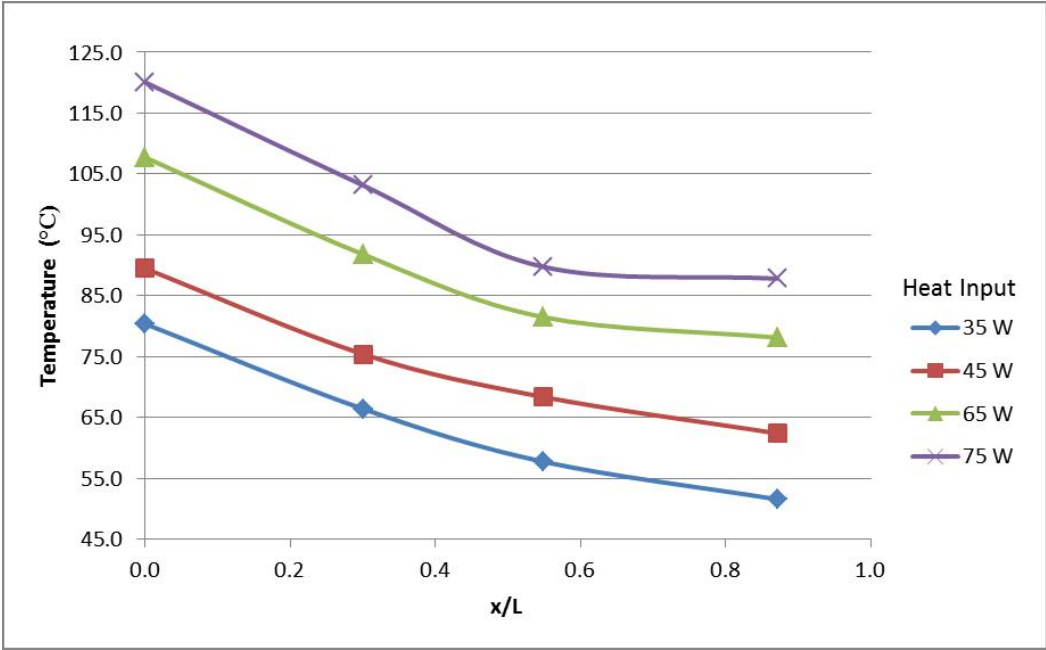


Figure 4.6 Lengthwise Temperature Distributions of the Sector Heat Pipe with Different Heat Inputs ( $f = 30$  Hz)

From Figure 4.6, it is evident that the evaporator section of the sector heat pipe begins working when the heat input reaches 35 W; it is also apparent from the lengthwise temperature distributions in the evaporator section that they are nearly uniform. Due to the working section in the condenser being relatively short, the temperatures along the condenser section drop sharply; this is seen because the temperatures near the condenser end are nearly that of the surrounding air temperature. By increasing the heat input, the operating temperature in the

evaporator section will increase and the vapor flow rate will also increase accordingly. Concurrently, the working section in the condenser will be prolonged to the condenser end, causing the lengthwise temperatures of the condenser section to increase rapidly. Nonetheless, the temperature gradient proximate to the end of the condenser section continues to remain large due to the heat sink formed from the outer cylinder. Considering the high conductivity of the shell (copper), this lowered temperature near the condenser end is understandable.

## 4.2 Effects of Heat Input

As stated previously, heat input has a significant effect on the heat transfer characteristics and temperature distribution of the heat pipe. Once the inner diameter of the heat pipe and dimensionless centripetal force are established, an increase in heat input will cause the lengthwise temperature distribution in the condenser section to be more uniform and the operating temperature in the evaporator section to rise rapidly.

### 1. Single Radially Rotating Miniature Heat Pipe

This is depicted for the single radially rotating miniature heat pipe in Figure 4.7 and Figure 4.8.

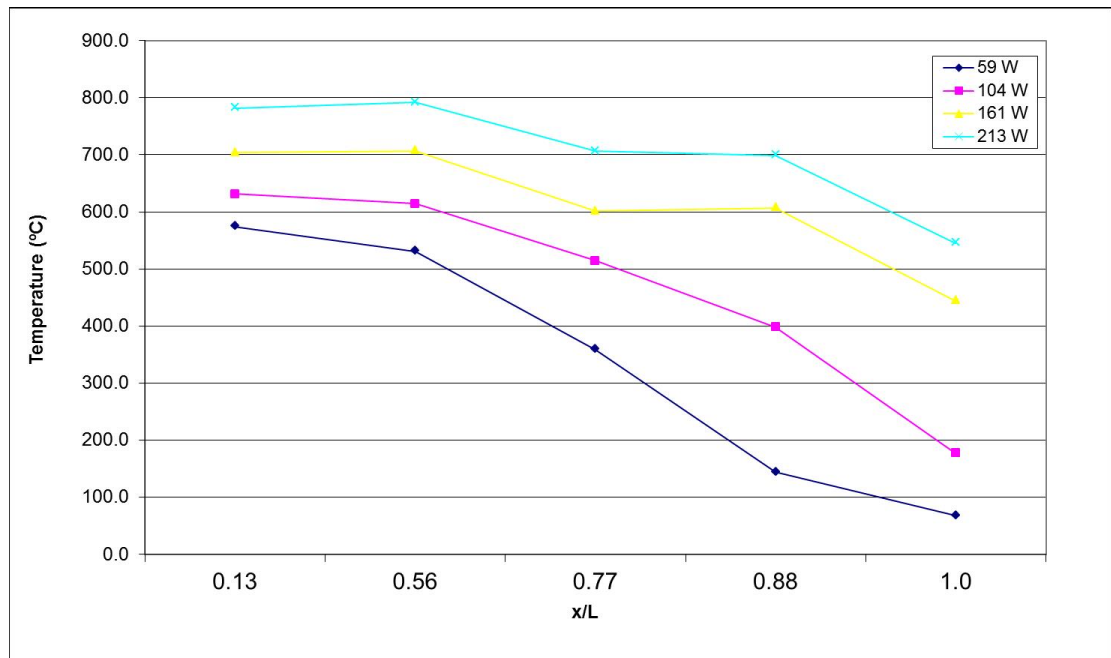


Figure 4.7 Lengthwise Temperature Distribution for Different Heat Inputs ( $d_i = 1.5 \text{ mm}$ ,  $f = 30 \text{ Hz}$ )



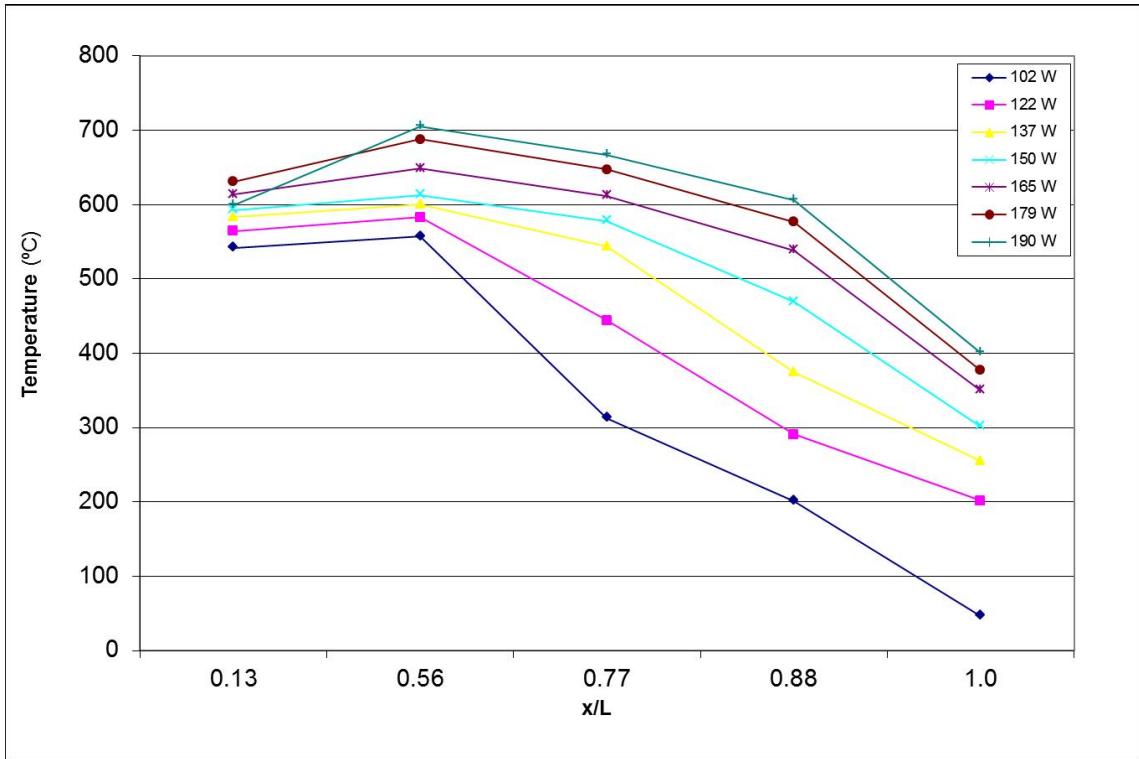


Figure 4.8 Lengthwise Temperature Distribution for Different Heat Inputs ( $d_i=2$  mm ,  $f = 30$  Hz)

Hence, the effective thermal conductance and the heat transfer characteristics are enhanced considerably. If the dimensionless centripetal force is fixed and the heat input is approximately 285 W for the heat pipe with an inner diameter of 1.5 mm and 300 W for the heat pipe with an inner diameter of 2 mm, the lengthwise temperature distribution of the heat pipe remains rather uniform, with the exception of the region near the end of the condenser. It is not uncommon to observe a temperature spike near the evaporator end; this is due to an increase in vapor production in the evaporator section caused by the increase in heat input in the same section of the heat pipe, resulting in additional vapor to flow towards the condenser section. In the condenser section, the velocity of the vapor is gradually diminished to zero and the vapor kinetic

energy may be transformed into thermal energy, which may cause a slight temperature rise in that section. Due to the heat sink at the end of the condenser and the effect of non-condensable gases, the observed temperature at the condenser end is still comparatively low.

## 2. Sector Heat Pipe (Design 2)

The effects of heat input are depicted for the sector heat pipe (design 2) in Figure 4.9 and Figure 4.10.

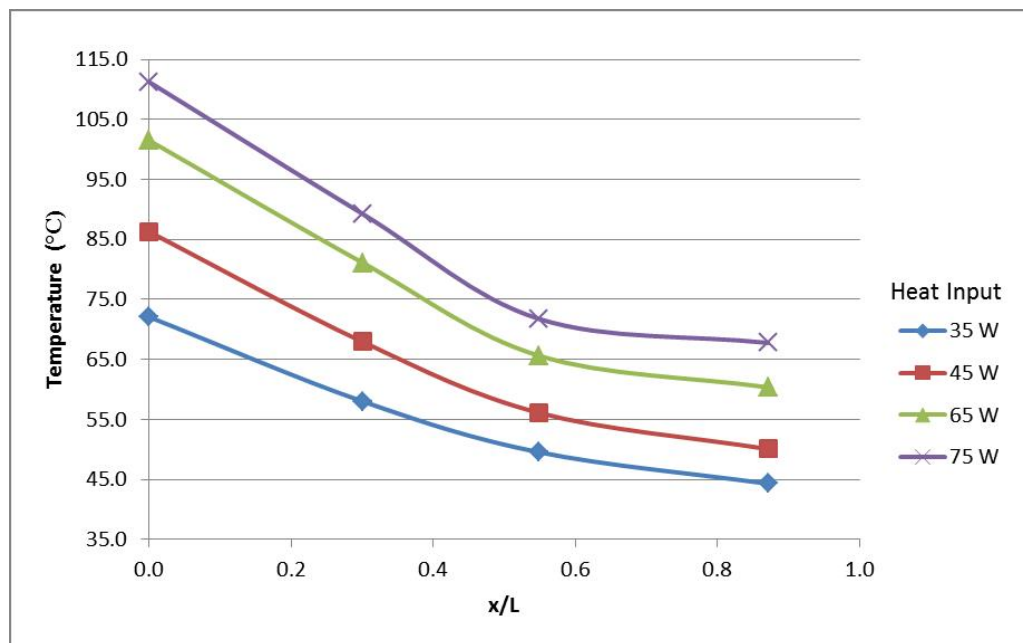


Figure 4.9 Sector Heat Pipe (Design 2) Lengthwise Temperature Distribution ( $f = 30$  Hz)

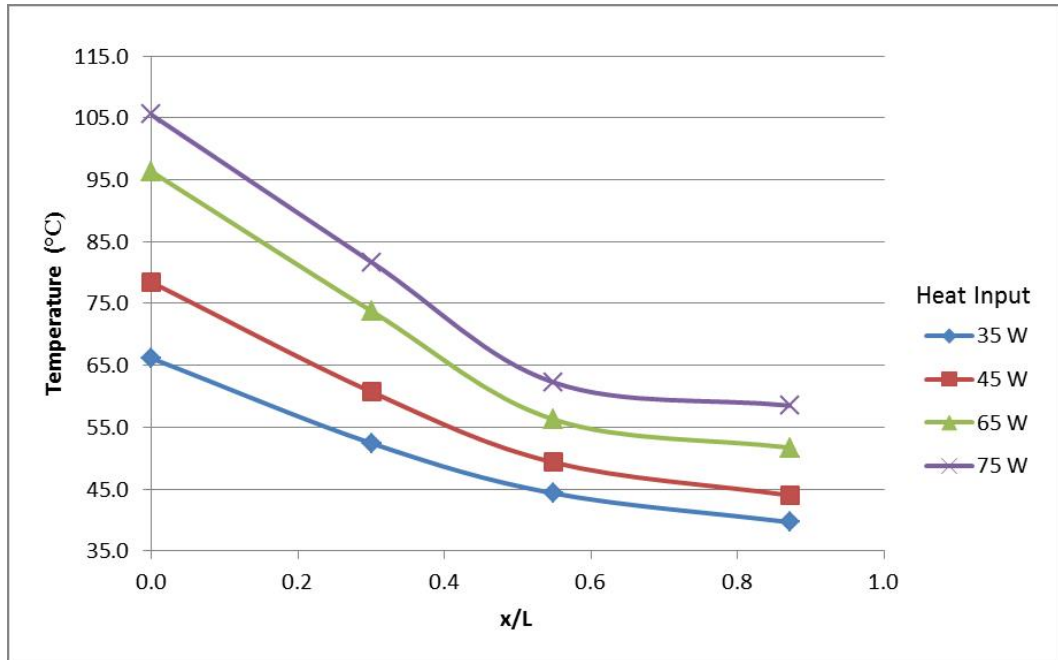


Figure 4.10 Sector Heat Pipe (Design 2) Lengthwise Temperature Distribution ( $f = 45$  Hz)

Because of the convective cooling condition in the condenser of the heat pipe, it can be seen from Figure 4.9 and Figure 4.10 that as the heat input is increased, the heat pipe operational temperature is increased, as a higher temperature in the condenser is required to reject a higher heat load. The slope of the temperature gradient is also improved and therefore the effective thermal conductance and the heat transfer characteristics are enhanced accordingly.

### **4.3 Effects of the Dimensionless Centripetal Forces**

As stated previously during the analysis in Section 2, at higher rotational frequencies, the dimensionless centripetal force becomes a dominant factor for the lengthwise temperature gradient of the heat pipe. If geometrical dimensions of the heat pipe and the heat input are fixed, as the dimensionless centripetal force is increased, the lengthwise temperature gradient and pressure drop of the heat pipe will increase. This occurs because as the dimensionless centripetal force is increased, the film thickness of condensate will decrease. Accordingly, the heat transfer amongst the inner wall of the condenser will be improved. Additionally, as the rotating speed is increased, the heat transfer coefficient associated with the air cooling in the condenser section will increase, which reduces the condenser temperature and increases the temperature gradient along the hat pipe. Hence, the dimensionless centripetal force moderately governs the total lengthwise temperature drop of the heat pipe and the slope of the temperature distribution.

Though the dimensionless centripetal force and the flow rate of cooling air have a similar trend for the total lengthwise temperature drop of the heat pipe, the mechanism creating the alteration of the temperature drop is different. The convection at the surface of the condenser section is increased as the cooling air flow rate is increased, causing the effective working section in the condenser to be reduced, which in turn causes the lengthwise temperature distribution in the condenser to become steeper if the heat flux is kept constant. However, the slope of the lengthwise temperature distribution in the evaporator section will remain constant. Accordingly, the total lengthwise temperature drop for the heat pipe is increased.

Therefore, the proceeding analysis is restricted to the slope of the lengthwise temperature distribution of the evaporator section, to demonstrate the influence of the dimensionless centripetal force.

1. Sector Heat Pipe (Design 2)

When the geometrical dimensions and heat inputs are fixed, and the dimensionless

centripetal force,  $\frac{\omega^2 \bar{Z}_a}{g}$ , is increased from 119 to 1072, the observed lengthwise

temperature distribution for the dimensionless heat pipe length are depicted by Figure 4.11.

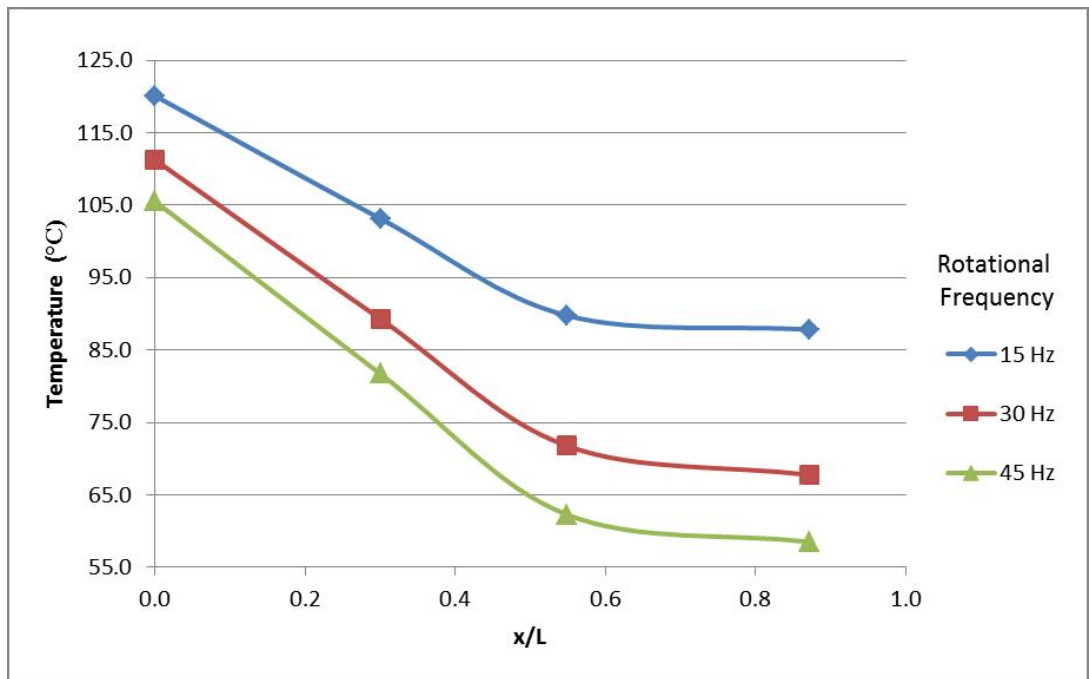


Figure 4.11 Lengthwise Temperature Distributions for Sector Heat Pipe with Different Rotational Frequencies (Q = 75 W)

As can be observed in Figure 4.11, when the rotating frequency is low,  $f = 15\text{Hz}$ , which corresponds to a dimensionless centripetal force,  $\frac{\omega^2 \bar{Z}_a}{g}$ , of 119, the lengthwise slope of the temperature distribution for the evaporator section is comparatively minor, and the lengthwise temperature distribution for the evaporator section is nearly uniform (when the effects of convective heat transfer are taken into consideration). When the rotating frequency is increased, the lengthwise slope of temperature distribution for the evaporator section becomes steeper, with an increased temperature drop in the evaporator section of the heat pipe. At a higher rotating frequency of  $f = 45\text{Hz}$ , equivalent to  $\frac{\omega^2 \bar{Z}_a}{g} = 1072$ , the lengthwise temperature drop of the evaporator section and the slope of the temperature distribution are comparatively high. It can be assumed, that with additional increases in rotating frequencies the trend will become more apparent. However, the temperature in the evaporator section is also reduced due to a lower condenser temperature, which results in a better cooling condition for the evaporator.

#### **4.4 Effects of Fill Volume on the Sector Heat Pipe**

Proper fill volume in heat pipes is essential to proper operation and effectiveness. When a heat pipe does not have the proper fill volume, two issues may occur; the dry-out limitation can be reached, for too little working fluid, or heat pipe flooding due to too much working fluid in the heat pipe.

The dry-out limitation can be reached when the fill volume of the working fluid is very small that could only sustain a comparatively small radial evaporator heat flux. With this scenario, although the falling film of condensate could continue to return back to the evaporator section, the liquid film thickness may approach zero at the top of the evaporator section. Consequently, the entire amount of working fluid may be distributed throughout the heat pipe, either as vapor or as liquid film, causing the necessary pool at the top of the evaporator section without enough liquid. Increasing the heat input in the evaporator section will initiate dry-out in the top of the heat pipe. The size of the dry area will continue to enlarge with increasing heat input. Subsequently, the wall temperature increases progressively, due to evaporation not occurring in the dry area. This phenomenon is illustrated in Figure 4.12, Figure 4.13, and Figure 4.14 for a fill ratio less than 50%. Also, it can be seen from these figures that a 100 % fill volume (the reservoir is mostly filled with liquid) provides the best performance of the heat pipe sector.

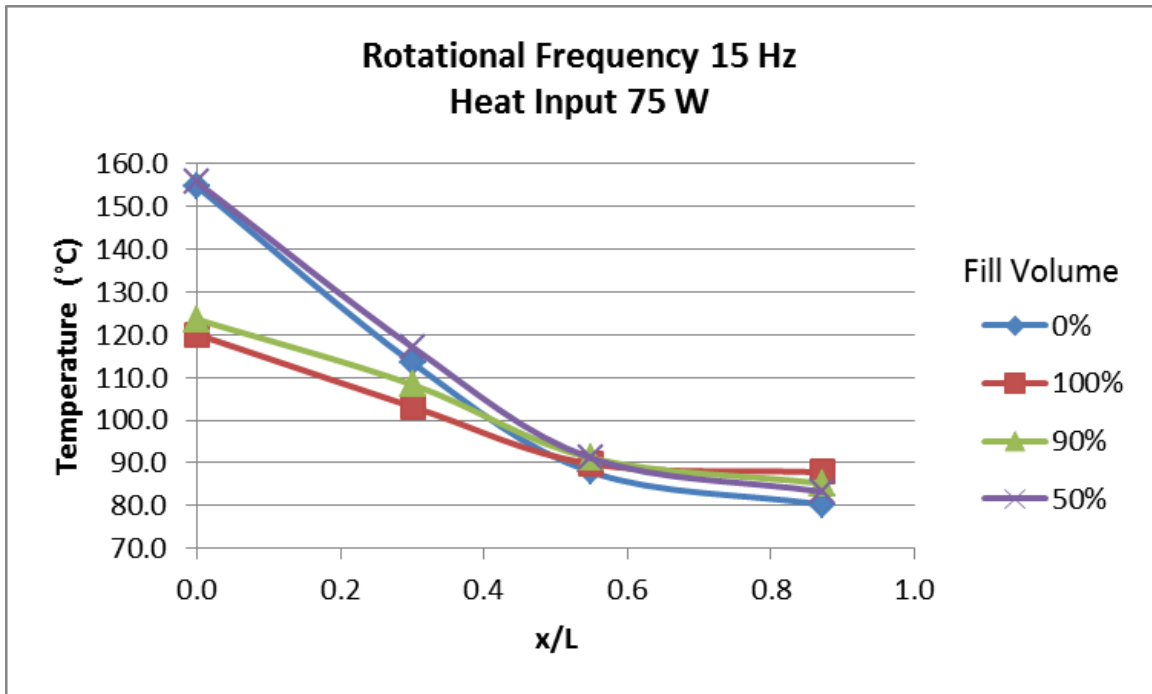


Figure 4.12 Sector Heat Pipe with Heat Input of 75 W ( $f = 15\text{Hz}$ )

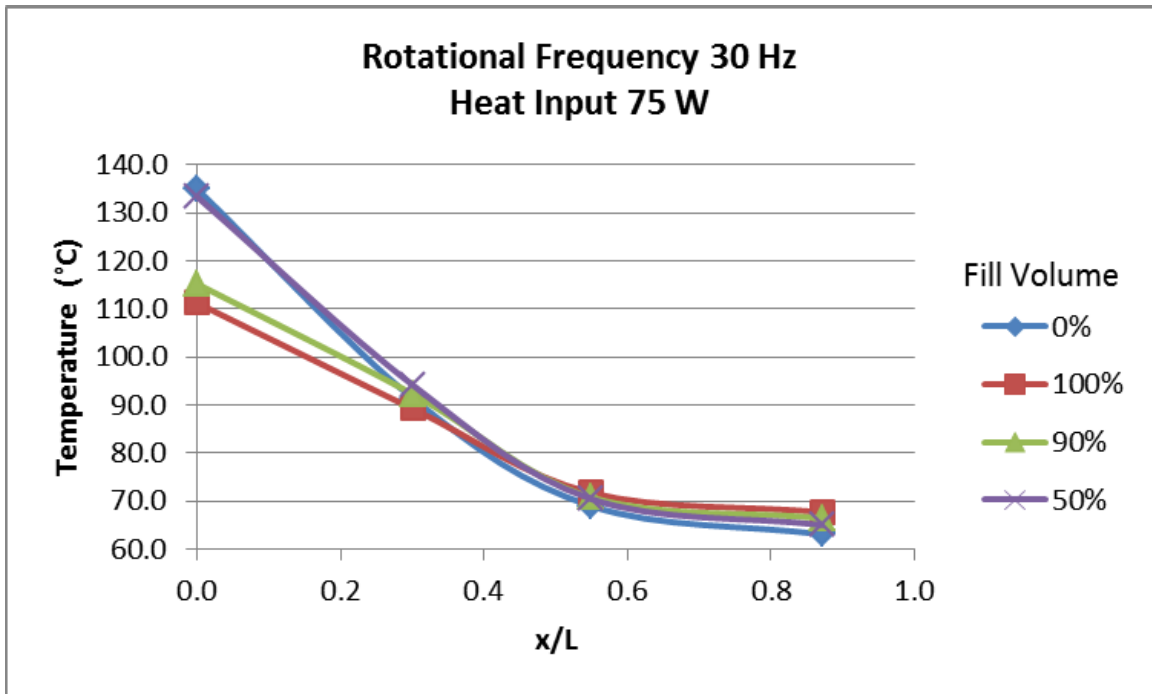


Figure 4.13 Sector Heat Pipe with Heat Input of 75 W ( $f = 30\text{Hz}$ )



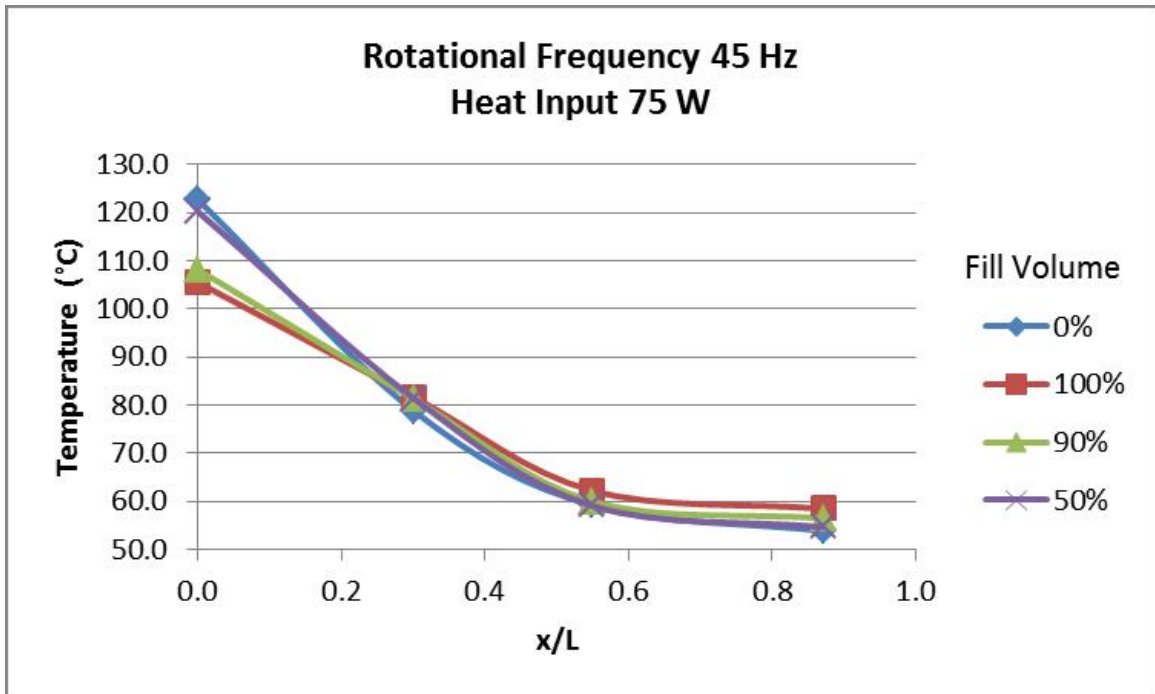


Figure 4.14 Sector Heat Pipe with Heat Input of 75 W ( $f = 45\text{Hz}$ )

The flooding limitation in heat pipes is described as the dry-out of the evaporator section due to the vapor-liquid interfacial shear suspending the condensate in the condenser section. With heat pipe flooding, large transient vapor pressure and temperature fluctuations may occur.

#### 4.5 Comparisons of the Theoretical Results with Experimental Data for the Lengthwise Temperature Distributions

It was observed that non-condensable gases can be very influential on the lengthwise temperature distribution of the heat pipe. With the analytical solution of the single heat pipe, the lengthwise temperature distribution for the heat pipe, without the diffuse effects of non-condensable gases, can be calculated. Accordingly, by modifying the analytical solution of the single heat pipe, the closed form analytical solution of the lengthwise temperature distribution of the heat pipe, with the diffuse effects of non-condensable gases, can be calculated [16]. The computed solutions for these equations are compared with the experimental results under identical operating conditions and geometrical dimensions of the heat pipes.

Table 4-4, Table 4-5, Figure 4.15, and Figure 4.16 illustrate the comparison between the experimental data and the calculated solutions with and without the diffuse effects of non-condensable gases.

Table 4-4 Comparisons of Calculated and Experimental Lengthwise Temperature Distributions of a Single

$$\text{Heat Pipe ( } d_i = 1.5\text{mm, } Q = 250\text{W, } \frac{\omega^2 \bar{Z}_a}{g} = 1881)$$

Dimensionless Single Heat Pipe Length $z/L$	Analytical Solution ( $^{\circ}\text{C}$ )	Analytical Solution with Non-Condensable Gases ( $^{\circ}\text{C}$ )	Experimental Results ( $^{\circ}\text{C}$ )
0.000	754.5	754.5	754.5
0.500	745.5	745.5	730.0
0.750	739.5	680.3	720.0
0.875	737.8	642.2	520.0
1.000	737.2	433.8	235.7

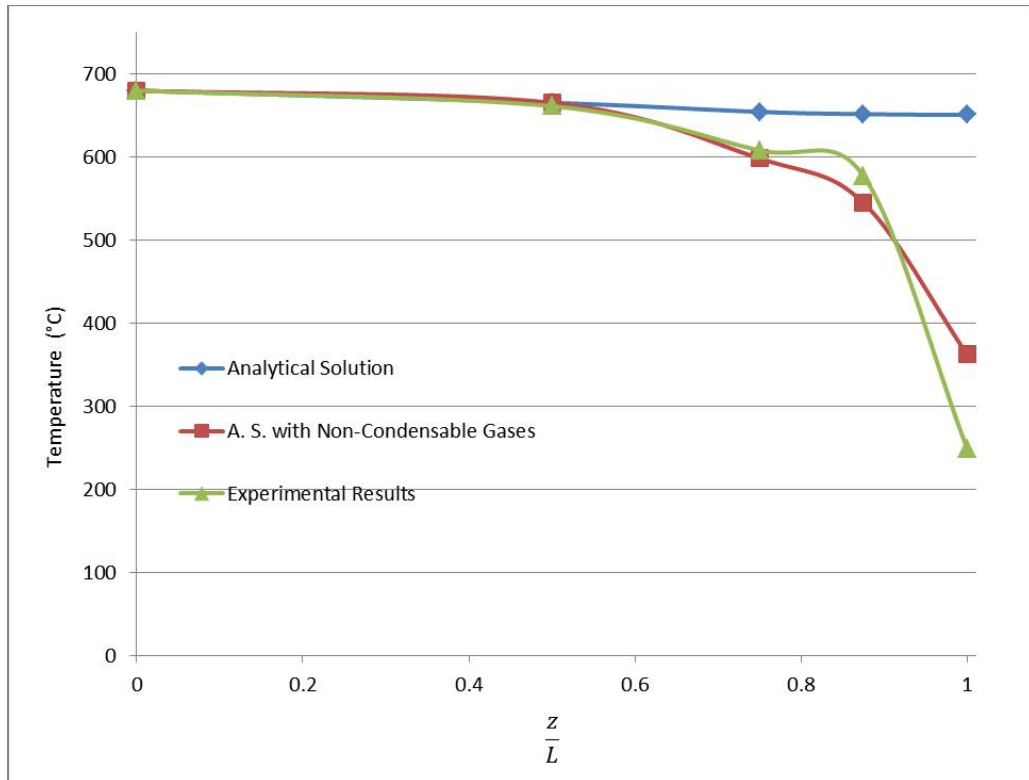


Figure 4.15 Comparisons of Calculated and Experimental Lengthwise Temperature Distributions of a Single Heat Pipe ( $d_i = 1.5mm$ )

Table 4-5 Comparisons of Calculated and Experimental Lengthwise Temperature Distributions of a Single

Heat Pipe ( $d_i = 2.0mm$ ,  $Q = 280W$ ,  $\frac{\omega^2 \bar{Z}_a}{g} = 1881$ )

Dimensionless Single Heat Pipe Length $z/L$	Analytical Solution (°C)	Analytical Solution with Non-Condensable Gases (°C)	Experimental Results (°C)
0.000	680.0	680.0	680.0
0.500	665.3	665.3	661.2
0.750	654.4	598.3	608.0
0.875	651.6	545.0	577.5
1.000	650.7	362.2	248.9

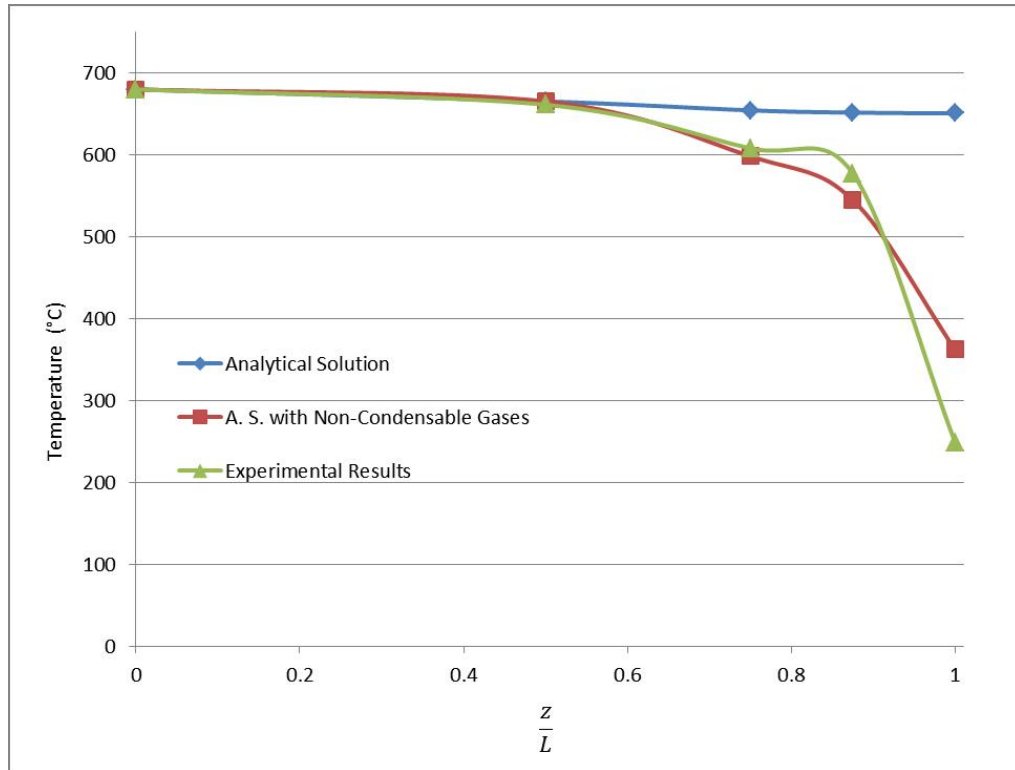


Figure 4.16 Comparisons of Calculated and Experimental Lengthwise Temperature Distributions of a Single Heat Pipe ( $d_i = 2.0mm$ )

It is evident that when using the analytical solution to calculate the temperature distribution, what is given is an ideal prediction neglecting the effects of the non-condensable gases. When using the analytical solution to calculate the lengthwise temperature distribution for the heat pipe, only the friction of the liquid-vapor interface and the centripetal force effect on the vapor are taken into account. Consequently, at higher operating temperatures, the lengthwise temperature drops for the heat pipe are very minor, making the slope of the temperature distribution approximately zero, as illustrated with Figure 4.15.

When coordinating the experimental values with the analytical ones, large discrepancies are observed between the experimental results and those calculated from the analytical equations, particularly with the area closest to the condenser end.

For the lengthwise temperature distribution of the heat pipe, with a flat front for the vapor-gas interface, the length dominated by non-condensable gases in the condenser section,  $L_{c,n}$ , is 4 mm; as calculated by modifying Equations (2.69), (2.70) and (2.71) to account for non-condensable gases. When comparing the experimental results to the closed form calculations shown in Table 4-4 and Figure 4.15, it is apparent that the calculated values that take into account non-condensable gases are in better agreement with the general analytical solution. This is apparent with the results for the entire evaporator section and the majority of the condenser section. The main discrepancy comes from a large deviation occurring at the condenser end, due to the condenser end cap of the heat pipe forming a large heat sink with the outer cylinder of the rotating experimental apparatus. Accordingly, the experimental data at the end of the condenser is caused to be lower than the calculated values from the closed form solution.

#### 4.6 Determination of the Effective Thermal Conductivity

Because of the thick shell and high-conductivity of the copper shell material associated with sector heat pipe design 2, the true performance of the sector heat pipe, which is largely associated with the vapor space of the sector, has been significantly blurred. To determine the effective thermal conductance of the sector heat pipe, a simulation was performed using SolidWorks Simulation. This was accomplished by constructing two three-dimensional models using SolidWorks. The first was a representation of the empty sector heat pipe, a sectional view of the model is depicted in Figure 4.17.

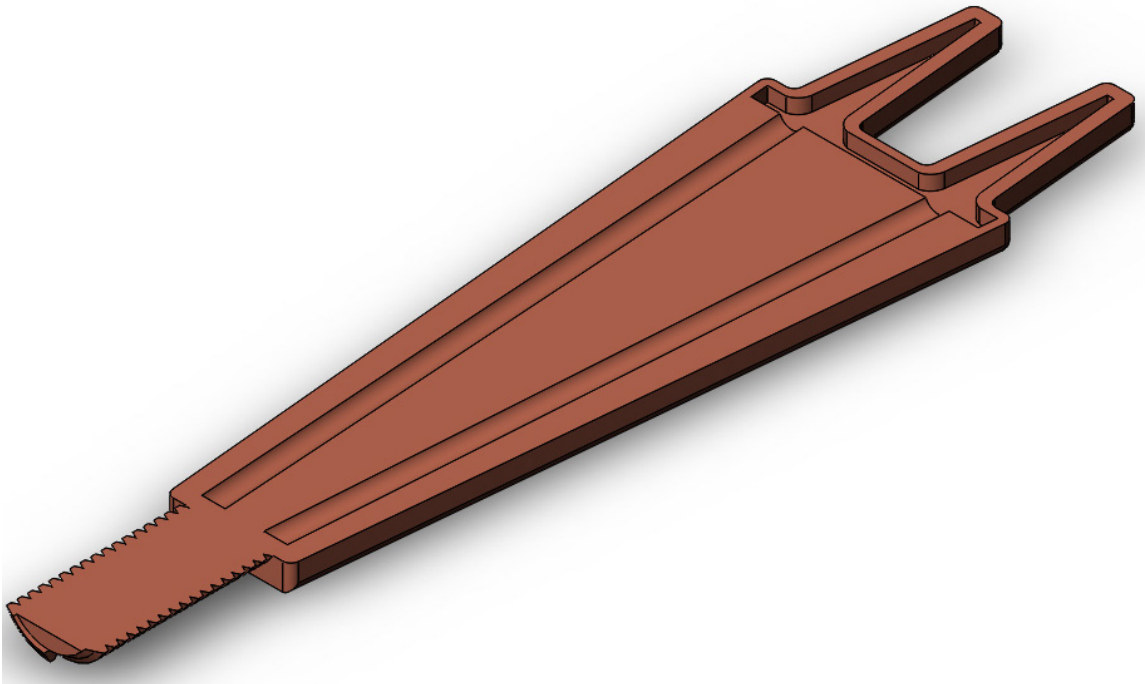


Figure 4.17 Sectional View of Empty Sector Heat Pipe

The second three-dimensional model was constructed in the exact same manner as the empty sector heat pipe, with the addition of a conductive solid material inserted into the

cavity of the sector heat pipe. Figure 4.18 depicts a sectional view of the second three-dimensional model.

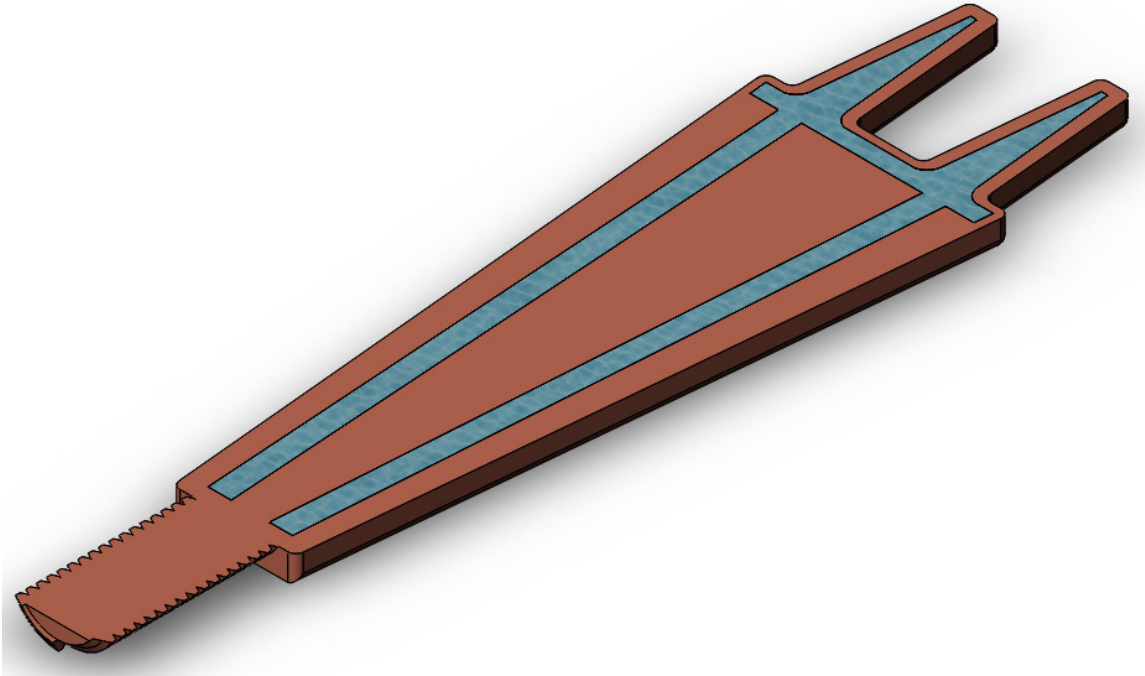


Figure 4.18 Sectional View of Sector Heat Pipe with a Conductive Solid within the Cavity

The performance of the empty model was then simulated in SolidWorks Simulation and a 75 Watt heat load was applied to the dovetail section of the sector. Many iterations were conducted until the probe points on the sector heat pipe matched the experimental results. The same parameters and heat load were then applied to the sector heat pipe with the conductive material filled cavity.

To determine the effective thermal conductivity of the sector heat pipe, the thermal conductivity of the conductive solid was varied until the probe points matched the experimental results for the 100% reservoir filled volume. The effective thermal

conductivity of the sector heat pipe was then determined to be  $\kappa \cong 3500 \frac{W}{m \cdot K}$ , which is

almost 10 times as high as that of standard copper.

Figure 4.19 and Figure 4.20 depict the resulting three-dimensional thermal plots of the simulation. As can be seen with the thermal plots, the empty sector heat pipe gives an expected linear temperature profile. While the filled sector heat pipe gives an almost flat temperature profile, which is similar to that of single miniature rotating heat pipes.



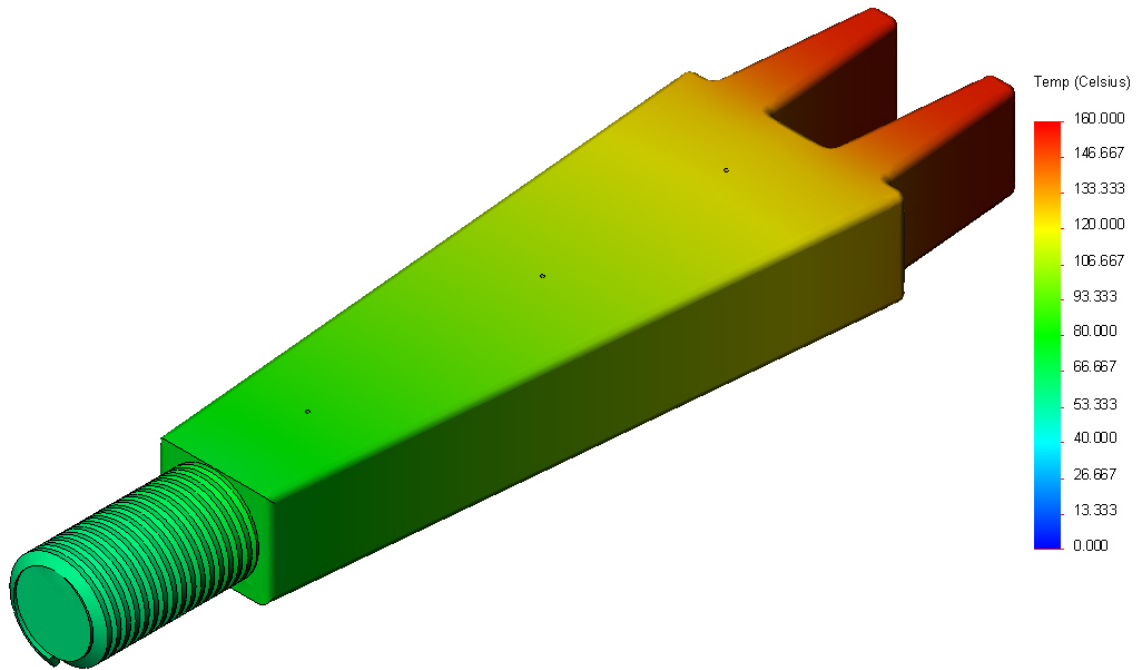


Figure 4.19 Three-dimensional Temperature Plot of Empty Sector Heat Pipe

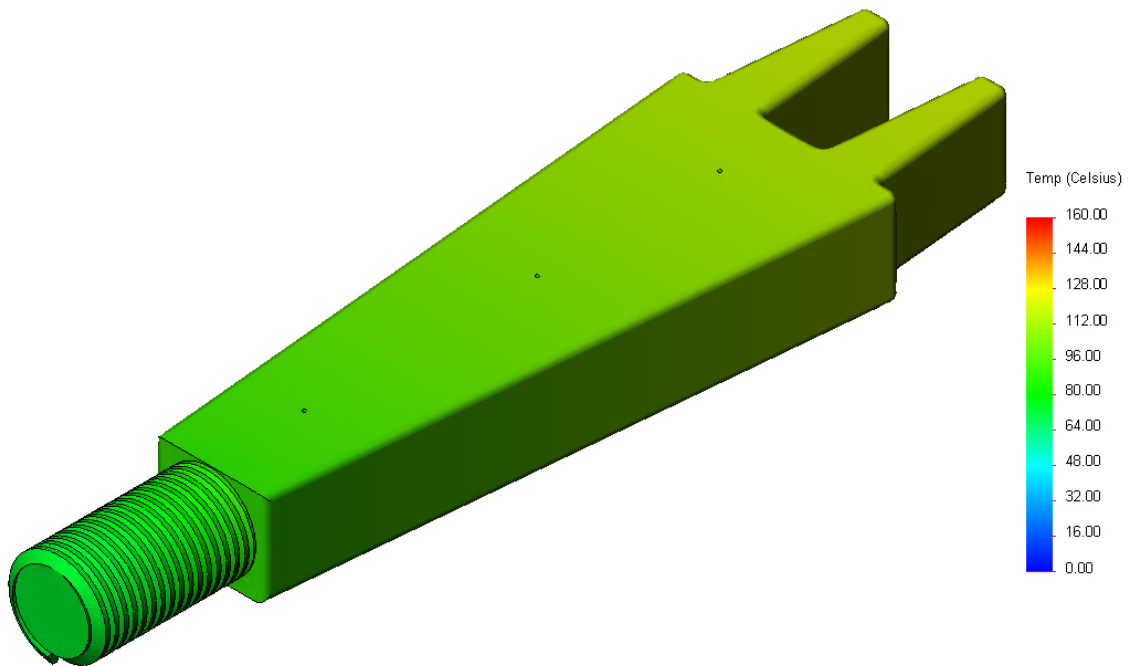


Figure 4.20 Three-dimensional Temperature Plot of Filled Sector Heat Pipe

#### 4.7 Error Analysis for Experimental Measurements

The experimental and calculated lengthwise temperature distributions of the heat pipe are in reasonable agreement; however, considerable deviations exist in the condenser section. These deviations could be due to many influential factors. An error analysis is postulated in this section, and the discrepancy amongst the experimental results and calculated values could be credited to the following influences:

1. The errors in the calculated values could be attributed to the one-dimensional heat transfer and flow modeling. The calculated values are established entirely on one-dimensional heat transfer and flow generalizations, whereas the heat transfer and flow characteristics in actual heat pipes have three-dimensional characteristics. Observing that the flow passages in radially rotating miniature heat pipes is very small, one-dimensional heat transfer and flow modeling would be adequate to portray the major characteristics of the flow and heat transfer. Nevertheless, the one-dimensional simplification will create particular deviations amongst the experimental and calculated results.
2. Errors can also arise by the experimental apparatus, specifically, the interference created by the vibrations of experimental apparatus. Ideally, because the flow passages in a single radially rotating miniature heat pipe are very small, the heat transfer and flow characteristics can be described by a one-dimensional model. However, during actual testing, as the frequency of rotation is increased, relatively large vibrations in the experimental apparatus are produced. This creates interruptions in the flow and heat transfer characteristics. Consequently, three-dimensional characteristics for the flow and heat transfer may have been

created during testing, which amplifies the deviations between the experimental and calculated results.

3. Errors can also arise from the uncertainties in the heat input and temperature measurements.

The following devices and their uncertainties were used for all experiments.

- i. Type K thermocouples, which have an uncertainty of 0.5%
- ii. Slip Ring, used to connect to the thermocouples, has an uncertainty of 0.5%
- iii. High Temperature Cement, used to attach the thermocouples. Errors could arise from the contact thermal resistance and can be assumed to be 1%.

Devices particular to the Single and Sector (Design 1) Heat Pipe Experiments

- i. HP34970 Data Acquisition Device, used to record the thermocouple readings, has an uncertainty of 0.2%
- ii. Radio Shack Multi-meter, for measuring voltage and current, has an uncertainty of 0.5%

Devices particular to the Sector (Design 2) Heat Pipe Experiments

- i. National Instruments NI-9213 module, used to measure the thermocouple readings, has an uncertainty of 0.03%
- ii. National Instruments NI-9219 module, used to measure the voltage readings from the current meter and the power supply of the heater, has an uncertainty of 0.3%
- iii. Fluke 80i-110s, used to measure the current of the heater, has an uncertainty of less than 3% of reading + 50 mA

iv. Milwaukee 2277-20 Laser Temperature gun, used to measure the surface temperature of the evaporator insulation, has an uncertainty of 1.5%

The total maximum uncertainty for the temperature measurement for the single and sector heat pipe (design 1) is approximately 2.2% and 2.03% for the sector heat pipe (design 2).

## **5. Conclusions and Recommendations**

### **5.1 Conclusions**

In this dissertation, extensive studies of radially rotating miniature heat pipes have been conducted both experimentally and analytically. The analytical solutions for the film thickness, condensate film and vapor flows, and lengthwise temperature distribution for the heat pipe were calculated, including the diffuse effects of non-condensable gases on the temperature distribution. Extensive experimental tests on both single radially rotating miniature heat pipes and a new sector heat pipe were conducted, with distinctive instrumental parameters varied. Conferring to the experimental and analytical studies reported in this dissertation, the following conclusions can be made:

1. Multiple radially rotating miniature heat pipes can be integrated into a device, such as a disk, and connected with a common reservoir. With its simple structure, lower manufacturing costs, ability to withstand strong vibrations, high effective thermal conductance, and high heat transfer capacity, the radially rotating miniature heat pipe is feasible for integration into large and complex structures.
2. The effective thermal conductance of the sector heat pipe is nearly 10 times that of the copper, indicating that the configuration of the interconnected heat pipe sharing a common reservoir is feasible. If the working fluid of the sector heat pipe is replaced by a liquid metal working fluid at a high temperature, the effective thermal conductance of the sector heat pipe should be even much higher.
3. With a large revolving radius or a moderately high rotational speed, the maximum temperature drop across the liquid film is negligible. Conversely, a lower heat pipe operating temperature may increase the liquid film temperature drop.

4. The cross-sectional area of the vapor flow is determined by the heat pipe inner diameter. Accordingly, for a larger heat pipe the friction of the vapor flow causes a lower temperature drop. Conversely, the friction of the vapor flow will be larger for smaller inner diameter heat pipes, causing a larger lengthwise temperature drop.
5. The heat transfer characteristics and lengthwise temperature distribution of the heat pipe are significantly influenced by the heat input. When the dimensionless centripetal force and inner diameter of the heat pipe are fixed, an increase in heat input will cause the operating temperature in the evaporator section to rise, increasing the length of the working section in the condenser, and increase the temperature in the condenser section. Thus, the effective thermal conductance and heat transfer characteristic can be improved significantly. Nonetheless, if a heat pipe is subjected to an excessively high heat input its heat transfer limitation will be reached.
6. The dimensionless centripetal force is very influential in the lengthwise temperature drop of the heat pipe. The pressure and lengthwise temperature drop of the heat pipe will increase as the rotational speed (concurrently the dimensionless centripetal force) is increased. At high rotational speeds, the centripetal forces become a dominant factor, becoming particularly evident in comparatively large diameter heat pipes.

## 5.2 Recommendations

1. The sector heat pipe should be investigated with larger individual heat pipe inner diameters.
2. Investigation of the sector heat pipe should be made with the container material being 304 Stainless Steel and sodium as the working fluid.
3. The body to cavity ratio of the sector heat pipe should be further examined. In order to determine the limit where the effectiveness of the heat pipe in a body is zero.
4. The testing apparatus should be upgraded to allow for more thermocouples, the housing enlarged to allow for larger test specimens, and the motor upgraded to allow for higher rotational speeds.
5. Some detailed analyses on the sector heat pipe should be undertaken. The experimental results from this dissertation could be employed to verify the analytical model. Once the model analysis is successful, it could provide a very useful tool for sector heat pipe design.

## References

- [1] D. Reay and P. Kew, *Heat Pipes Theory, Design and Applications*, 5 ed., Burlington, MA: Butterworth-Heinemann, 2006.
- [2] A. Faghri, *Heat Pipe Science and Technology*, Washington D.C.: Taylor & Francis, 1995.
- [3] Y. Lee and A. Bedrossian, "The characteristics of heat exchangers using heat pipes or thermosyphons," *International Journal of Heat and Mass Transfer*, vol. 21, no. 2, pp. 221-229, 1978.
- [4] A. Faghri, M. M. Chen and M. Morgan, "Heat Transfer in Two Phase Closed Conventional and Concentric Annular Thermosphon," *American Society of Mechanical Engineers*, vol. 111, no. Heat Transfer, pp. 611-618, 1989.
- [5] A. Faghri and S. Thomas, "Performance Characteristics of a Concentric Annular Heat Pipe, Part I, Experimental Prediction and Analysis of the Capillary Limit," *ASME Journal of Heat Transfer*, vol. 111, no. 4, pp. 844-850, 1989.
- [6] M. Groll and J. P. Kirkpatrick, "Heat pipes for spacecraft temperature control; an assesment of the state of the art," in *Second International Heat Pipe Conference*, Bologna, Italy, 1976.
- [7] J. Ku, E. J. Kroliczek and R. McIntosh, "Analytical Modeling of the Capillary Pumped Loop," in *6th International Heat Pipe Conference*, Grenoble, France, 1987.
- [8] P. Marto, "Performance Characteristics of Rotating Wickless Heat Pipes," in *2nd International Heat Pipe Conference*, Bologna, 1976.
- [9] y. Cao, Q. Wang and J. Ling, "Operating Limitation of Reciprocating Heat Pipes for Piston Cooling Applications," in *ASME International Mechanical Engineering Congress and Exposition*, San Francisco, 1995.
- [10] A. Rehman, "Turbine blade cooling design," 08 02 2013. [Online]. Available: <http://www.bestinnovativesource.com/2013/02/08/turbine-blade-cooling-design/>. [Accessed 31 05 2013].
- [11] "Film Cooling of Turbine Blades in Gas Turbines," [Online]. Available: <http://littwww.epfl.ch/research/htprojects/filmcool.htm>. [Accessed 31 05 2013].



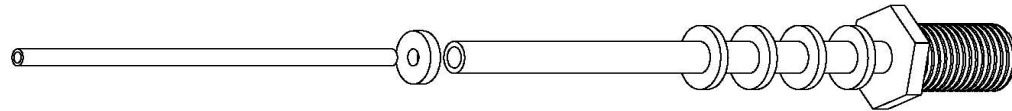
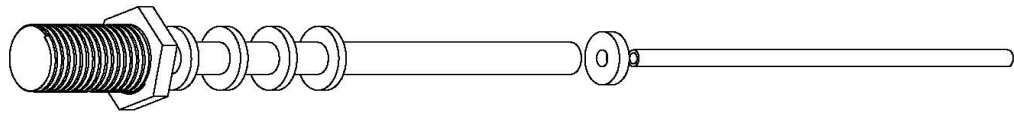
- [12] H. Cohen, G. F. Rogers and H. I. Saravanamuttoo, *Gas Turbine Theory*, England: Longman Scientific & Technical, 1994.
- [13] Y. Cao, "Rotating Micro/Miniature Heat Pipes for Turbine Blade Cooling Applications," AFOSR Contractor and Grantee Meeting on Turbulence and Internal Flows, Atlanta, 1996.
- [14] Y. Cao, J. Ling and W. S. Chang, "Analyses of Liquid and Vapor Flows in a Miniature Radially Rotating Heat Pipe for Turbine Blade Cooling Applications," in *11th International Heat and Mass Transfer Conference*, South Korea, 1998.
- [15] Y. Cao, W. S. Chang and C. D. MacArthur, "An Analytical Study of Turbine Disk Incorporating Radially Rotating Heat Pipes," in *IMECE*, Anaheim, 1998.
- [16] J. Ling and Y. Cao, "Closed Form Analytical Solutions for the Radially Rotating Miniature High-Temperature Heat Pipes Including Non-Condensable Gas Effects," *International Journal of Heat and Mass Transfer*, vol. 43, no. 19, pp. 3661-3671, 2000.
- [17] J. Ling, Y. Cao and W. S. Chang, "Analysis of Radically Rotating High-Temperature Heat Pipes for Turbomachinery Application," *ASME Journal of Engineering for Gas Turbines and Power*, vol. 121, pp. 306-312, 1999.
- [18] Y. Cao and W. S. Chang, "Analyses of Heat Transfer Limitations of Radially Rotating Heat Pipes for Turbomachinery Applications," in *AIAA 32nd Thermophysics Conference*, Atlanta, 1997.
- [19] S. W. Chi, *Heat Pipe Theory and Practice: a Sourcebook*, New York: Hemisphere Publishing, 1976.
- [20] R. T. Harman, *Gas Turbine Engineering*, New York: John Wiley & Sons, Inc, 1981.
- [21] G. P. Peterson, *An Introduction to Heat Pipes*, New York: John Wiley & Sons, Inc., 1994.
- [22] Y. Cao and J. Ling, "An Experimental Study of Micro Radially Rotating Heat Pipes with Water as the Working Fluid," in *ASME MNHT2008, Micro/Nano Scale International Heat Transfer Conference*, Tainan, Taiwan, 2008.
- [23] S. V. Ekkad, Y. Huang and J. C. Han, "Detailed Heat Transfer Distributions in Two-Pass Smooth and Turbulated Square Channels With Bleed Holes," *Fundamentals of Augmented Single-Phase Convection*, vol. 330, pp. 133-140, 1996.

- [24] A. Faghri, S. Gogineni and S. Thomas, "Numerical Analysis of Vapor Flow in an Axially Rotating Heat Pipe," *American Society of Mechanical Engineers*, vol. 221, pp. 11-21, 1992.
- [25] J. C. Han, Y. M. Zang and K. Kalkuehler, "Uneven Wall Temperature Effect on Local Heat Transfer in a Rotating Two-Pass Square Channel With Smooth Walls," *American Society of Mechanical Engineers*, vol. 115, no. Heat Transfer, pp. 912-920, 1993.
- [26] J. C. Han, Y. M. Zang and C. P. Lee, "Influence of Surface Heating Condition on Local Heat Transfer in a Rotating Square Channel With Smooth Walls and Radial Outward Flow," *American Society of Mechanical Engineers*, vol. 116, no. Turbomachinery, pp. 149-158, 1994.
- [27] M. Streby, P. Ponnappan, J. Leland and J. Bean, "Design and Testing of a High Speed Rotating Heat Pipe," *Institute of Electrical and Electronics Engineers*, vol. 96301, pp. 1453-1458, 1996.
- [28] W. W. Bathie, *Fundamentals of Gas Turbines*, Chichester: John Wiley & Sons, Inc, 1996.
- [29] Y. Cao, J. Ling and Q. Wang, "Analytical and Experimental Investigations for the Critical Working Frequency of Reciprocating Heat Pipes with Piston Cooling Applications," *ALCHE Symposium Series*, vol. 92, pp. 317-323, 1996.
- [30] T. Daniels and F. Al-Jumaily, "Investigations of the Factors Affecting the Performance of a Rotating Heat Pipe," *International Journal of Heat and Mass Transfer*, vol. 18, pp. 961-973, 1975.
- [31] P. D. Dunn and D. A. Reay, *Heat Pipe*, New York: Pergamon Press, 1982.
- [32] V. H. Gray, "The Rotating Heat Pipe - A Wickless, Hollow Shaft for Transferring Heat Fluxes," in *ASME / AICHE Heat Transfer Conference*, Minneapolis, 1969.
- [33] C. Harley and A. Faghri, "Two Dimensional Rotating Heat Pipe Analysis," *American Society of Mechanical Engineers*, vol. 117, no. Heat Transfer, pp. 418-426, 1995.
- [34] J. Ling, Y. Cao and Q. Wang, "Critical Working Frequency of Reciprocating Heat Transfer Devices in Axially Reciprocating Mechanisms," *International Journal of Heat and Mass Transfer*, vol. 41, pp. 73-80, 1998.

- [35] J. Ling, Y. Cao and Q. Wang, "Transversally Reciprocating Heat Pipe (TRHP) and its Application in Cutting Tools," in *ASME 32nd National Heat Transfer Conference*, Baltimore, 1997.
- [36] J. Ling, Y. Cao and Q. Wang, "Experimental Investigations and Correlations for the Performance of Reciprocating Heat Pipe," *Heat Transfer Engineering*, vol. 17, no. 4, pp. 34-35, 1996.
- [37] S. Maezawa, Y. Suzuki and A. Tsuchida, "Heat Transfer Characteristics of Disk Shaped Rotating, Wickless Heat Pipes," in *4th International Heat Pipe Conference*, London, 1981.
- [38] H. Nomoto and et al, "The Advanced Cooling Technology for the 1500 C Class Gas Turbines: Steam Cooled Vanes and Air Cooled Blades," *ASME Journal of Engineering for Gas Turbines and Power*, vol. 119, pp. 624-632, 1997.
- [39] E. R. Norster, *Combustion and Heat Transfer in Gas Turbine Systems*, Oxford, New York: Pergamon Press, 1969.
- [40] D. G. Shepherd, *Aerospace Propulsion*, New York: American Eseevier, 1972.
- [41] N. V. Suryanarayana, *Engineering Heat Transfer*, New York: West Publishing Company, 1995.
- [42] J. H. Wagner, B. V. Johnson and T. J. Hajek, "Heat Transfer in Passages with Smooth Walls and Radial Outward Flow," *American Society of Mechanical Engineers*, vol. 113, no. Heat Transfer, pp. 42-51, 1991.
- [43] B. D. Marcus, "Theory and Design of Variable Conductance Heat Pipes," Ames Research Center, Washington, D.C., 1972.
- [44] J. Ling, Y. Cao and W. S. Chang, "Analysis of Radially Rotating High Temperature Heat Pipes for Turbomachinery Application," *ASME Journal of Engineering for Gas Turbines and Power*, vol. 121, 1999.
- [45] J. Ling and Y. Cao, "Closed Form Analytical Solutions for the Radially Rotating Miniature High Temperature Heat Pipes Including Non-Condensable Gas Effects," *International Journal of Heat and Mass Transfer*, vol. 43, no. 19, pp. 3661-3671, 2000.

## Appendix

**Appendix A**  
**Mechanical Drawing**



NAME		DATE	TITLE:	
DRAWN	Brian D. Reding II	01 MAR 07	1.5 mm Single Radially Rotating Miniature Heat Pipe Assembly	
ENG APPR.				
MFG APPR.				
Q.A.				
COMMENTS:			SIZE	DWG. NO.
			<b>A</b>	1
			SCALE: 1:1	SHEET 1 OF 4

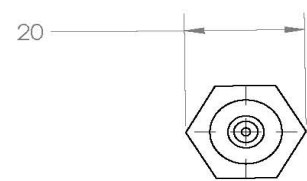
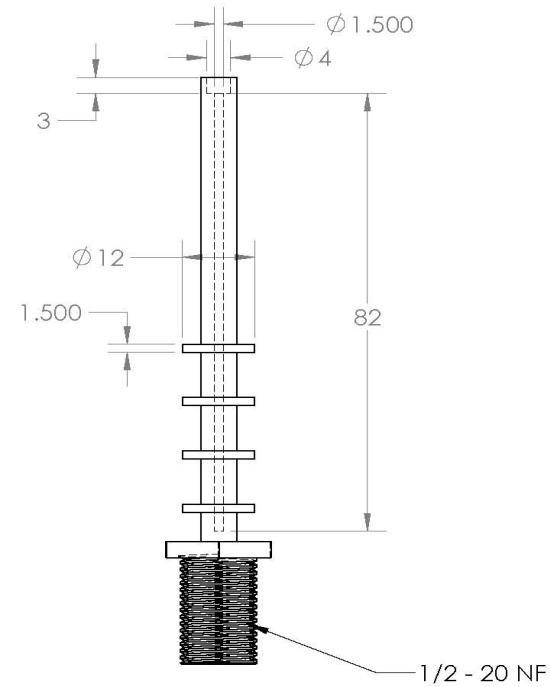
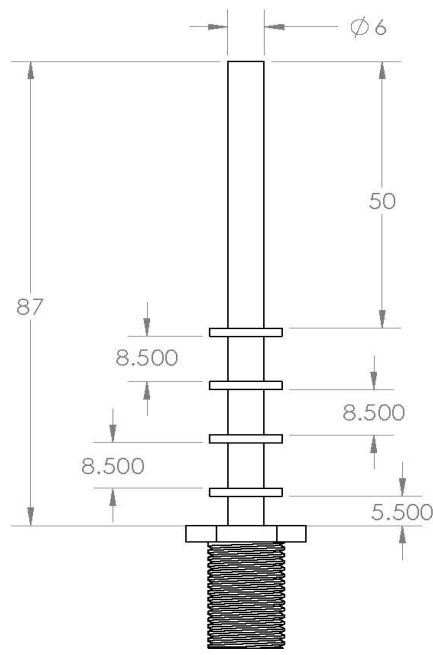
5

4

3

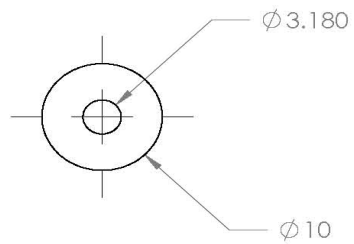
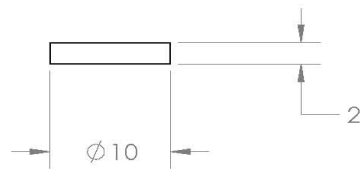
2

1



NAME		DATE	TITLE:	
DRAWN	Brian D. Reding II	01 MAR 07	1.5 mm Heat Pipe Body	
ENG APPR.				
MFG APPR.				
Q.A.				
COMMENTS:			SIZE	DWG. NO.
Material: 304 Stainless Steel			<b>A</b>	2
SCALE: 1:1		Units: mm	SHEET 2 OF 4	

5 4 3 2 1



NAME		DATE	TITLE:	
DRAWN	Brian D. Reding II	01 MAR 07	1.5 mm Heat Pipe End Cap	
ENG APPR.				
MFG APPR.				
Q.A.				
COMMENTS:			SIZE	DWG. NO.
Material: 304 Stainless Steel			<b>A</b>	3
SCALE: 2:1		Units: mm	SHEET 3 OF 4	

5

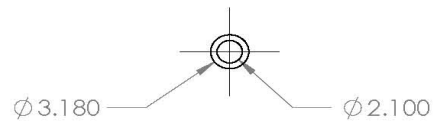
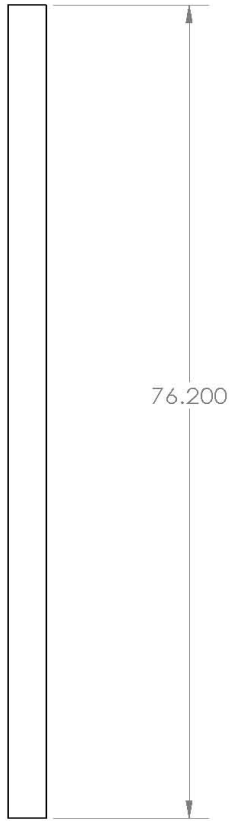
4

3

2

1





		NAME	DATE		
DRAWN	Brian D. Reding II	01 MAR 07	TITLE:		
ENG APPR.			1.5 mm Heat Pipe Fill Tube		
MFG APPR.					
Q.A.					
COMMENTS:			SIZE	DWG. NO.	
Material: 304 Stainless Steel			<b>A</b>	4	
SCALE: 2:1		Units: mm	SHEET 4 OF 4		

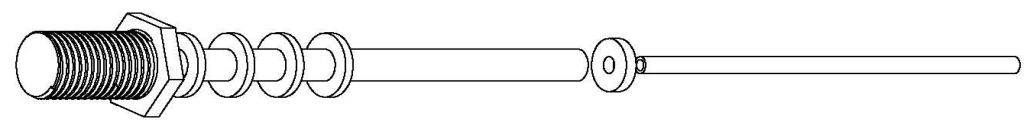
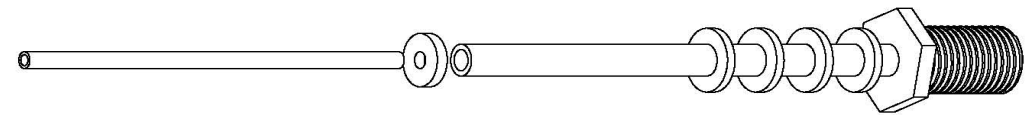
5

4

3

2

1



NAME		DATE	TITLE:	
DRAWN	Brian D. Reding II	01 MAR 07	2mm Single Radially Rotating Miniature Heat Pipe Assembly	
ENG APPR.				
MFG APPR.				
Q.A.				
COMMENTS:			SIZE	DWG. NO.
			<b>A</b>	1
			SCALE: 1:1	SHEET 1 OF 4

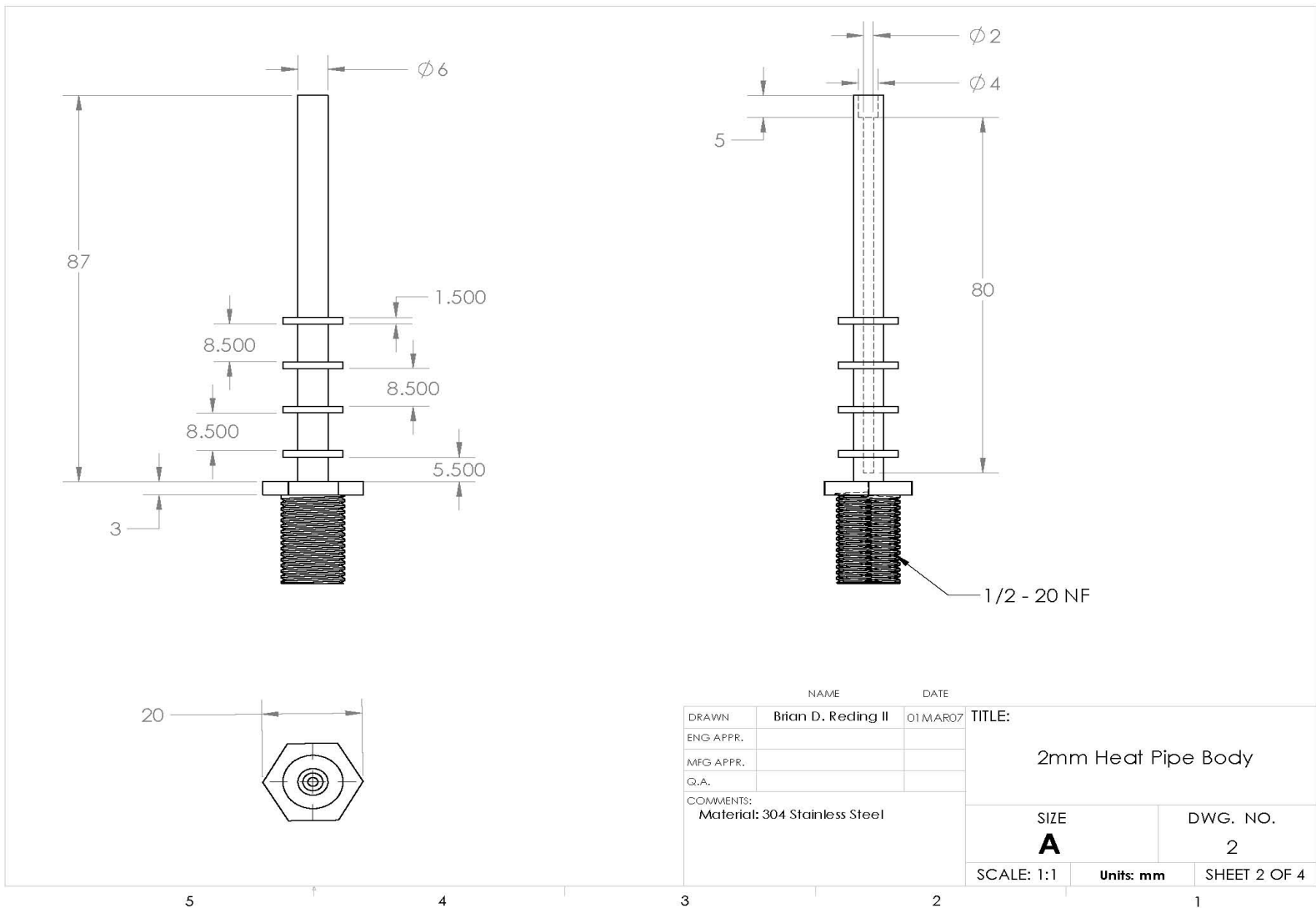
5

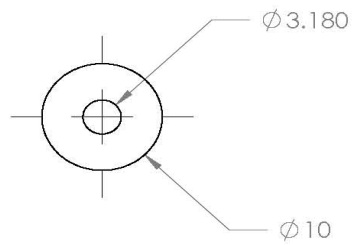
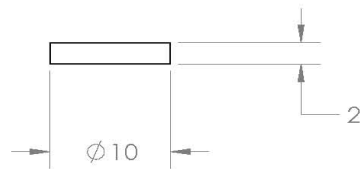
4

3

2

1





NAME		DATE	TITLE:	
DRAWN	Brian D. Reding II	01 MAR 07	2mm Heat Pipe End Cap	
ENG APPR.				
MFG APPR.				
Q.A.				
COMMENTS:			SIZE	DWG. NO.
Material: 304 Stainless Steel			<b>A</b>	3
SCALE: 2:1		Units: mm	SHEET 3 OF 4	

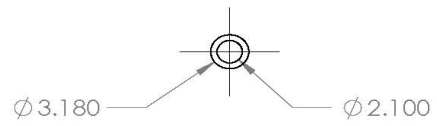
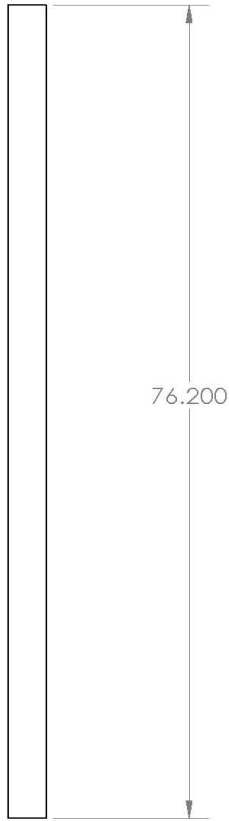
5

4

3

2

1



NAME		DATE	TITLE:	
DRAWN	Brian D. Reding II	01 MAR07	2mm Heat Pipe Fill Tube	
ENG APPR.				
MFG APPR.				
Q.A.				
COMMENTS:			SIZE	DWG. NO.
Material: 304 Stainless Steel			<b>A</b>	4
SCALE: 2:1		Units: mm	SHEET 4 OF 4	

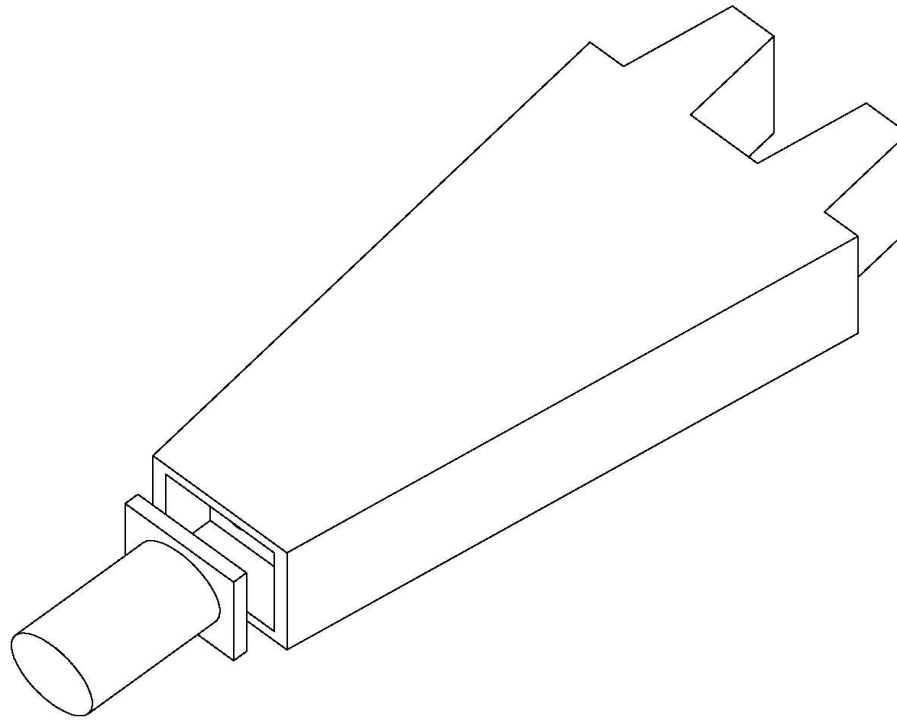
5

4

3

2

1



MATERIAL	Drawn By Designed By	NAME Brian D. Reding II	DATE	TITLE: Sector Sector Heat Pipe (Design 1) (Design 1)
Units: mm	Florida International University College of Engineering Miami, FL.		SIZE DWG. NO. <b>A</b>	
			SCALE: 1.75:1	SHEET 1 OF 3

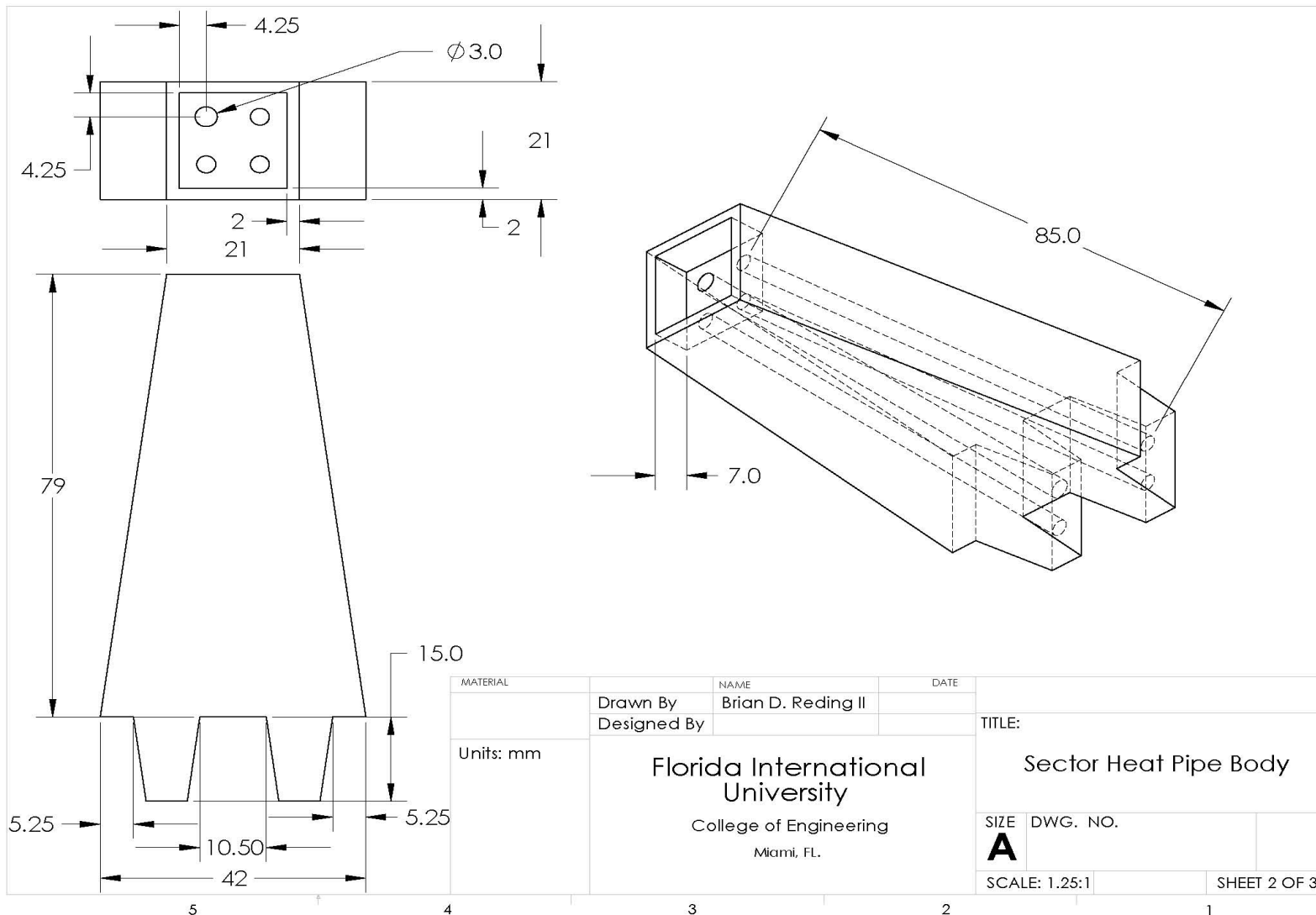
5

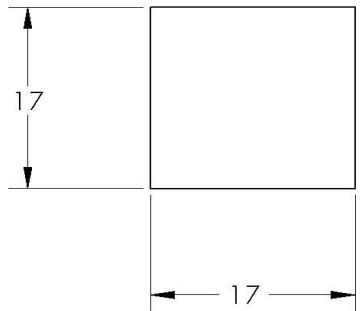
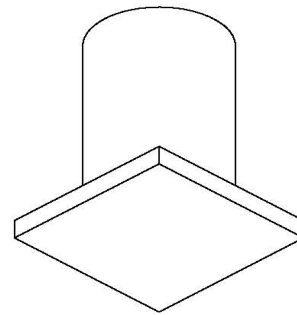
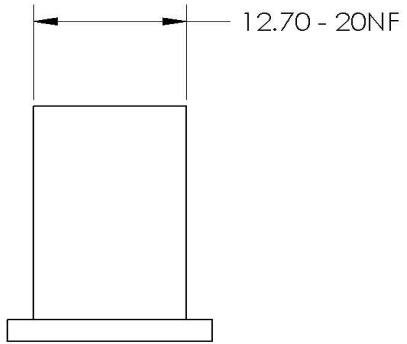
4

3

2

1

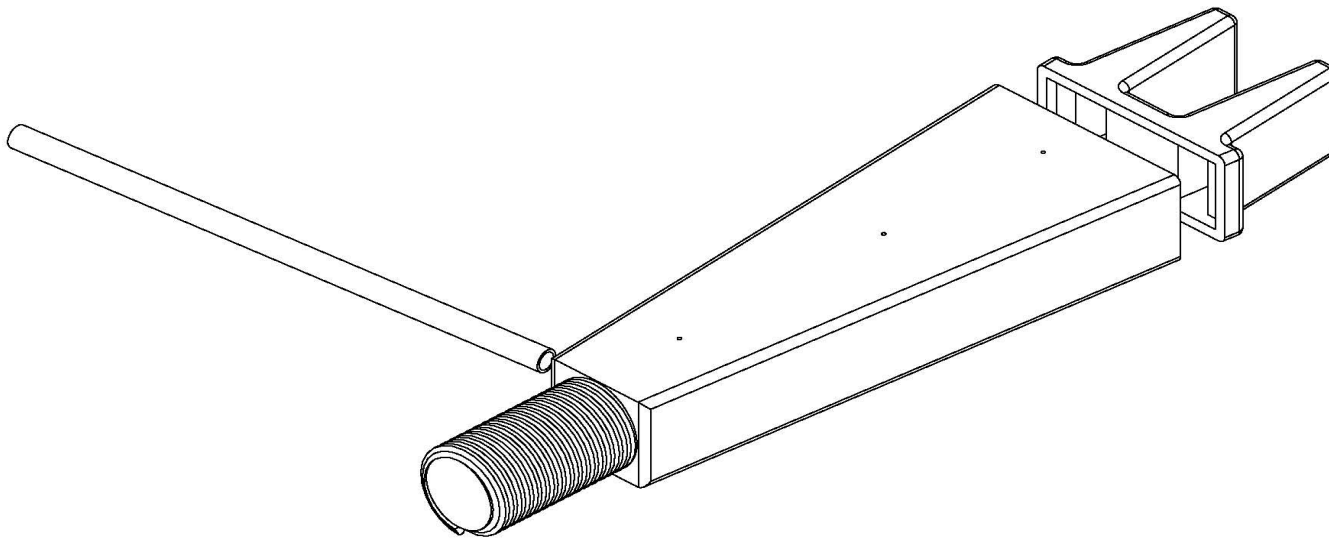




MATERIAL	Drawn By	NAME	DATE	TITLE:	
	Designed By	Brian D. Reding II		Sector Heat Pipe Cap	
Units: mm	Florida International University		SIZE	DWG. NO.	
	College of Engineering		<b>A</b>		
	Miami, FL.		SCALE: 2:1		SHEET 3 OF 3

5 4 3 2 1





NAME		DATE	TITLE:	
DRAWN	Brian D. Reding II	04APR11	Sector Heat Pipe (Design 2) Assembly	
ENG APPR.				
MFG APPR.				
Q.A.				
COMMENTS:			SIZE	DWG. NO.
Material: Multipurpose Copper (Alloy 110)			<b>A</b>	1
SCALE: 3:2		Units: mm	SHEET 1 OF 4	

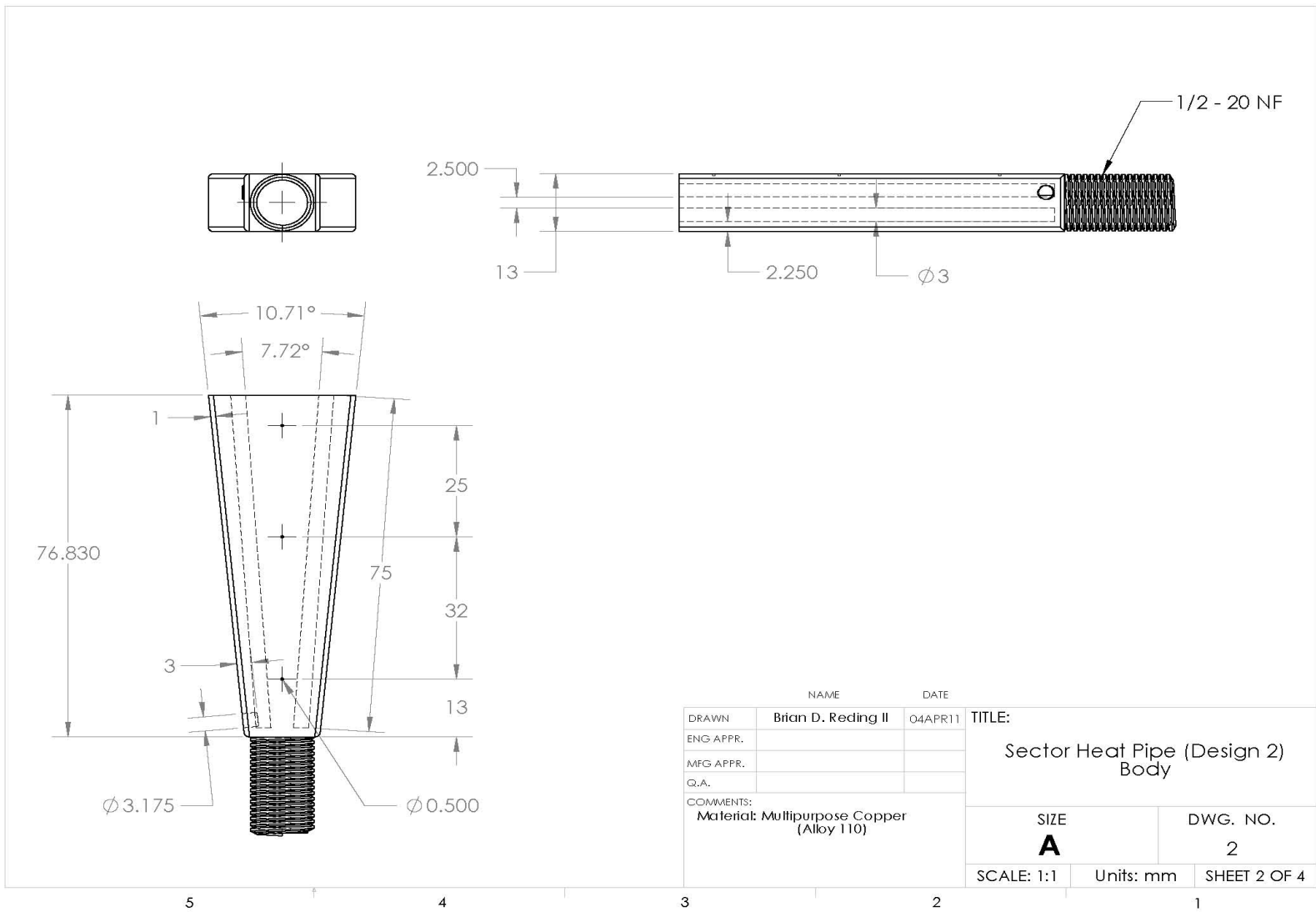
5

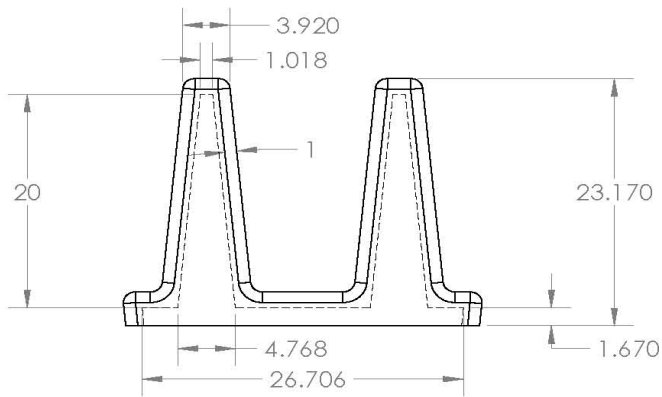
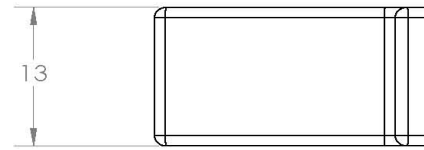
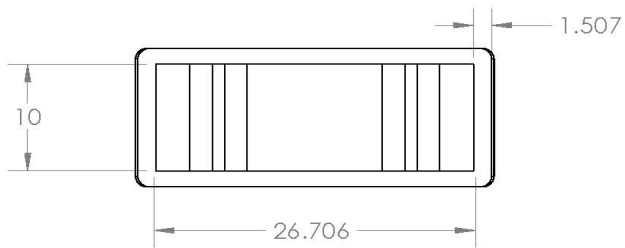
4

3

2

1





NAME		DATE	TITLE: Sector Heat Pipe (Design 2) Dovetail Cap
DRAWN	Brian D. Reding II	04APR11	
ENG APPR.			
MFG APPR.			
Q.A.			
COMMENTS: Material: Multipurpose Copper (Alloy 110)			SIZE <b>A</b>
			DWG. NO. 3
SCALE: 2:1		Units: mm	SHEET 3 OF 4

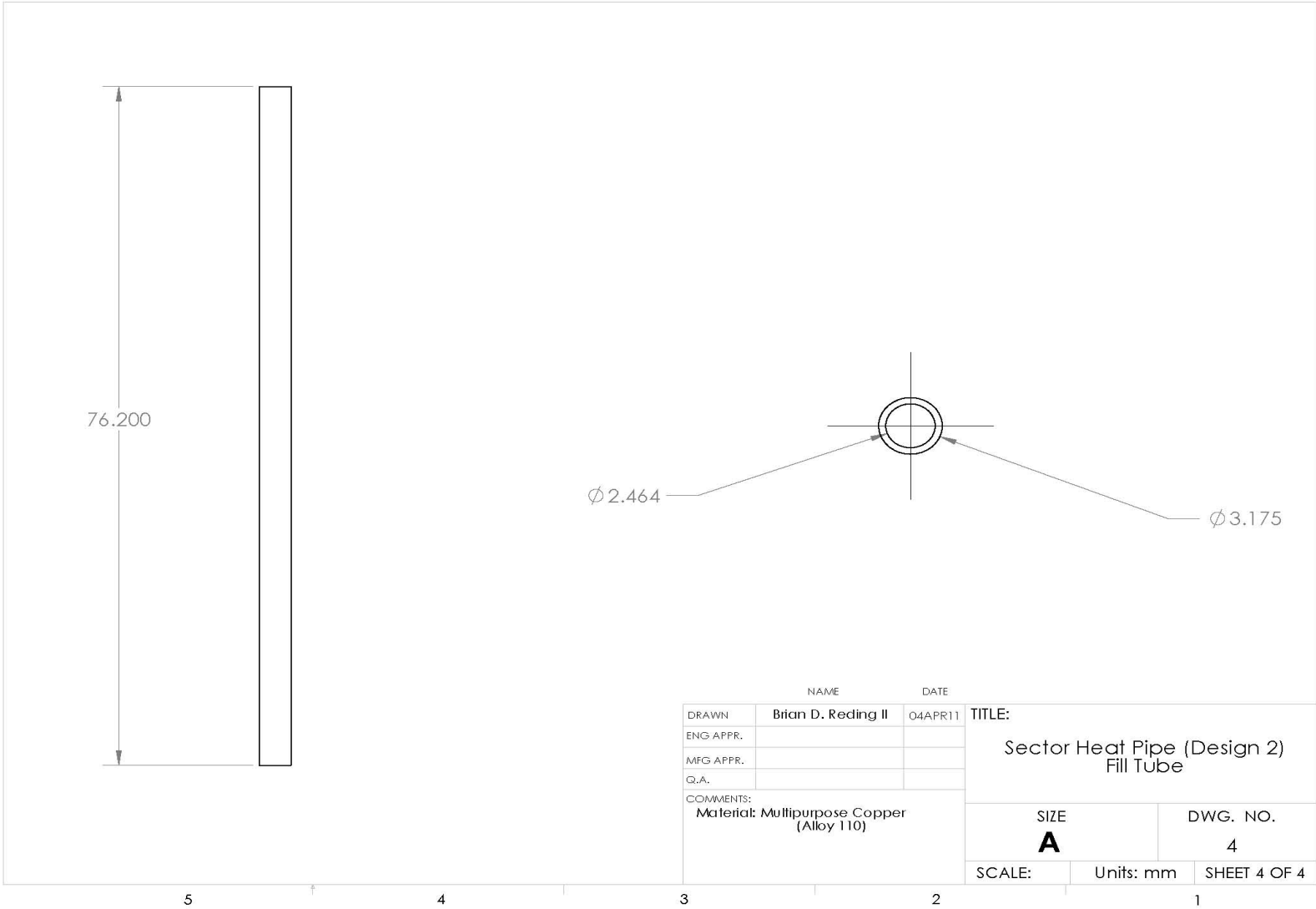
5

4

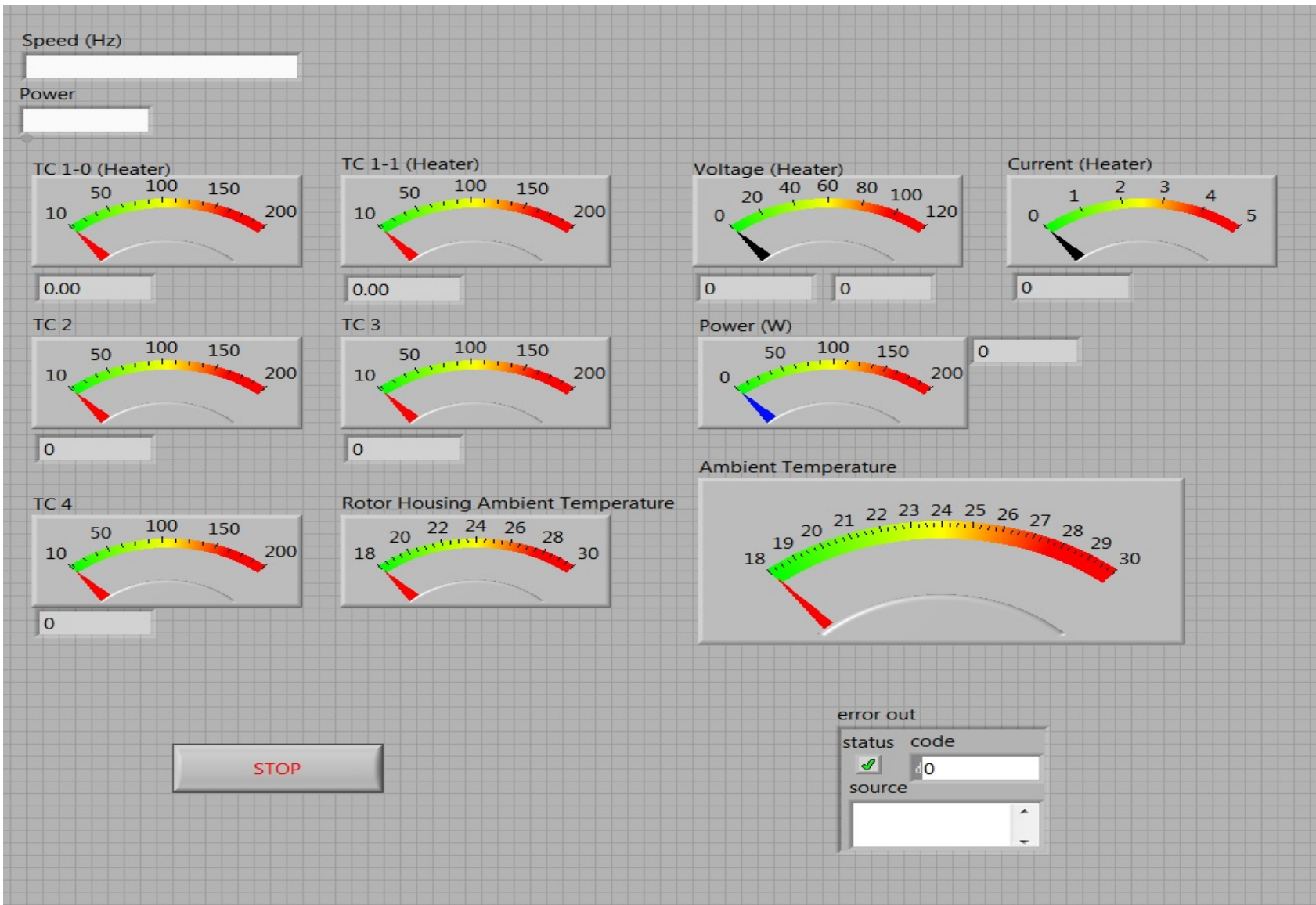
3

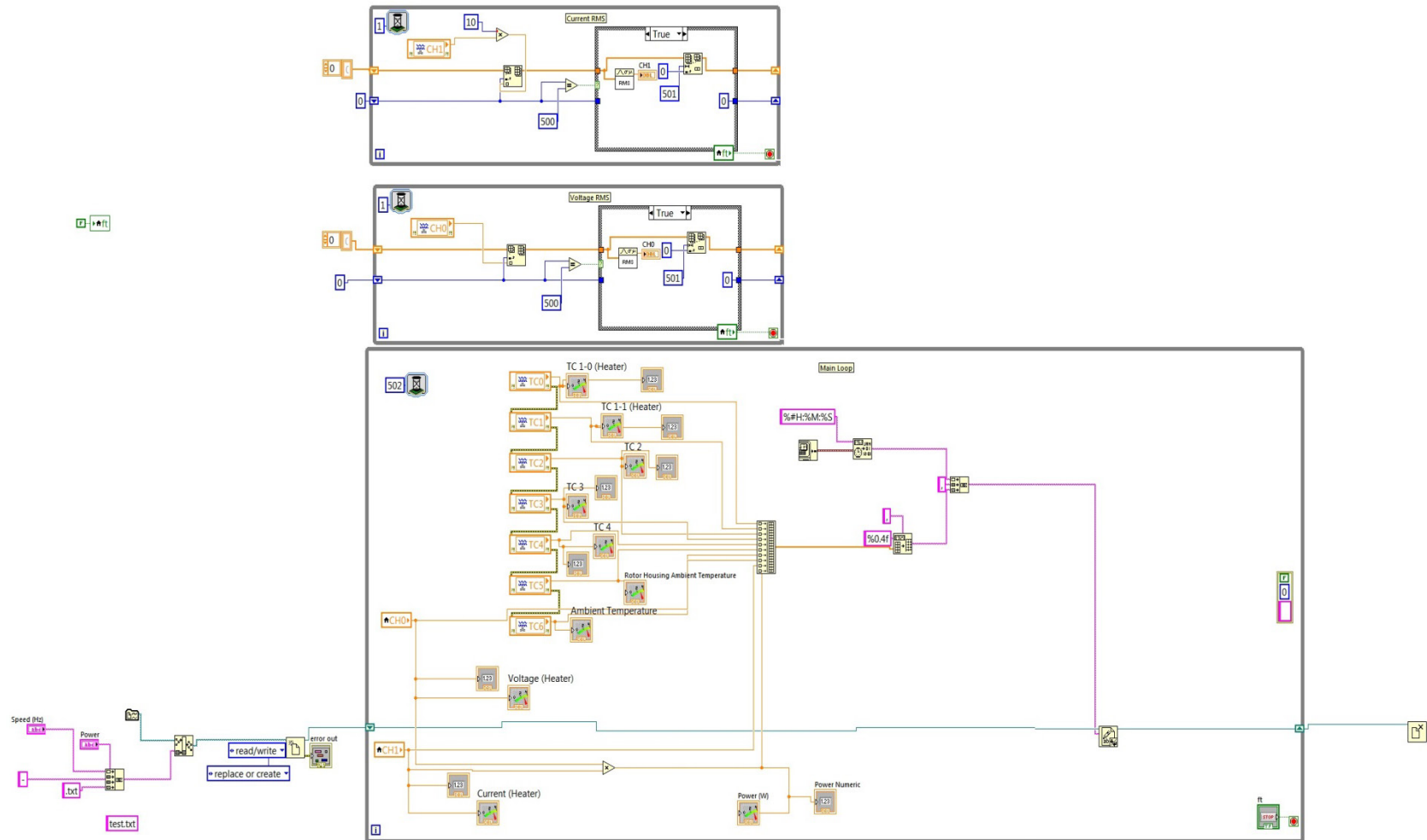
2

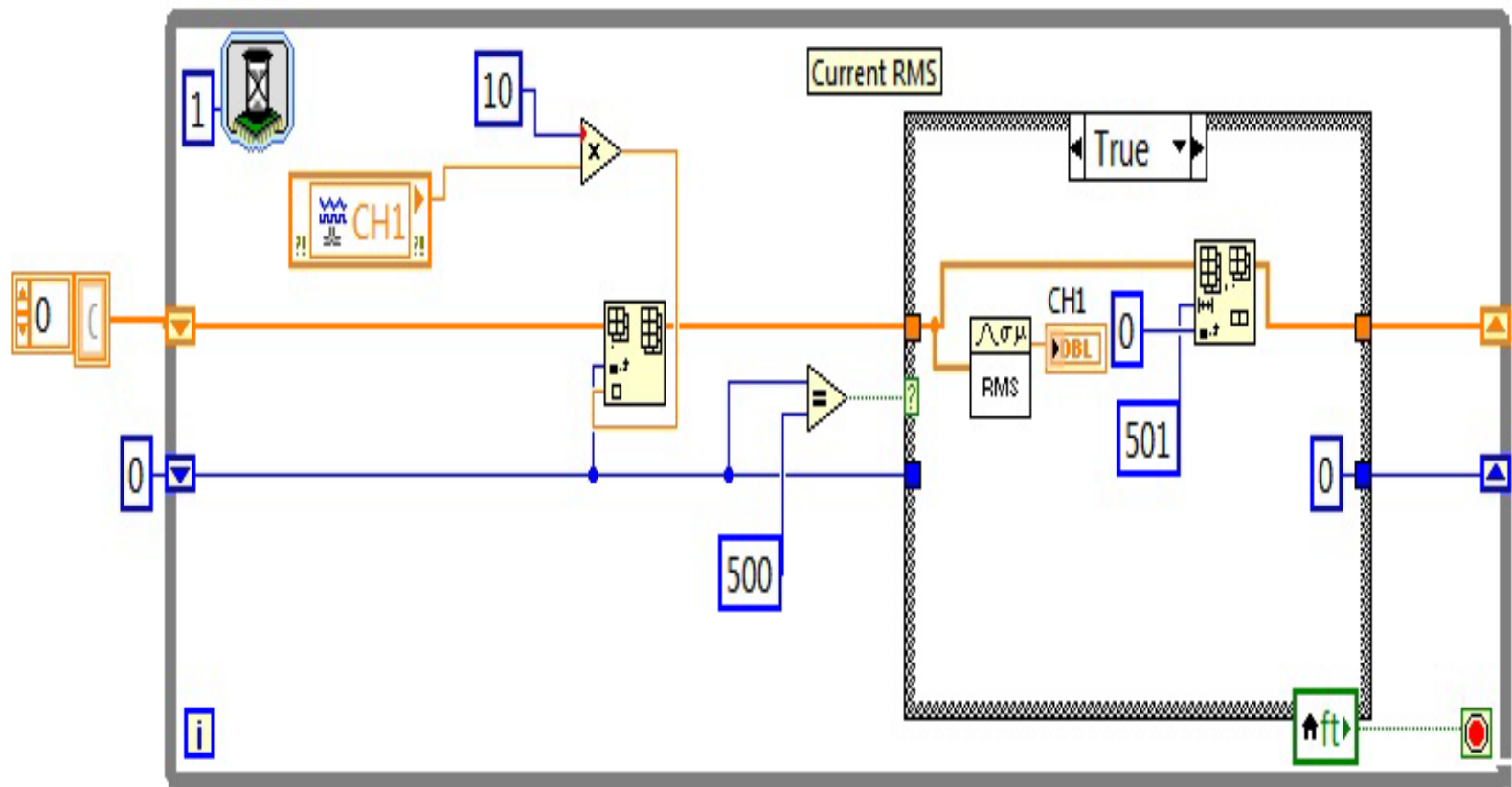
1



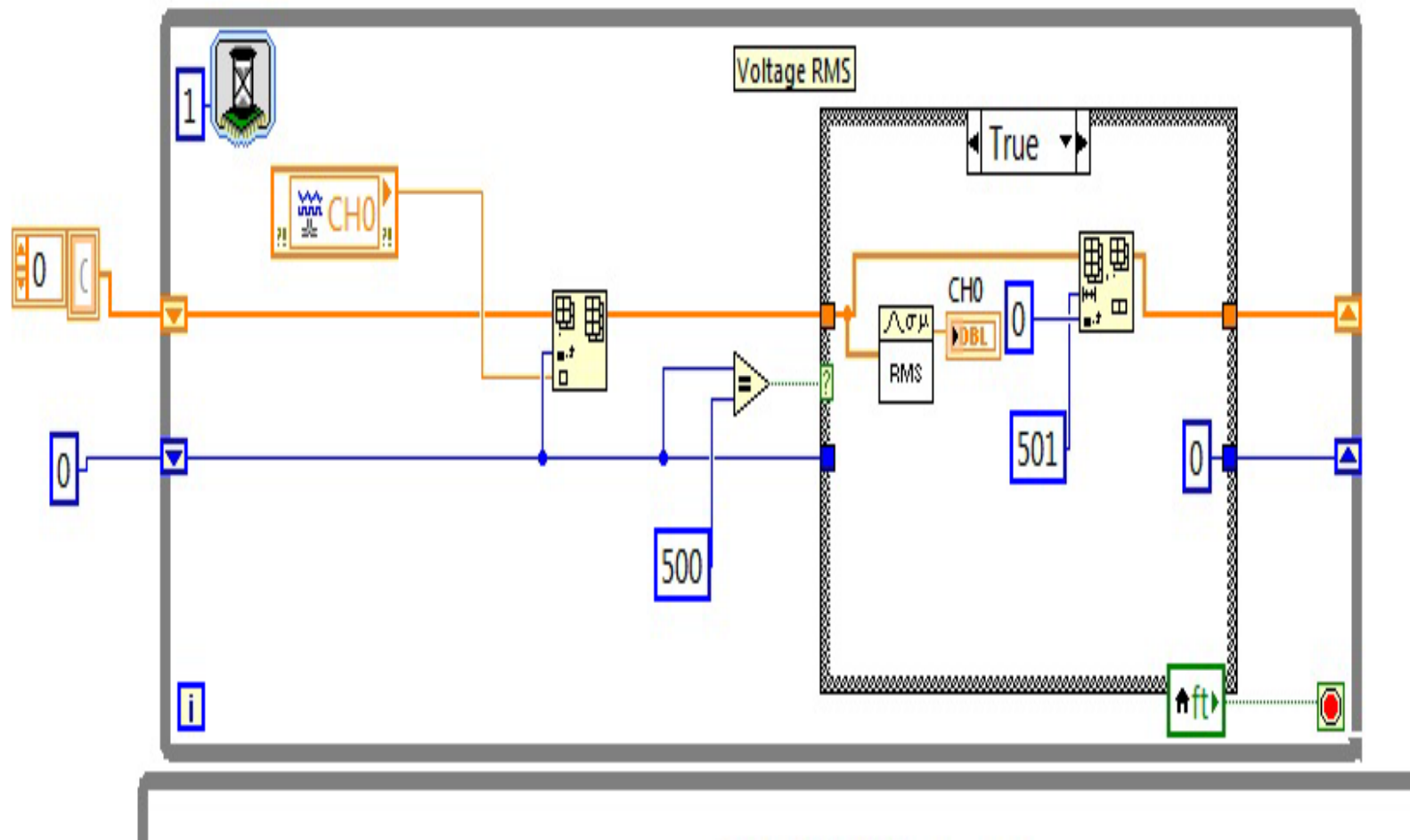
**Appendix B**  
**LabView Program**

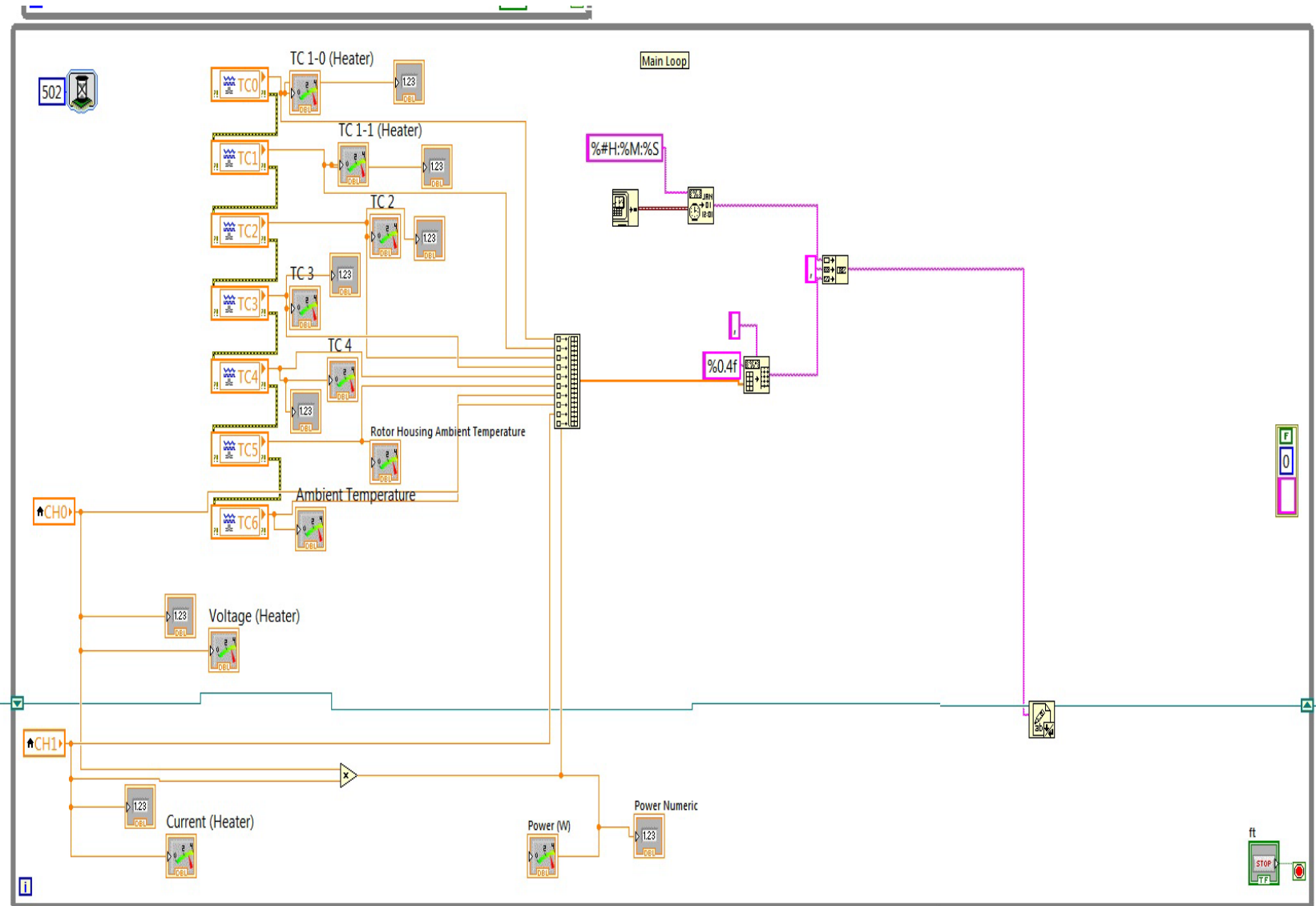


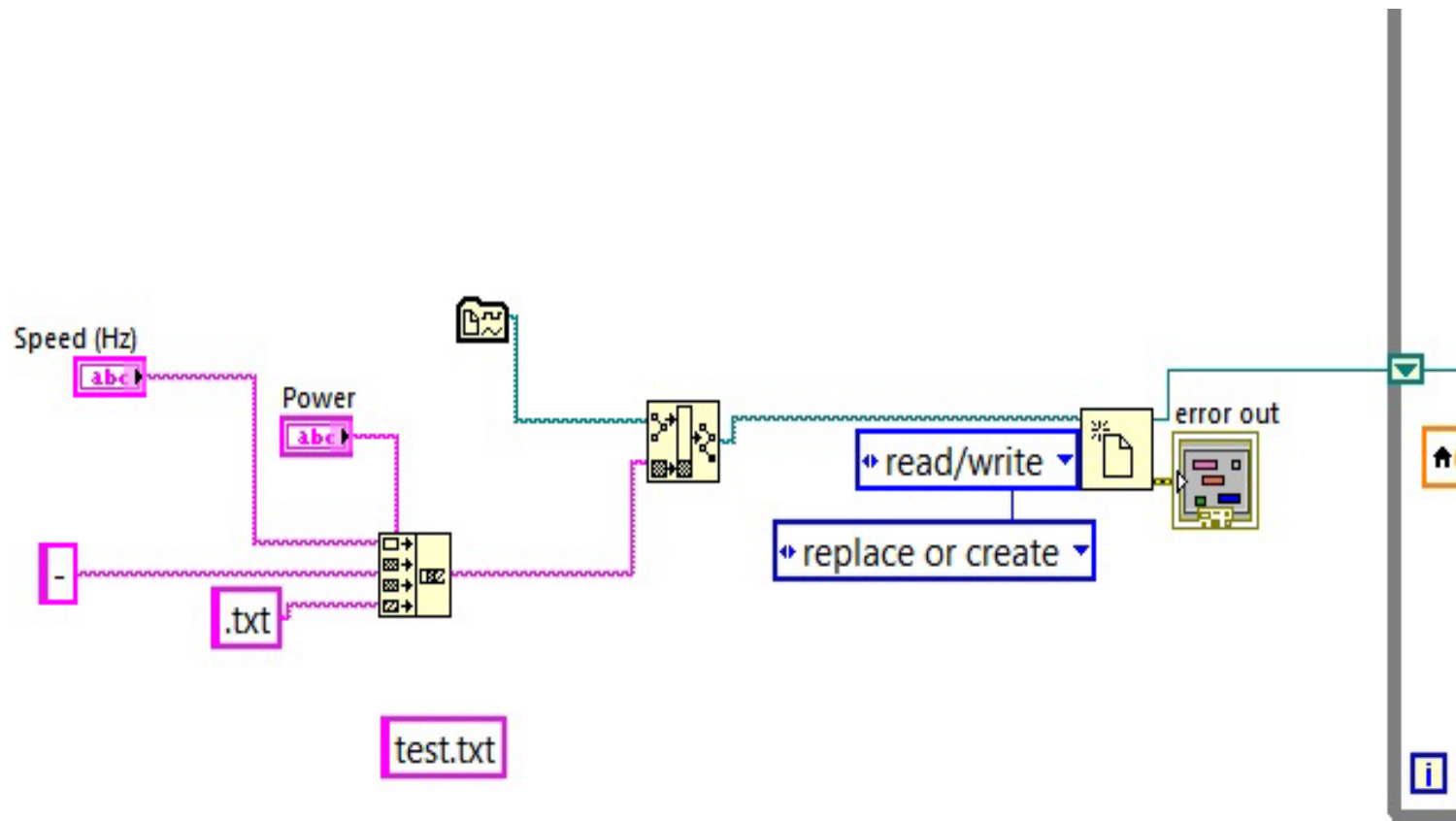


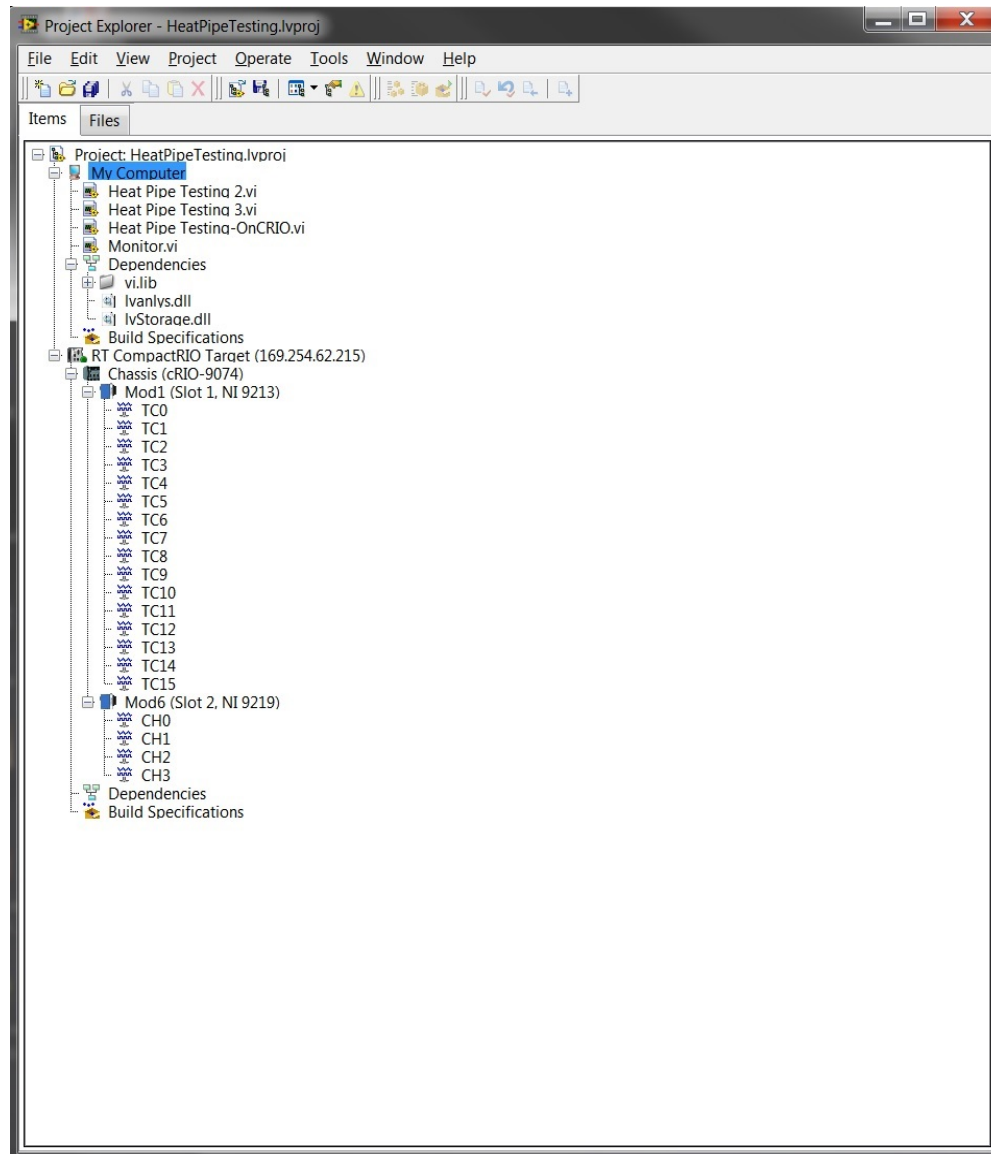












## VITA

BRIAN D REDING II

Born, Bridgeport, Connecticut

- 2002-2006            B.S. Mechanical Engineering  
University of Miami  
Coral Gables, Florida
- 2009-2010            Western Hemisphere Information Exchange FY07  
Florida International University / Universidad Tecnológica  
de Panamá  
Miami, FL. / Panama City, Panama
- 2010-2011            Western Hemisphere Information Exchange FY08  
Florida International University / Universidad Tecnológica  
de Santiago  
Miami, FL. / Santo Domingo, Dominican Republic
- 2010                    Graduate Certificate in Robotics  
Florida International University  
Miami, FL
- 2011                    Certificate of Appreciation  
U.S. Southern Command
- 2010-2013            Doctoral Candidate  
Florida International University  
Miami, FL
- 2012                    Air Force Summer Faculty Fellowship Program  
University of Colorado Boulder  
Boulder, CO

## PUBLICATIONS AND PRESENTATIONS

### Peer-Reviewed Journal Publications

Y. Cao, B. Reding and M. Gao, "*Rotating Miniature and Sector Heat Pipes for Cooling Gas Turbine Rotor Blades and Disks*," Heat Transfer Research, vol. 44, no. 1, pp. 101-114, 2013.

A. Higier, A. Arbide, A. Awaad, J. Eiroa, J. Miller, N. Munroe, A. Ravinet and B. Reding, "*Design, development and deployment of a hybrid renewable energy powered mobile medical clinic with automated modular control system*," Renewable Energy, vol. 50, pp. 847-857, 2013.

I. N. Tansel, B. Reding and W. L. Cooper, "*Lagrangian Point State Estimation with Optimized, Redundant Induction Coil Gauges*," Experimental Mechanics, vol. 53, no. 6, pp. 1065-1072, 2013.

Peer-Reviewed Papers Presented at Conferences and Published in the Conference Proceedings

Cao, Y., Gao, M., and Reding, B., 2009, *Experimental Studies of Rotating Heat Pipes for Cooling Gas Turbine Rotor and Disks*," AIAA paper No. 2009-1427

Presentations

Brian Reding, et al., "*Unmanned Aerial Vehicles using Biofuels*", Western Hemisphere Information Exchange Project and U.S. Southern Command Science and Technology Annual Unmanned Systems Conference, Miami, Florida, December 2009

Brian Reding, et al., "*Biofuel Production and Uses*", Western Hemisphere Information Exchange Project Renewable Energy Conference, Panama City, Panama, May 2010

Brian Reding, et al., "*Use of Eolic Energy for Mobile Operations*", Beyond the Horizons Renewable Energy Mobile Medical Clinic Field presentation, Santo Domingo, Dominican Republic, March 2011

Brian Reding and Adrian Arbide, "*Construction, Utilization, and Management of a suite of renewable energy sources to power a micro grid system (presented in English and Spanish)*", Western Hemisphere Information Exchange Project Renewable Energy Training Conference, Santo Domingo, Dominican Republic, April 2011

Brian Reding, "*Biofuel Production and Chemistry (presented in English and Spanish)*", Western Hemisphere Information Exchange Project Renewable Energy Training Conference, Santo Domingo, Dominican Republic, April 2011

Brian Reding, et al., "*Using a Suite of Renewable Energy Sources to power a mobile medical clinic*", Beyond the Horizons Exercises and Presentation, Mao, Dominican Republic, May 2011

Brian Reding, et al., "*Powering a micro-grid system with a suite of renewable energies*", Annual U.S. Southern Command Science and Technology Conference, Miami, Florida, February 2011